

PLATE TO BACKSTOP: A GEOPHYSICAL INVESTIGATION OF TWO JAPANESE  
SUBDUCTION ZONES, FROM THE OUTER RISE TO THE FOREARC SLOPE

A DISSERTATION SUBMITTED TO THE GRADUATE DIVISION OF THE UNIVERSITY  
OF HAWAI'I AT MĀNOA IN PARTIAL FULFILLMENT OF THE REQUIREMENTS FOR  
THE DEGREE OF

DOCTOR OF PHILOSOPHY

IN

GEOLOGY AND GEOPHYSICS

DECEMBER 2015

By

Brian Boston

Dissertation Committee:

Gregory F. Moore, Chairperson  
Clinton Conrad  
Patricia Fryer  
Stephen Martel  
Horst Brandes

Keywords: Subduction Zones; Japan Trench; Nankai Trough; Outer Rise; Accretionary Prism;  
Forearc Slope

## Acknowledgements

This dissertation is an accumulation of work that greatly benefited from the support, guidance, and encouragement of others, some mentioned and too many others to name individually. My undergraduate experience at the University of Wisconsin ingrained a passion for geology and geophysics originating in classes and field trips, fellow students, and from research. From there I would specifically thank Harold Tobin, who introduced me to many subduction zone processes and to seismic reflection and the Nankai Trough (and would later serve as my co-chief scientist during my PhD). This initial introduction led to a strong curiosity covering a range of topics, including the work of this dissertation.

For this dissertation's work, I thank my advisor, Greg Moore, first and foremost. He provided tremendous opportunities, both at sea and in the lab, and provided a watchful eye as I learned multiple processing and interpretation techniques. I thank my committee, Horst Brandes, Clint Conrad, Patty Fryer, and Steve Martel, for providing helpful comments and discussions that have greatly improved the dissertation.

I thank all my collaborators: Yasuyuki Nakamura and Shuichi Kodaira for helping with data collection and access on the Japan Trench projects; Takeshi Sato for my first seismic cruise; my logging team from my first drilling experience on Expedition 348, María José Jurado and Hiroki Sone; the expedition co-chiefs, Harold Tobin, Demian Saffer, and Takehiro Hirose; and I thank the whole Expedition 348 Scientific Party, logging staff, and crew, who made it a wonderful experience. Additionally, I am thankful for all the other marine experiences I participated in while at the University of Hawaii, which gave me a broader understanding of marine geology and geophysics.

Last but not least, I thank my family and friends, especially my parents, brother, and sister for encouraging me to pursue my passion wherever that may lead and for providing tremendous support. I thank my eighth floor G&T friends for the many conversations covering geology and geophysics: Jess Barnes, Katie Taladay, Dana Brodie, Sarah Maher, Jonathan Sleeper, Sam Howell, Harrison Togia, Jonathan Weiss, and many more. Finally, I thank Sarah Crites who helped me navigate the rough seas of a PhD for most of my time here.

## Abstract

Subduction zones are among the most tectonically dynamic regions. To help resolve the tectonics of such a complex and poorly understood region, this dissertation focuses on three different settings within subduction zones, from seaward to landward, at two Japanese subduction zones, the Japan Trench and the Nankai Trough. I use multiple geophysical methods and datasets including 2D and 3D seismic reflection data, multibeam bathymetry, and logging-while-drilling data to investigate the outer rise to the forearc slope. The first part of this dissertation starts with the incoming plate's structures influencing the deformation front along the Japan Trench. I imaged 199 basement-cutting normal faults finding faults first from striking parallel to the trench axis and reactivate pre-existing seafloor structures as the plate moves landward. The sediment thickness of the incoming Pacific Plate fluctuates between 0 to 600 m with late stage deposition occurring in multiple low relief regions. I find that the incoming outer-rise faults directly influence the location and geometry of the up-dip décollement at the Japan Trench. The second part of this dissertation moves landward to the inner accretionary prism of the Nankai Trough. I find multiple preserved structures of the outer prism with reactivation of one buried thrust estimated to have ~580 m of slip since ~1.04 Ma, after forearc basin deposition started, based on kinematic modeling. I show that the interior of the inner prism has steeply dipping beds with multiple fracture populations. The final part of this dissertation looks at deformational processes at the forearc slope of the Japan Trench. I find forearc basins that dip landward in both bathymetry analysis and in the seismic reflection data that follows basement uplift. The regional basal unconformity is mapped throughout the survey region and exhibits >1 km of relief with slope fill varying by up to ~3000 m and thinning on the seaward edge of the upper slope setting,

the same location where the regional basal unconformity consistently dips seaward. This pattern indicates a landward limit to major subduction erosion and that the upper slope has deformed from additional processes at the Japan Trench margin.

## Table of Contents

Abstract.....	iv
List of Figures.....	ix
List of Abbreviations and Variables.....	xi
Chapter 1: Introduction.....	1
1.1. Dissertation Overview.....	1
1.2. Background.....	1
1.3. Tectonic Setting.....	3
1.4. Dissertation Organization.....	5
References.....	6
Chapter 2: Outer-rise normal fault development and influence on near-trench décollement propagation along the Japan Trench, off Tohoku.....	8
2.1. Background.....	9
2.2. Methods.....	13
2.3. Results.....	14
2.3.1. Distribution of outer-rise normal faults off Tohoku.....	14
2.3.2. Basement-cutting faults.....	17
2.3.3. Incoming Pacific Plate sediments.....	18
2.3.3.1. Sediment thickness.....	19
2.3.3.2. Near-trench, sediment-restricted faults.....	21
2.3.4. The deformation front along the Japan Trench.....	23
2.4. Discussion.....	27
2.4.1. Fault development.....	27
2.4.2. Incoming plate sediment thickness.....	28
2.4.3. Décollement propagation.....	30
2.5. Conclusions.....	36

References.....	37
Chapter 3: The Outer to Inner Accretionary Prism Transition of the Nankai Trough, Southwest Japan.....	43
3.1. Introduction.....	44
3.2. Tectonic Setting.....	46
3.3. Data and Methods.....	50
3.3.1. Seismic Data.....	50
3.3.2. Well Data.....	50
3.3.3. Velocity-Corrected Seismic Volume.....	51
3.3.4. Trishear Model.....	52
3.4. Results.....	52
3.4.1 Top of the Miocene Prism.....	53
3.4.2. Inner Prism Thrusts.....	56
3.4.2.1. Inferring Inner Prism Thrusts.....	56
3.4.2.2. Recent Uplift in the Kumano Basin.....	57
3.4.2.3. Kinematic Model of Uplift.....	59
3.4.3. Interior of the Inner Prism.....	60
3.5. Discussion.....	64
3.5.1. Development and Stability of the Inner Accretionary Prism.....	64
3.5.2. Fluid Localization.....	67
3.6. Conclusions.....	69
References.....	70
Chapter 4: Forearc Slope Deformation above the Japan Trench Megathrust: Implications for Subduction Erosion.....	77
4.1. Introduction.....	78
4.2. Methods.....	81

4.3. Results and Interpretations.....	83
4.3.1. Tilted Forearc Basins .....	83
4.3.2. The Regional Basal Unconformity and Slope Sediments.....	85
4.3.3. Characteristics of the Upper to Middle Slope Break .....	87
4.4. Discussion.....	91
4.5. Conclusions.....	96
References.....	97
Chapter 5: Concluding Remarks.....	102
5.1. Dissertation Summary.....	102
5.2. Broader Impacts.....	104

## List of Figures

Figure 1.1	Tectonic setting of the two Japanese subduction zones of this dissertation ..2
Figure 1.2	Generalized cross-sections between the two study regions .....4
Figure 2.1	Regional and survey location maps .....12
Figure 2.2	Bathymetry and seaward portion of the seismic survey .....15
Figure 2.3	Bathymetry view of intersecting structures .....16
Figure 2.4	Throw analysis of basement-cutting normal faults.....18
Figure 2.5	A subducting horst and trench sediments .....20
Figure 2.6	Small-scale faults within the sediment section .....22
Figure 2.7	Trench graben with deformed sedimentary section .....23
Figure 2.8	Subducted structures parallel to the trench .....24
Figure 2.9	Trench axis bathymetry .....26
Figure 2.10	A schematic model for near-trench décollement propagation .....33
Figure 3.1	Bathymetric map of the Kumano section of the Nankai Trough .....47
Figure 3.2	Seismic inline 2468 across the outer and inner accretionary prisms .....49
Figure 3.3	Well compressional velocity and velocity-corrected seismic data .....53
Figure 3.4	Map view of deep seismic horizons.....54

Figure 3.5	Seismic inline 2147 through the Kumano Basin .....	57
Figure 3.6	Reactivated buried thrusts within the inner prism .....	58
Figure 3.7	Structural reconstruction on seismic inline 2645 (Figure 3.6) using a kinematic trishear model .....	60
Figure 3.8	LWD logs from Hole C0002P .....	62
Figure 3.9	Structure data from Hole C0002P resistivity image log .....	63
Figure 4.1	Japan Trench survey location and tectonic setting .....	79
Figure 4.2	Regional-residual separation of bathymetry .....	82
Figure 4.3	Seismic profiles of landward dipping basins .....	85
Figure 4.4	Shallow basins at the Japan Trench forearc .....	87
Figure 4.5	Seafloor and RBU profiles from seismic lines .....	88
Figure 4.6	Map view of the RBU and slope fill sediment thickness map .....	89
Figure 4.7	Bathymetry and residual bathymetry at the upper to midslope boundary and structural interpretations .....	91
Figure 4.8	Seismic profiles of the western midslope boundary (left column) and general interpretations (right column) .....	94

## List of Abbreviations and Variables

<u>Abbreviation/Variable</u>	<u>Definition</u>
°	degree
~	approximately
>	greater than
<	less than
1D	one-dimensional
2D	two-dimensional
3D	three-dimensional
AFR	azimuthal focused resistivity
$\alpha$	difference between borehole azimuth and dip azimuth
BSR	bottom-simulating reflector
CGG	Compagnie Générale de Géophysique
CMP	common mid-point
DSDP	Deep Sea Drilling Program
E	east
EP	Eurasian Plate

GAPI	gamma ray American Petroleum Institute unit
I-B	Izu-Bonin arc
IBT	Izu-Bonin Trench
IODP	Integrated Ocean Drilling Program
JT	Japan Trench
JAMSTEC	Japan Agency for Marine-Earth Science and Technology
kHz	kilohertz
km	kilometer
LWD	logging while drilling
m	meter
Ma	million years ago
MAD	median absolute deviation
mbsf	meters below seafloor
mbsl	meters below sealevel
MCS	multichannel seismic
MHz	megahertz
mm	millimeter

MT	measured thickness
M <sub>w</sub>	moment magnitude
N	north
NW	northwest
ODP	Ocean Drilling Program
Ωm	ohm meter
OOST	out-of-sequence thrust
PGS	Petroleum GeoServices
φ	bed dip
Ψ	borehole inclination
PoSDM	post-stack depth migration
PP	Pacific Plate
PSDM	pre-stack depth migration
PSP	Philippine Sea Plate
PSTM	pre-stack time migration
RBU	regional basal unconformity
s	second

S	south
SE	southeast
SW	southwest
TIC	top of igneous crust
TST	true stratigraphic thickness
W	west

# **Chapter 1**

## **Introduction**

### **1.1. Dissertation Overview**

This dissertation investigates multiple aspects of subduction zones. In particular, I focus on the incoming outer-rise and the overriding plate, from the trench to the forearc slope. Chapter 1 provides a general introduction to the dissertation topics and structure. Chapters 2, 3, and 4 are written as articles that are to be submitted, are submitted, or are published in peer-reviewed journals. They are ordered seaward to landward to provide insight into each subduction setting, and cover two different subduction zones: the Japan Trench and the Nankai Trough (Figure 1.1). Chapter 2 focuses on the outer-rise normal faults and their influence on the near-trench accretionary prism and décollement. Chapter 3 covers the transition from the outer prism to the inner prism. Chapter 4 focuses on forearc basin development and deformation. Finally, Chapter 5 concludes the work in Chapters 2 through 4 and examines potential broader impacts of this research.

### **1.2. Background**

Subduction zones produce the most numerous and generally largest earthquakes on Earth, accounting for more than 90% of the global seismic moment release (Pacheco and Sykes, 1992). These can produce the highest peak ground accelerations, causing havoc at nearby cities. Additionally, as a fault slips, the overlying water can be displaced, creating a tsunami in response to vertical and horizontal displacement of the seafloor (Tanioka and Satake, 1996). Tsunamis are often stories of lore, as the sea erases entire towns, but they are still very much a threat to modern civilization, as seen from the 2004 Sumatra and 2011 Tohoku tsunamis. New technology and developments in tsunami warning systems have greatly diminished imminent public threats

(e.g., National Research Council, 2011). However, a detailed understanding of the geology of these regions has been elusive due to their offshore locations.

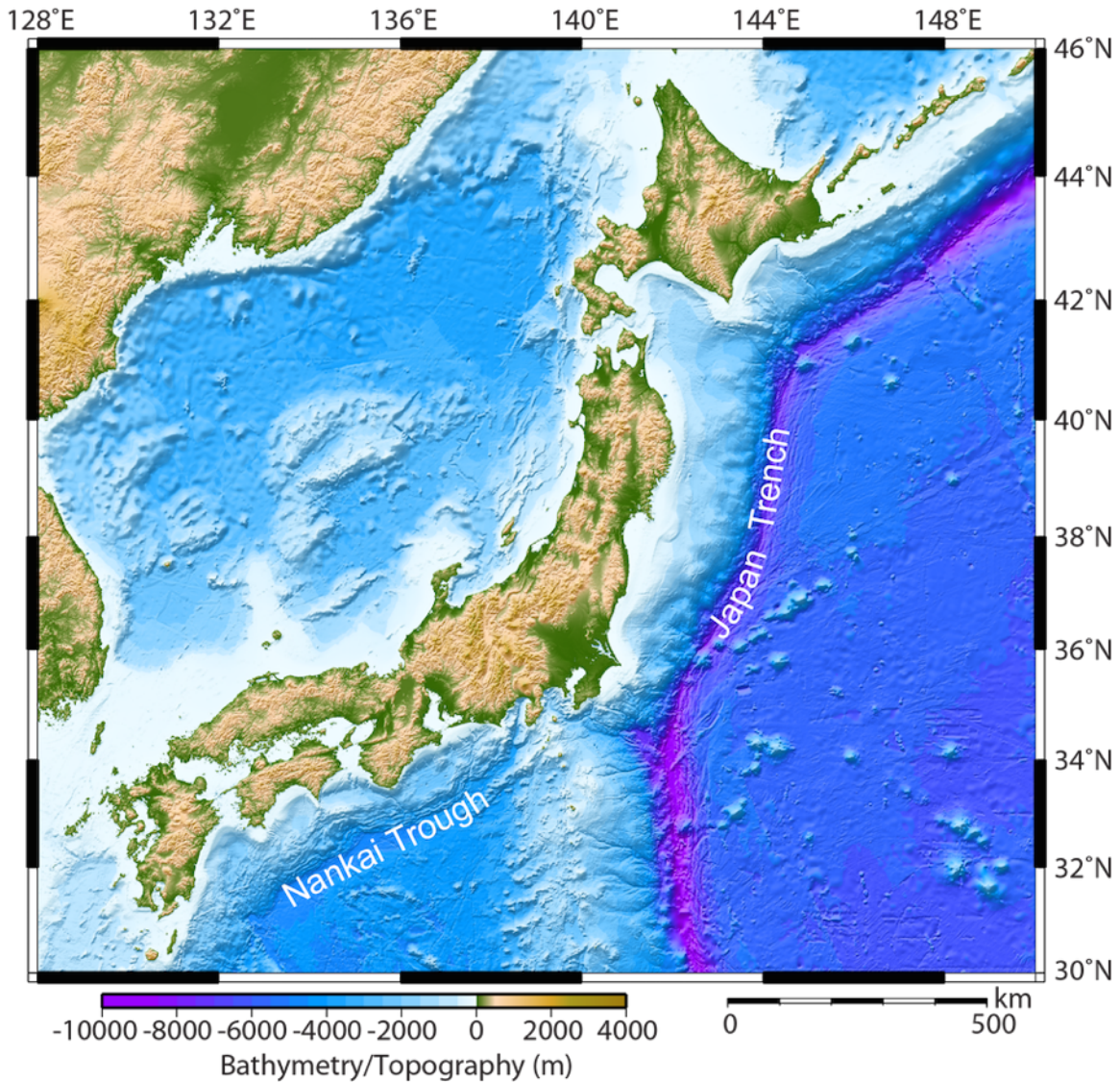


**Figure 1.1.** Tectonic setting of the two Japanese subduction zones of this dissertation. Chapters 2 and 4 focus on the Japan Trench, whereas Chapter 3 covers the Nankai Trough.

This dissertation focuses on two Japanese subduction zones: the Japan Trench and the Nankai Trough (Figure 1.1). Both subduction zones are known for large earthquakes and tsunamis. The Japan Trench was previously known for frequent events of  $M_w$  7-8 (Kanamori et al., 2006). However, the 2011  $M_w$  9.0 Tohoku earthquake broke from this trend, surprising

many. Shaking did affect many towns, but most buildings were engineered for earthquakes and survived. Most of the ~16,000 fatalities came instead from the devastating tsunami. The Nankai Trough is also known for large earthquakes, including two  $M_w > 8.0$  events in the 1940s (Kanamori, 1972), and has a recorded earthquake history going back over 1,000 years (Ando, 1975). In spite of each subduction zone being able to generate large earthquakes, the geology of these subduction zones differs substantially. This dissertation addresses selected geologic aspects of the two subduction zones.

### **1.3. Tectonic Setting**

Subduction zones occur where tectonic plates descend into the Earth's mantle, forming the descending portion of the mantle's convection cells (e.g., Stern, 2002). Subduction zone processes occur on the incoming plate many kilometers from a subduction zone, help form the ocean's deepest trenches, and influence mantle processes down to the core-mantle boundary. This dissertation focuses largely on deformation and sedimentation in the upper lithosphere, within both the overriding plate and the incoming plate, and locations near the seismogenic zone, where earthquakes nucleate and rupture. Great earthquakes since 2004 have revealed a more complex picture of the seismogenic zones than previously known (Lay, 2015).

The Nankai Trough (Figure 1.2A) has been recognized as a sediment-dominated accretionary margin since the first migrated seismic lines were published more than 30 years ago (Aoki et al., 1982). Here, sediment is scraped off of the downgoing plate and accreted on the overriding plate (Clift and Vannucchi, 2004). This process forms a large accretionary prism of accreted sediment. The Nankai Trough has been studied using multiple seismic reflection and refraction surveys, as well as multiple drill sites, including the most recent ones from the Kumano region (e.g., Kinoshita et al., 2006; Park et al., 2002; Kodaira et al., 2000).

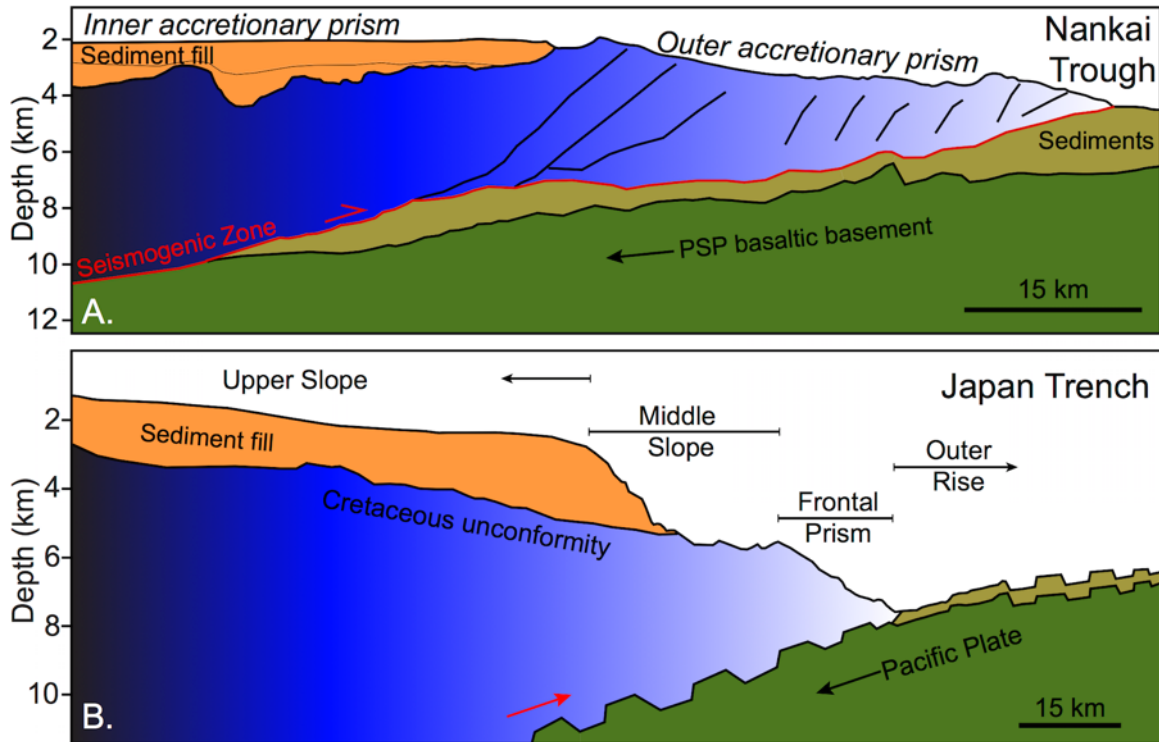


**Figure 1.2.** Generalized cross-sections between the two study regions. **A.** The Nankai Trough, PSP=Philippine Sea Plate. **B.** The Japan Trench. The Nankai Trough has a clear slope break between the inner and outer prisms. The Japan Trench’s accretionary frontal prism is poorly imaged and understood. The subducting Pacific Plate has clear normal fault populations. Chapter 2 focuses on these normal faults and their role in deforming the frontal prism. Chapter 3 looks into the inner accretionary prism at the Nankai Trough. Chapter 4 investigates the middle and upper forearc slopes of the Japan Trench.

In contrast, the Japan Trench (Figure 1.2B) is viewed as an erosional or non-accretionary margin (von Huene and Lallemand, 1990). This type of margin forms small frontal prisms where sediment is initially accreted but may be removed later. Multiple drill sites at the Japan Trench indicated that the forearc has had over 2 km of subsidence since the late Oligocene (von Huene et al., 1982). This subsidence has generally been related to subduction erosion of the upper plate considered to be caused by hydrofracturing and subducting the overriding plate’s fractured sediments (von Huene and Culotta, 1989; von Huene et al., 2004). However, temporal changes in

the geometry of the subducting plate may also account for some the subsidence patterns seen at the Japan Trench (Regalla et al., 2013).

Accretionary prisms form from the incorporation of material from the downgoing plate, so information on that plate is vital for understanding how a prism forms. Seaward of the trench, flexural bending of the downgoing plate creates the outer rise, a feature with a broad-wavelength (>100 km) and small (~0.5 km) vertical relief (Bodine et al., 1981). These bending stresses also produce brittle deformation in the form of normal faults on the incoming plate (Ranero et al., 2003). The lithology and physical properties of the incoming plate also affect prism deformation (Underwood, 2007).

#### **1.4. Dissertation Organization**

This dissertation focuses on three different geologic settings at two Japanese subduction zones. Chapter 2 begins by investigating the region between the outer-rise and the frontal prism. This chapter looks into the outer-rise normal fault population and explores how the incoming normal faults may influence the growth of the frontal prism along the Japan Trench. Chapter 2 was originally published in *Earth, Planets and Space* in 2014. While Chapter 2 focused on near-trench properties, Chapter 3 delves into inner wedge dynamics, in particular topics of inner wedge growth and stability, which active field-based studies have barely treated. Chapter 3 uses a three-dimensional seismic reflection volume, modeling, and deep drilling to address the inner prism. I investigate how an outer prism transitions into the stable environment of the inner prism. This chapter will be submitted for peer-reviewed publication. Chapter 4 considers the most landward part of the subduction system, focusing on forearc basins at the Japan Trench. It will also be published in a peer-reviewed journal. Chapters 2 and 4 use two-dimensional seismic

reflection data that were collected over the course of multiple cruises, and I participated in one of these cruises. Chapter 5 concludes the dissertation with a summary of Chapters 2, 3, and 4.

## References

- Ando, M., 1975. Source mechanisms and tectonic significance of historical earthquakes along the Nankai Trough, Japan. *Tectonophysics* 27, 119-140. doi:10.1016/0040-1951(75)90102-x.
- Aoki, Y., Tamano, T., Kato, S., 1982. Detailed structure of the Nankai Trough from migrated seismic sections. in Watkins, J. S., and Drake, C. L., eds., *Studies in continental margin geology*, American Association of Petroleum Geologists Memoir 34, 309-322.
- Bodine, J.H., Steckler, M.S., Watts, A.B., 1981. Observations of Flexure and the Rheology of the Oceanic Lithosphere. *J. Geophys. Res.* 86, 3695-3707. doi:10.1029/Jb086ib05p03695.
- Clift, P., Vannucchi, P., 2004. Controls on tectonic accretion versus erosion in subduction zones: Implications for the origin and recycling of the continental crust. *Rev. Geophys.* 42, RG2001. doi:10.1029/2003rg000127.
- Kanamori, H., 1972. Tectonic implications of the 1944 Tonankai and the 1946 Nankaido earthquakes. *Phys. Earth Planet. Inter.* 5, 129-139.
- Kanamori, H., Miyazawa, M., Mori, J., 2006. Investigation of the earthquake sequence off Miyagi prefecture with historical seismograms. *Earth Planets Space* 58, 1533-1541.
- Kinoshita, M., Moore, G.F., von Huene, R., Tobin, H., Ranero, C.R., 2006. The Seismogenic Zone Experiment. *Oceanography* 19, 28-38.
- Kodaira, S., Takahashi, N., Park, J.-O., Mochizuki, K., Shinohara, M., Kimura, S., 2000. Western Nankai Trough seismogenic zone: Results from a wide-angle ocean bottom seismic survey. *Journal of Geophysical Research: Solid Earth* (1978–2012) 105, 5887-5905.
- Lay, T., 2015. The surge of great earthquakes from 2004 to 2014. *Earth Planet. Sci. Lett.* 409, 133-146. doi:10.1016/j.epsl.2014.10.047.
- National Research Council, 2011. *Tsunami Warning and Preparedness: An Assessment of the U.S. Tsunami Program and the Nation's Preparedness Efforts*. The National Academies Press, Washington, DC.
- Pacheco, J.F., Sykes, L.R., 1992. Seismic moment catalog of large shallow earthquakes, 1900 to 1989. *Bulletin of Seismological Society of America* 82, 1306-1349.

- Park, J.O., Tsuru, T., Kodaira, S., Cummins, P.R., Kaneda, Y., 2002. Splay fault branching along the Nankai subduction zone. *Science* 297, 1157-1160. doi:10.1126/science.1074111.
- Ranero, C.R., Morgan, J.P., McIntosh, K., Reichert, C., 2003. Bending-related faulting and mantle serpentinization at the Middle America trench. *Nature* 425, 367-373. doi:10.1038/Nature01961.
- Regalla, C., Fisher, D.M., Kirby, E., Furlong, K.P., 2013. Relationship between outer forearc subsidence and plate boundary kinematics along the Northeast Japan convergent margin. *Geochem. Geophys. Geosyst.* 14, 5227-5243. doi:10.1002/2013gc005008.
- Stern, R.J., 2002. Subduction zones. *Rev. Geophys.* 40. doi:10.1029/2001rg000108.
- Tanioka, Y., Satake, K., 1996. Tsunami generation by horizontal displacement of ocean bottom. *Geophys. Res. Lett.* 23, 861-864. doi:10.1029/96gl00736.
- Underwood, M.B., 2007. Sediment inputs to subduction zones: Why lithostratigraphy and clay mineralogy matter, in: Dixon, T.H., Moore, J.C. (Eds.), *The Seismogenic Zone of Subduction Thrust Faults*. Columbia University Press, New York, pp. 42-85.
- von Huene, R., Culotta, R., 1989. Tectonic erosion at the front of the Japan Trench convergent margin. *Tectonophysics* 160, 75-90.
- von Huene, R., Lallemand, S., 1990. Tectonic erosion along the Japan and Peru convergent margins. *Geol. Soc. Am. Bull.* 102, 704-720. doi:10.1130/0016-7606(1990)102<0704:teatja>2.3.co;2.
- von Huene, R., Langseth, M., Nasu, N., Okada, H., 1982. A summary of Cenozoic tectonic history along the IPOD Japan Trench transect. *Geol. Soc. Am. Bull.* 93, 829. doi:10.1130/0016-7606(1982)93<829:asoch>2.0.co;2.
- von Huene, R., Ranero, C.R., Vannucchi, P., 2004. Generic model of subduction erosion. *Geology* 32, 913-916. doi:10.1130/g20563.1.

## Chapter 2

### **Outer-rise normal fault development and influence on near-trench décollement propagation along the Japan Trench, off Tohoku**

Published as:

Boston, B., Moore, G. F., Nakamura, Y., Kodaira, S., 2014. Outer-rise normal fault development and influence on near-trench décollement propagation along the Japan Trench, off Tohoku. *Earth, Planets and Space*, 66, 135. doi:10.1186/1880-5981-66-135

*Abstract*— Multichannel seismic reflection lines image the subducting Pacific Plate to approximately 75 km seaward of the Japan Trench and document the incoming plate sediment, faults, and deformation front near the 2011 Tohoku earthquake epicenter. Sediment thickness of the incoming plate varies from <50 to >600 m with evidence of slumping near normal faults. We find recent sediment deposits in normal fault footwalls and topographic lows. We studied the development of two different classes of normal faults: faults that offset the igneous basement and faults restricted to the sediment section. Faults that cut the basement seaward of the Japan Trench also offset the seafloor and are therefore able to be well characterized from multiple bathymetric surveys. Images of 199 basement-cutting faults reveal an average throw of approximately 120 m and average fault spacing of approximately 2 km. Faults within the sediment column are poorly documented and exhibit offsets of approximately 20 m, with densely spaced populations near the trench axis. Regional seismic lines show lateral variations in location of the Japan Trench deformation front throughout the region, documenting the incoming plate's influence on the deformation front's location. Where horst blocks are carried into the trench, seaward propagation of the deformation front is diminished compared to areas where a graben has entered the trench. We propose that the décollement's propagation into the trench graben may be influenced by local

stress changes or displacements due to subduction of active normal faults. The location and geometry of the up-dip décollement at the Japan Trench is potentially controlled by the incoming outer-rise faults.

## **2.1. Background**

When large bathymetric features, such as seamounts, fracture zones, ridges, and oceanic plateaus, are subducted at convergent margins, they strongly deform the landward trench slopes (e.g., McCann and Sykes 1984; Lallemand and Le Pichon 1987; Dominguez et al. 1998; Taylor et al. 2005). Smaller features, such as subducting horst and graben structures, were once considered to play a role in sediment subduction and upper plate abrasion by horst blocks (Hilde 1983), but better imaging of the subducting plate suggested the subduction plane was well above the top of such features (von Huene and Culotta 1989). Sediment thickness and lithostratigraphy of the incoming plate may further influence the landward trench slope by controlling the physical properties of the margin and inducing lateral heterogeneities in prism formation (Underwood 2007; Ike et al. 2008). Although large-scale features can dominate the upper plate morphology, small-scale features are likely more common at most trenches and may also play a role in modifying the upper plate over time.

Normal faults, found on the outer rise of many Pacific trenches (e.g., Masson 1991), are one type of small-scale feature with potential impacts on the upper plate morphology. As the plate enters a subduction zone, flexural bending of the plate produces the outer rise (e.g., Bodine et al. 1981). Brittle failure manifested by normal faults permanently deforms the surface of the downgoing plate. Faults can form parallel to the trench axis in subduction zones. However, in regions where the abyssal hill fabric, formed at oceanic spreading centers, strikes at a low angle (<25° to 30°) to the trench, the abyssal hill faults are reactivated instead of forming new faults

(Masson 1991). Reactivated abyssal hill faults are identified by their strike, which is parallel to the abyssal hill fabric or magnetic lineations seaward of the trench (Billen et al. 2007). Flexural bending structures and seafloor spreading fabrics along the outer rise are the major contributors to strikes of incoming topographic features on the Northwestern Pacific Plate (Nakanishi 2011). Furthermore, normal faults produced by plate flexure seaward of the trench penetrate into the mantle are thought to allow hydration of the upper mantle and crust (Ranero et al. 2003; Grevemeyer et al. 2007) leading to a potential role in overpressuring and hydrofracturing of the upper plate at depth (von Huene et al. 2004).

The dominant features observed on the incoming Pacific Plate are bending-related normal faults, abyssal hill fabric, fracture zones, seamounts, and elongated ridges (Nakanishi 2011). The incoming outer-rise faults are largely active structures before and during subduction. Following a large megathrust earthquake at a subduction zone, shallow intraplate earthquakes are often detected along the outer rise (Christensen and Ruff 1988); these earthquakes might be caused by the Coulomb stress change from the main thrust event (e.g., Sato et al. 2013). After the 2011 Mw 9.0 Tohoku earthquake, the outer rise of the Japan Trench was dominated by normal fault earthquakes of varying size, depth, and spatial location. These earthquakes may still be potential tsunamigenic hazards, as several Mw >7.0 events have occurred since the main shock, including a large outer-rise event of Mw 7.7 (Lay et al. 2011) and two Mw 7.2 earthquakes in 2012 (Obana et al. 2014). Historically, large outer-rise events within this region include the 2005 Mw 7.0 (Hino et al. 2009) and the 1933 Mw 8.4 (Kanamori 1971) events. Precise measurements from ocean bottom seismographs (OBSs) detected numerous intraplate earthquakes after the 2011 event ranging in location from approximately 120 km seaward of the trench to approximately

90 km landward of the trench with mainly normal fault focal mechanisms in the uppermost subducting Pacific Plate (Obana et al. 2012; Obana et al. 2013).

Geophysical analysis of the Tohoku earthquake revealed large coseismic slip that extended to the trench (Ide et al. 2011; Ito et al. 2011; Fujiwara et al. 2011; Fujii et al. 2011). Differential bathymetry from before and after the earthquake also revealed the largest vertical displacements near the trench axis (Fujiwara et al. 2011), and seismic reflection data imaged frontal thrust development after the event (Kodaira et al. 2012). Seismic data collected in 2011 suggested that the décollement steps down into a local graben at the trench axis (Kodaira et al. 2012; Nakamura et al. 2013) rather than remaining at a constant depth above the overriding plate and ‘bulldozing’ the sediment from the top of the incoming horst blocks (e.g., Hilde 1983). Subduction of active bending-related normal faults may have larger implications for deformation of the near-trench upper plate and may be a small contributor to tsunamigenesis, with large seafloor displacements but small areal extent. To better determine the role of the incoming plate on near-trench coseismic processes, we first examine the nature of the crust that is subducting at the Japan Trench.

This study focuses on the basement and sediment structure of the incoming Pacific Plate off Tohoku. We investigate the morphology of outer-rise normal fault systems and their lateral variations along the Japan Trench. These fault systems are particularly important in the Japan Trench because the lack of significant trench sediment fill means that, along many parts of the margin, the morphologic trench is defined where a graben has entered the trench. Therefore, it is important to define the characteristics of the subducting normal fault system. We use recently collected seismic reflection data seaward of the Tohoku earthquake epicenter to image the sediment and basement structure of the Pacific Plate. In the present study, we analyze the

bending-related normal faults off Tohoku with a goal of establishing relationships among the subducting horst-graben structures, their sediment cover, and deformation in the Japan Trench and the adjacent landward trench slope.

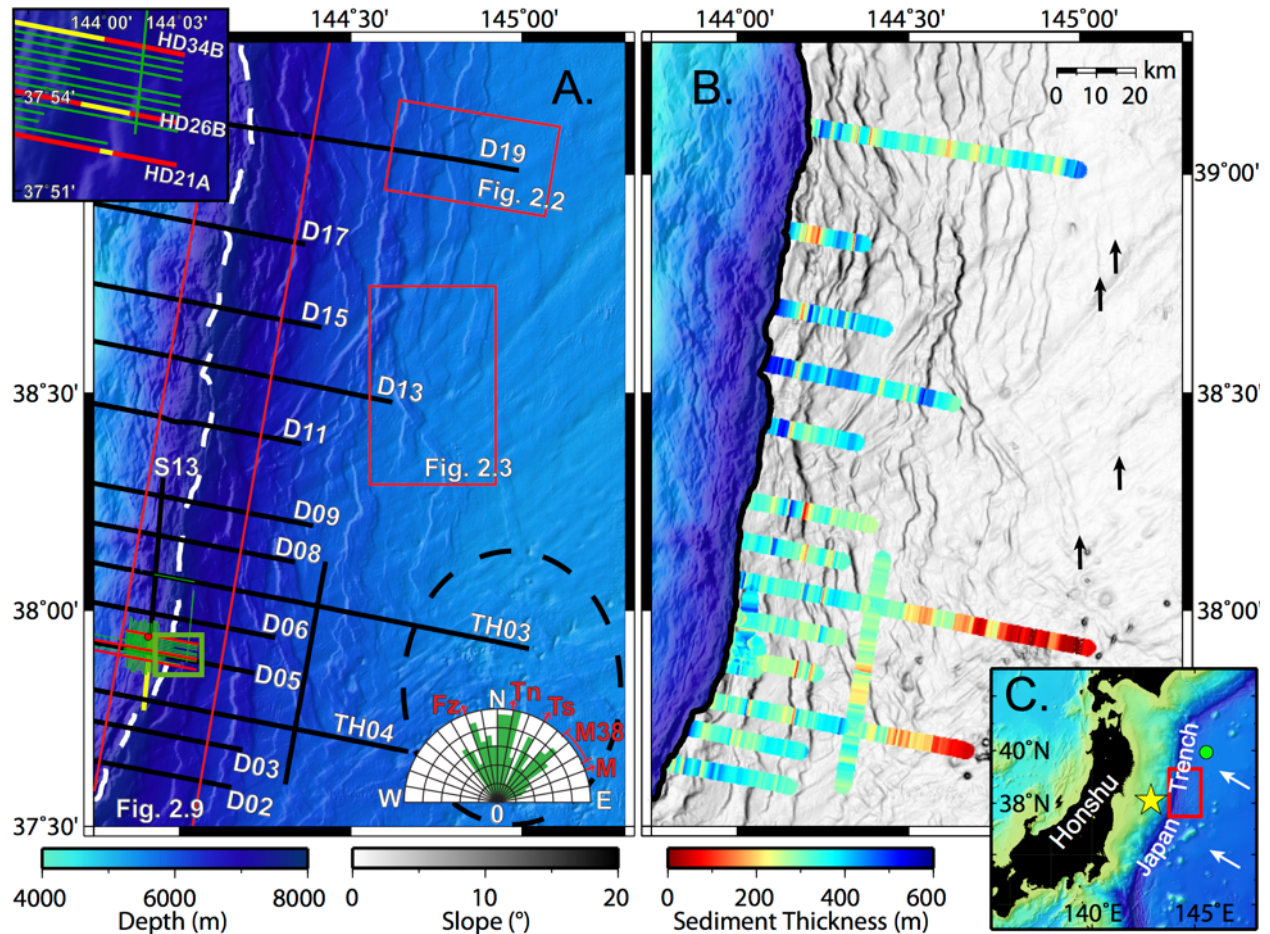


**Figure 2.1.** Regional and survey location maps. **(A)** Black lines are the regional seismic lines and green lines are the high-resolution seismic lines. The green box is the location of the inlet in the upper left corner showing high-resolution seismic line locations with yellow sections marking shown sections. The red circle is location of IODP Site C0019 (J-FAST). The dashed white line is the trace of the deformation front. Labeled red boxes are locations of Figures 2.2, 2.3, and 2.9. The rose diagram displays the strike of topographic structures within  $38^{\circ}$  to  $39^{\circ} 20'$  N (modified from Nakanishi 2011). Abbreviations on the rose diagram are as follows: Fz, fracture zone; Tn, trench trend north of  $38^{\circ}$  N; Ts, trench trend south of  $38^{\circ}$  N; M38, magnetic anomaly orientation near  $38^{\circ}$  N; M, magnetic anomaly orientation elsewhere. Black dashed oval shows area of petite spot volcanoes (Hirano et al. 2008); **(B)** slope map of the Pacific Plate is overlain on top of the bathymetry, highlighting normal fault scarps (dark regions). Arrows point to seaward trench-parallel fault scarps outside the region of the 2D seismics. Black line marks the deformation front. Colored profiles indicate the stratigraphic thickness of the sediment column of the Pacific Plate. Thinning near normal faults is expected. **(C)** Regional tectonic map.

The yellow star is the location of the 2011 Tohoku earthquake epicenter. The red box is the location of Figure 2.1A,B. Green circle is the location of Deep Sea Drilling Project (DSDP) Site 436. White arrows show the convergence direction of the Pacific Plate.

## 2.2. Methods

We use four two-dimensional (2D) multichannel seismic (MCS) surveys carried out by the Japan Agency for Marine-Earth Science and Technology (JAMSTEC) for a total of 28 dip lines and 19 strike lines along the Japan Trench. JAMSTEC's vessel R/V *Kairei* conducted three MCS surveys in March, April to May, and August to September 2011, collecting a total of 15 regional lines. The seismic system used a 444-channel hydrophone streamer, 12.5-m group interval, 6,000-m-long receiver cable, with a 7,800 in.<sup>3</sup> air gun array fired at 50-m intervals, producing a common mid-point (CMP) interval of 6.25 m. R/V *Kaiyo* collected 32 high-resolution seismic lines in October to November 2011. The acquisition system used a 192-channel, 6.25-m group interval, 1,200-m-long receiver cable, with a 320 in.<sup>3</sup> cluster gun array fired at 37.5-m intervals. Line spacing for the *Kaiyo* seismic grid was approximately 500 m with a CMP interval of 3.125 m. Both regional and high-resolution lines were processed through conventional workflows (e.g., Yilmaz 2001) that included trace edit, CMP binning, band-pass filter, velocity analysis, normal moveout correction, and CMP stacking. We performed Kirchhoff post-stack depth migration (PoSDM) on the regional *Kairei* lines using previous local refraction and reflection studies (e.g., Tsuru et al. 2000) to constrain our velocity model. For the high-resolution *Kaiyo* lines, we performed Kirchhoff pre-stack depth migration (PSDM). Due to the short streamer-cable length, the velocity model for the PSDM is poorly constrained, so our starting velocity models were based on velocity values of PoSDM migrations for each line. We performed 2 to 4 iterations of velocity analyses for PSDM creating a final model that produced

the clearest image. Because of the great water depths (>6,000 m), the water velocity (which does not vary greatly) has a large effect on the migrations. We estimate that within the sediment section, which is less than 1,000-m-thick, our velocity errors are no more than approximately 200 to 400 m s<sup>-1</sup> based on PSDM sediment velocity sensitivity in the high-resolution lines (e.g., Tsuru et al. 2000; Costa Pisani et al. 2005). Such velocity errors would result in a maximum of approximately 5% to 10% error in depth that would not affect our structural interpretations.

We combined multibeam echosounder data collected during more than 150 JAMSTEC cruises (available from the JAMSTEC DARWIN database, <http://www.godac.jamstec.go.jp/darwin>) to produce our bathymetry map. All of these JAMSTEC cruises used SeaBeam systems. Regions with no multibeam ship tracks are plotted with the GEBCO 30 arcsec grid (<http://www.gebco.net>). We applied noise reduction and merging techniques, gridding, and filtering to produce a final dataset (Figure 2.1). The detailed bathymetry and a computer-generated slope map delineate the surface expression of the normal faults, allowing us to map their orientations.

## **2.3. Results**

### **2.3.1. Distribution of outer-rise normal faults off Tohoku**

The bathymetric and slope maps clearly show normal faults on the Pacific Plate seaward of the Japan Trench (Figure 2.1). Surface breaks are detected as far as approximately 120 km seaward of the trench axis with the strike of the faults parallel to the trench trend. Sixty kilometers landward from the most seaward surface breaks, the fault patterns become more intricate (Figures 2.2 and 2.3), presumably a reflection of these faults' interacting with the pre-existing fabric of the Pacific Plate and each other as they propagate (e.g., Ranero et al. 2003). The pre-existing fabric appears to limit certain fault orientations and promote others, as active

fault strikes coincide with the orientations of fracture zones and abyssal hill fabric (Nakanishi 2011). The southeast region of the survey area is slightly more complex due to potential petite spot volcanism (Site C of Hirano et al. 2008) making it difficult to determine the strike of basement-cutting faults because of more relief in the topography and regional sediment thinning (Figure 2.1). Fault interactions on the incoming Pacific Plate produce a heavily deformed and spatially complex fault pattern just seaward of the trench.

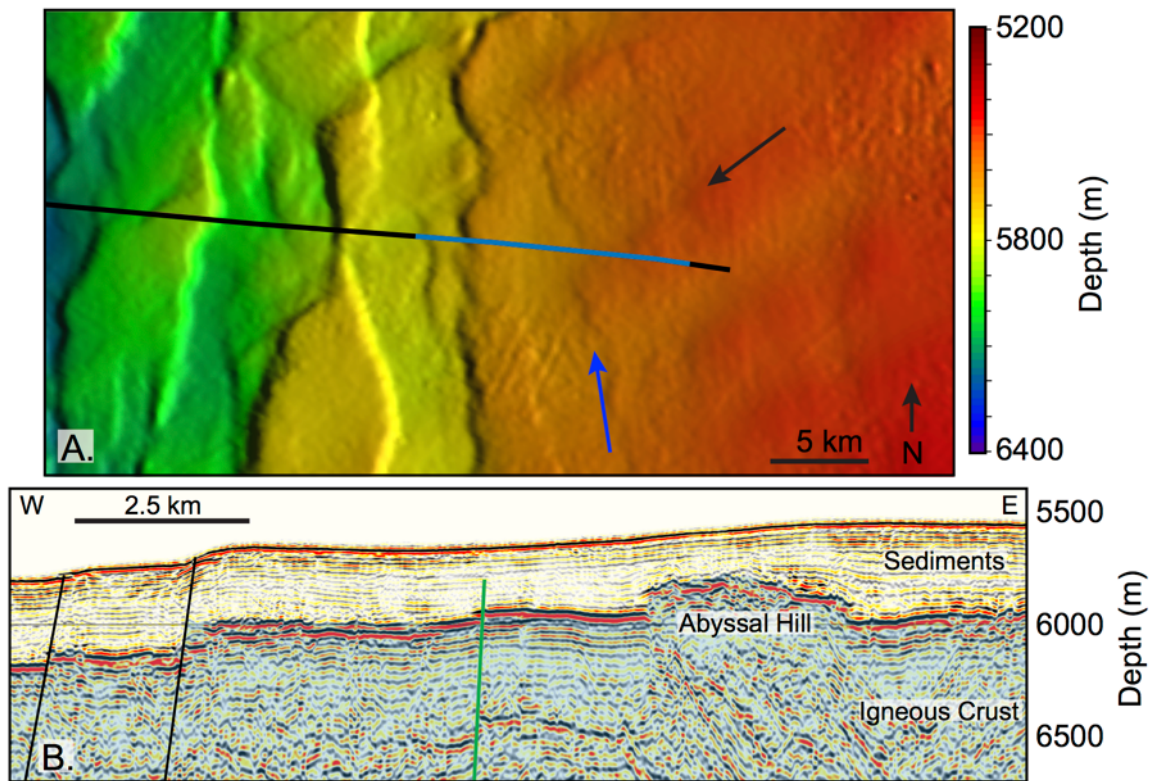


**Figure 2.2.** Bathymetry and seaward portion of the seismic survey. **(A)** Bathymetry around line D19 (black line), location is shown in Figure 2.1. Blue segment is shown in Figure 2.2B. Blue arrow shows trench-parallel faults and black arrow points to abyssal hill fabric. **(B)** Seismic line crossing abyssal hill fabric. Continuous horizons over the top of the abyssal hill indicate that this is a relatively old feature. Faulting parallel to the trench starts within approximately 3 km west of the green fault (blue arrow in Figure 2.2A).

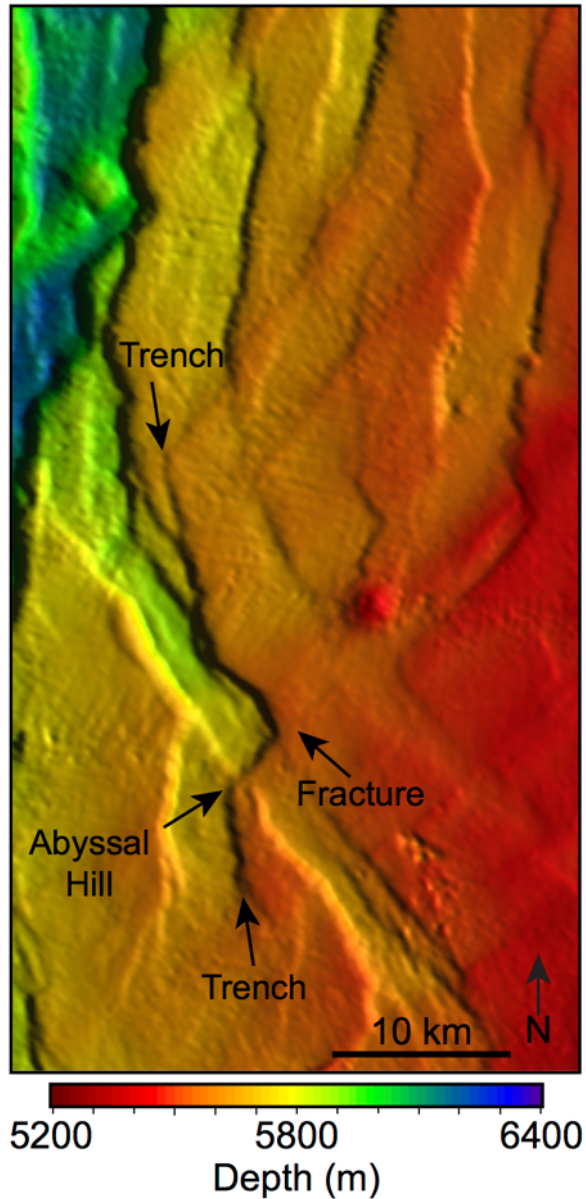


**Figure 2.3.** Bathymetry view of intersecting structures. Bathymetric map south of Figure 2.2A and the location is shown in Figure 2.1. Fault traces are parallel to the abyssal hills, fracture zones, and the trench. The zig-zag fault trace pattern reflects the intersection of pre-existing structures.

zig-zag surface traces containing sharp bends and irregular paths develop where the faults with differing strikes intersect (Figures 2.1 and 2.3). This indicates that trench-parallel faulting may

The MCS data only extend approximately 75 km seaward of the Japan Trench but still provide insight into the beginning of faulting. Line D19 intersects both abyssal hill and trench-parallel fabrics (Figure 2.2). Although the geometry of line D19 is not ideal for imaging those fabrics (its line is not perpendicular to the strike of the fabrics), the seismic line does show continuous horizons above the buried abyssal hill topography, which formed at the spreading center. The continuity of reflectors over the abyssal hill implies that the fault associated with the abyssal hill either is not active or has not slipped enough to offset the youngest sediments. A few kilometers west of the abyssal hill (Figure 2.2B), a trench-parallel fault (green fault in Figure 2.2B)

offsets the top of igneous crust (TIC) by approximately 30 m. Continued propagation of faults generates three sets of fault orientations: (a) parallel to the abyssal hills, (b) parallel to fracture zones, and (c) parallel to the trench. Faults with

control the early stage of brittle deformation with reactivation of pre-existing structures developing later.

### **2.3.2. Basement-cutting faults**

We interpreted 199 normal faults that cut the TIC within the area of the seismic data survey. Throws are based on the vertical offset of the interpreted TIC. In each seismic line, we calculate cumulative throw at the distance to the trench of each fault by summing the throws of all faults seaward of that point (Figure 2.4). However, the seismic lines' seaward-termination points are not constant, causing the region >30 km from the trench to be undersampled. Slopes of cumulative throw for each seismic line reveal deformation per distance. Linear regression of cumulative throw versus distance, using a maximum distance of 30 km from the trench to reduce sampling effects, indicates that there are small differences in cumulative throw between the south, central, and north regions. For seismic line groups (south to north) D02 to D06, TH03 to D13, and D15 to D19, the median absolute value of cumulative throw slope is 2.50°, 3.46°, and 3.66°, respectively. Maximum fault throw on a single fault is >500 m but more than half of the faults have throws of <100 m with the average offset being approximately 120 m. Of the 199 faults interpreted, 105 of them dip landward, whereas 94 faults dip seaward. The median number of faults increases towards the trench (Figure 2.4) with variations from line to line. There is a minor drop in the number of faults at a distance of 30 to 40 km from the trench. This is the result of the termination of multiple seismic lines near 30 km to the trench, which leads to low fault counts for that distance bin. Fault spacing averages approximately 2 km with a minimum and maximum spacing of 200 m to 10 km. Analysis of fault throw within our survey region from available seismic (Tsuru et al. 2000) and bathymetry data (Iwabuchi 2012; 2013) is prone to two types of error: variation in sediment thickness in the region complicates the bathymetry-based

analysis and limited number of previous seismic lines in this area is insufficient to provide complete regional coverage.

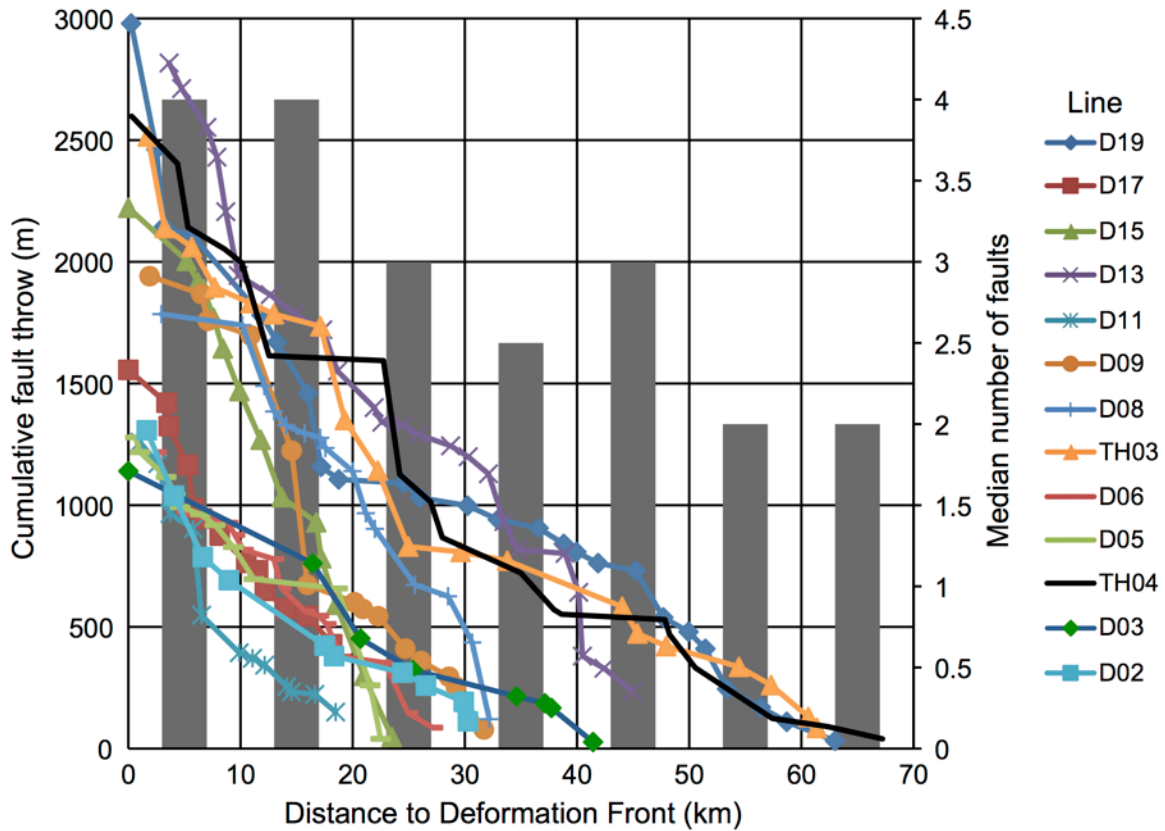


**Figure 2.4.** Throw analysis of basement-cutting normal faults. Left vertical axis is cumulative fault throw of basement-cutting normal faults that cut the TIC for each regional seismic line. Notice that the change in slopes varies from line to line with a slight slope change south to north. The histogram, gray bar graph, shows the median number of faults for each 10 km bin east of the trench (right vertical axis). A general increase in the number of faults towards the trench indicates that new faults form close to the deformation front.

### 2.3.3. Incoming Pacific Plate sediments

The Japan Trench margin has long been known for its relatively thin incoming sediment column of approximately 400 m from both seismic and DSDP drill cruises (e.g., Ludwig et al.

1966; Shipboard Scientific Party 1980). Our data provide new insight into regional variation in sediment thickness and internal deformation within the sediments.

### **2.3.3.1. Sediment thickness**

We evaluated sediment thickness along a series of profiles, based on interpretations of the seafloor and TIC, using both regional and high-resolution lines to plot the stratigraphic thickness of the sediment column (Figure 2.1B). Thinning of the sediment section is expected above the fault surface at footwalls of normal faults (Groshong 2006) and should not be interpreted as stratigraphic thickness. We find a range of sediment thickness of 0 to 600 m along the incoming Pacific Plate. Thinning in the southeast is largely found near potential ‘petite spot’ volcanoes (Figure 2.1A; Site C of Hirano et al. 2008) and is likely related to the formation of these small cones, or to erosion around them. Elsewhere, thickness is generally related to initial deposition or reworking of the sediment. Sediment thickness varies from line to line but generally increases towards the trench.

Evidence for variation in sediment thickness and near-trench sediment deposition is found throughout the survey region. As an example, Line D02 in the southern part of the survey area (Figure 2.5B) illustrates the sedimentary section surrounding the trench axis. The base of the sediment column is marked as the blue dashed line, which has an apparent dip to the west. An unconformity at the top of the sediment section is discernible near the trench axis, with a near horizontal dip, and is marked with a green dashed line. This pair of markers implies that the original sediment column was tilted landward during bending of the subducting plate, followed by deposition of horizontal sediments in the trench. High-resolution line HD21A also images recent sediments that onlap older, landward-tilted strata in a developing graben adjacent to a normal fault, seaward of the trench (Figure 2.5C). Slight rotation of the lower horizons (in the

blue region) indicates syndepositional faulting. Little faulting has occurred after this initial rotation, however, as the upper horizons are near horizontal. Seafloor displacement from this fault is small, indicating that either recent sedimentation has obscured any surface offsets or the fault currently is inactive.

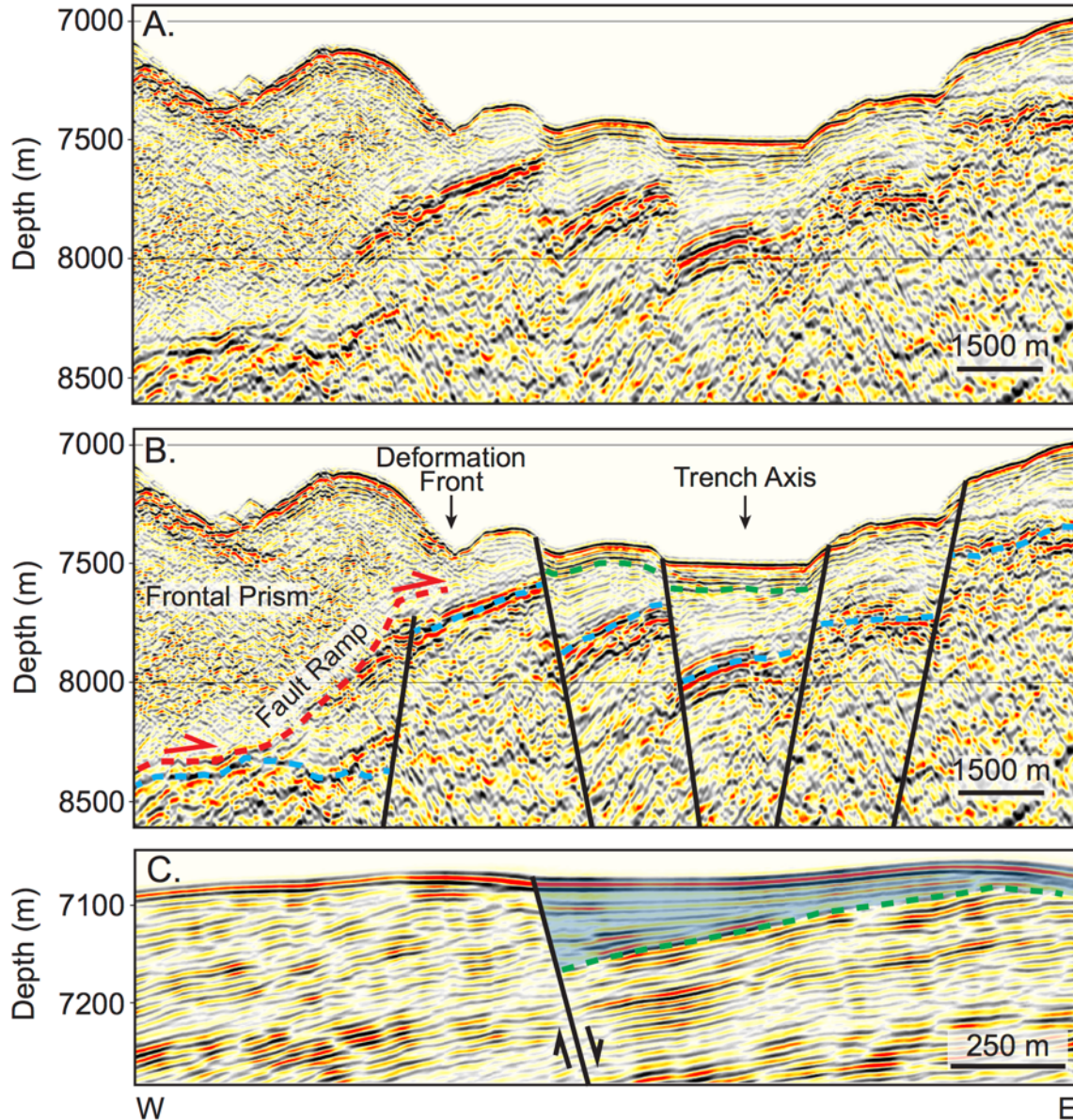


**Figure 2.5.** A subducting horst and trench sediments. (A) Line D02, located near the southern end of the survey (Figure 2.1). (B) Interpretation of line D02. Blue dashed line is the top of oceanic crust. Red dashed line is décollement. The green dashed line is an unconformity (note

angular relations below), implying recent sediment deposition of horizontal reflections. Variable thickness of sediments is also apparent on the seaward horst compared to the graben at the trench axis. Note also the distance between the deformation front and trench axis. The trench axis does not directly correlate with the deformation front location. **(C)** Section of high-resolution line HD21A (yellow section in Figure 2.1). A near-trench sediment deposit, likely a turbidite, found at a basement-cutting normal fault (black). The younger sediment (blue region) onlaps against an unconformity (green dashed line).

### **2.3.3.2. Near-trench, sediment-restricted faults**

Faulting and fracturing of the sediment column occurs along the outer rise. Dives with submersible *Shinkai 6500* in the 1990s were the first to observe open cracks striking parallel to the horst and graben system at the outer rise of the Japan Trench (Ogawa et al. 1997). Our high-resolution seismic lines image similar structures. Lines HD26B and HD27B (500 m north of HD26B) show an incoming horst approximately 1 km seaward of the trench axis (Figure 2.6). Lithologic units were correlated from DSDP Site 436 (Shipboard Scientific Party 1980). Faults within the sediment column (units 1 and 2) exhibit offsets of approximately 20 m or less and are densely spaced, with populations of approximately 20 faults occurring within an approximately 2-km-long interval on Figure 2.6. These faults do not appear to offset the top of the chert layer (unit 3). Unit 3 reflections are deformed internally, but the upper boundary of the unit is not disrupted. The fault pattern in unit 1 shows poor vertical fault connectivity. Faults do not appear to be confined to a specific sedimentary layer within unit 1. Increased sediment deformation around a nearby basement-cutting fault is common. There is no evidence for growth faulting along these sediment-restricted faults, indicating that the fault system is young. Landward (westward), towards a bounding basement-cutting fault, unit 1 reflections become discontinuous, indicating that the region is heavily deformed. Unit 1 thins in this discontinuous region, potentially from slumping of material into the graben to the west.

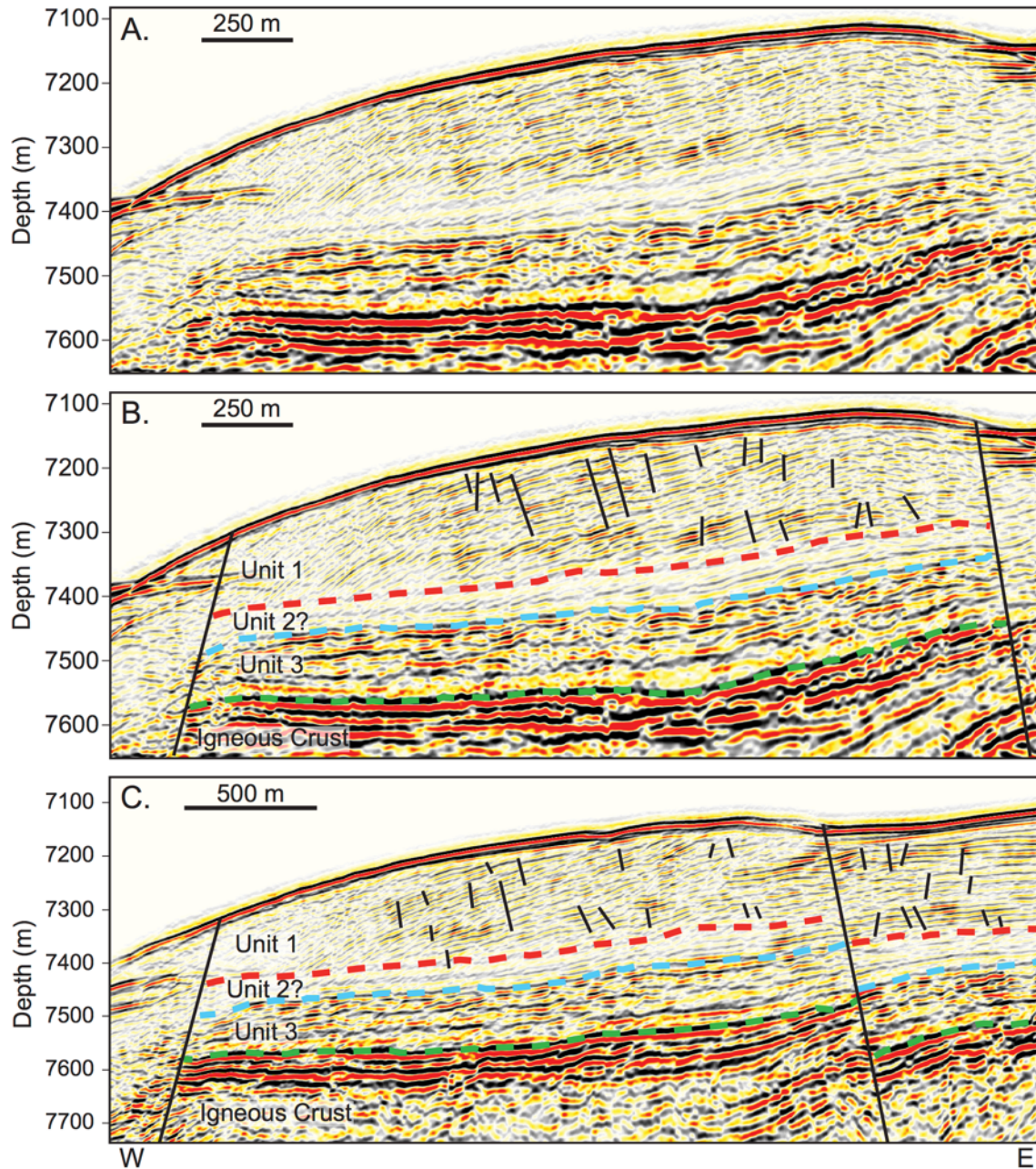


**Figure 2.6.** Small-scale faults within the sediment section. **(A)** A section of high-resolution line HD26B (yellow in Figure 2.1). **(B)** Interpretation of line HD26B with lithologies based on Site 436 of DSDP Leg 56, located further north on the Pacific Plate. Unit 1: vitric diatomaceous silty clay/ clay stone, unit 2: radiolarian diatomaceous clay stone/pelagic clay, unit 3: chert (Shipboard Scientific Party 1980). Note the pelagic clay layer is approximately 1-m-thick in the drill core, above the chert layer and within unit 2. Faults within the mudstones have small offsets, less than 20 m, and do not cut the chert layer or offset the seafloor. **(C)** Interpretation of a

section line HD27B, approximately 500 m north of HD26B, with lithologies based on Site 436 of DSDP Leg 56 (Shipboard Scientific Party 1980). This line also shows sediment-restricted faults.

### 2.3.4. The deformation front along the Japan Trench

Our seismic lines reveal the subduction of horst and graben systems and their interactions with the landward trench slope. We define the deformation front as the seafloor trace where either chaotic reflections of the landward slope or the frontal thrust contact coherent, continuous reflections of the incoming plate (Figures 2.5 and 2.7). We used the bathymetry grid to interpolate the deformation front between seismic lines, correlating similar topographic features identified on the seismic lines. The deformation front is better defined on the high-resolution lines, which also reveal an imbricate thrust structure in the trench (Figure 2.7). In many areas, the regional lines display only chaotic reflections around the imbricate thrusts due to their lower resolution.

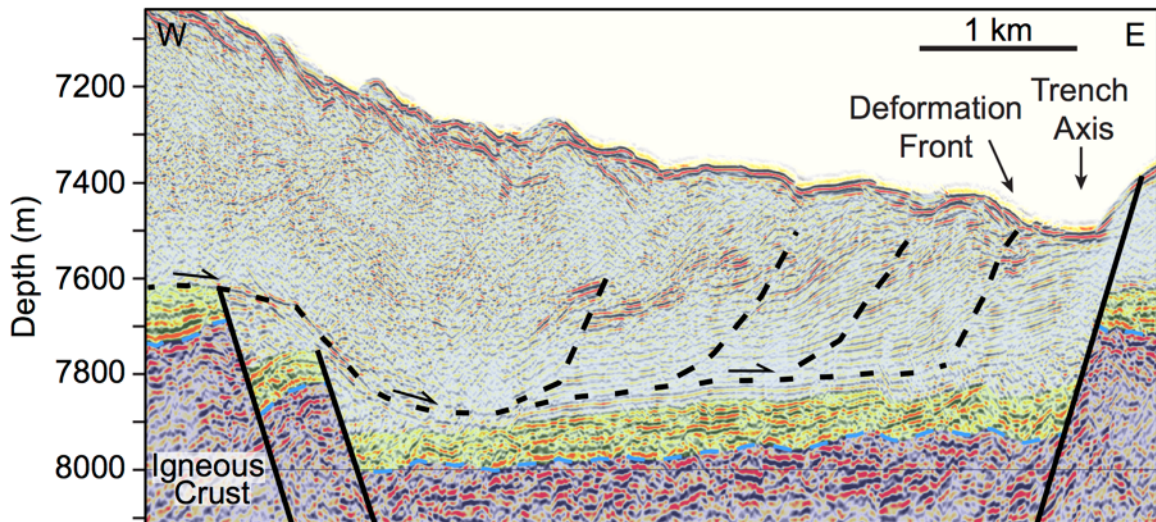


**Figure 2.7.** Trench graben with deformed sedimentary section. Section of high-resolution seismic line HD34B (Figure 2.1). The interpretation is based on the major features of Nakamura et al. (2013). Black dashed lines are thrust faults that sole into the décollement. The décollement is located above the chert boundary and within the sediment column in the graben. Light blue is the sediment column, units 1 and 2. Green region is unit 3. Dark blue region and dashed line marks the top portion of the igneous crust. Black solid lines are normal faults that offset the igneous crust.

Where a horst block is subducted beneath the base of the landward trench slope, the décollement is localized near the top of the chert layer at the top of the horst (Figure 2.7). At the seaward edge of the horst block, a low-angle, seaward-dipping reflection shows that the décollement drops down into the adjacent graben, where it localizes within the sediment column, approximately 10 to 20 m above the chert layer.

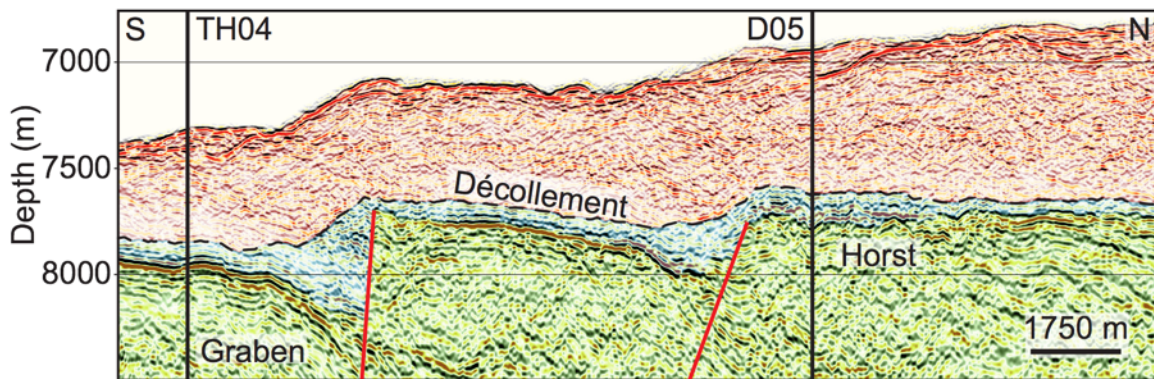


**Figure 2.8.** Subducted structures parallel to the trench. The southern portion of seismic strike line S13 (Figure 2.1). Red region shows chaotic reflectors and accreted sediments. Blue region contains more continuous reflectors and appears less deformed. The boundary between red and blue is the décollement (black dashed line). Green region is the upper part of the igneous crust offset by basement-cutting normal faults (red lines). Solid black lines show intersections of seismic dip lines (Figure 2.1).

North-south profiles aid in lateral interpretation between horst-graben systems. The high-resolution lines are concentrated over a single trench-graben system. However, strike line S13 images the adjacent section to the north showing both a subducted horst and graben system beneath the landward trench slope (Figure 2.8). We interpret the décollement as the surface between the continuous (blue) horizons beneath and the deformed (red) horizons above the plane. Across the main part of a horst or graben, approximately 100 m of sediments (blue region) are subducted with minimal variations along the profile, but adjacent to the bounding normal

faults, a large amount of sediment that has slumped from the adjacent horst block is being subducted. Furthermore, the seafloor appears to follow the morphology of the TIC indicating that seafloor topography is controlled by the underlying horst-graben morphology. To investigate effects of the subducting plate on the deformation front, we plot the location of the deformation front and the underlying structures (Figure 2.9). The continuous bathymetric expression of the horst blocks allows us to confidently interpolate our seismic interpretations between the seismic lines. An oblique horst is currently at the deformation front in the southern region, at lines D02 and D03 (Figure 2.9). The distance from the trench axis to the deformation front is to a maximum of approximately 4 km. At Line TH04 (Figure 2.9), a graben is being subducted under the deformation front (Figure 2.8). Here, the deformation front is located further seaward and near the trench axis. Bathymetric highs within the graben reflect the vertical growth of anticlines from the imbricate thrust faults (Figure 2.7). From line TH04 to D11, the deformation front is located within a graben (Figure 2.9). However, there is a topographic low at the deformation front at line TH03. This change in topography indicates lateral variation in the vertical growth of the thrust system within a graben, which may be related to previously subducted structures. At line D13 to D15, the deformation front is located above a horst and further west than at line D11. The deformation front at line D17 is above a half-graben (Figure 2.5). At the northern end of the survey, line D19, the deformation front is on the landward edge of a horst (Figure 2.9). We generally find that subduction of a horst temporarily impedes seaward propagation of the deformation front.

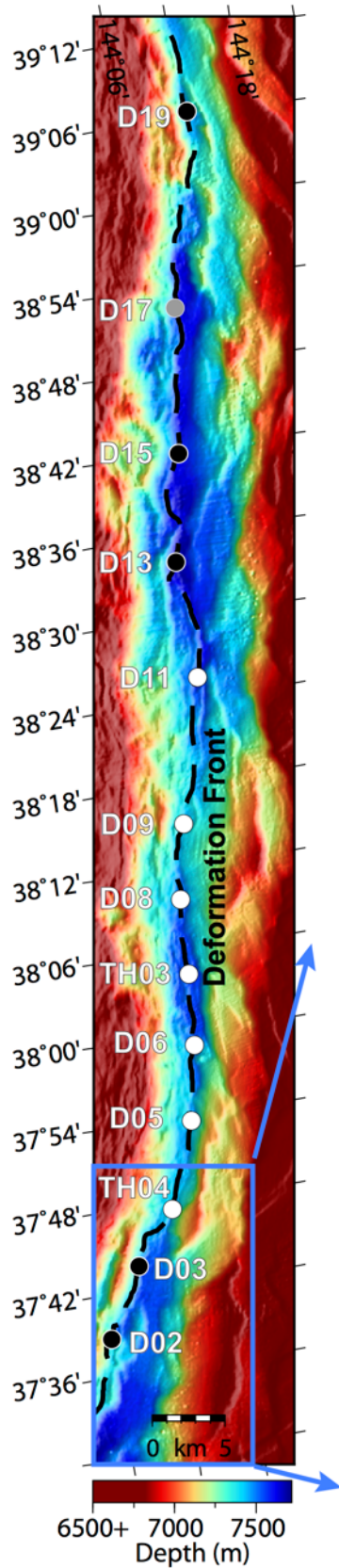
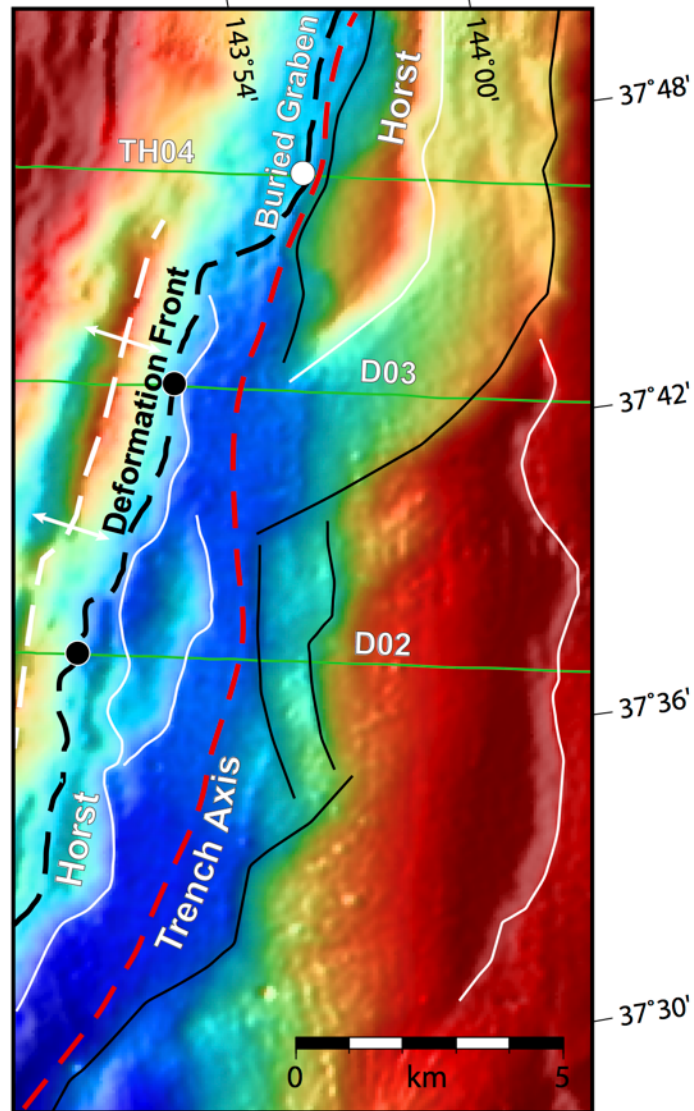


**Figure 2.9.** Trench axis bathymetry. The dashed black line marks the deformation front based on seismic and bathymetric interpretations. White and black circles mark the deformation front located above a graben or horst, respectively, whereas a gray dot marks a half-graben. Seismic line numbers (e.g., D02, D03) are plotted near respective circles. Blue box marks location of inlet to the right. White and black solid lines are normal faults dipping seaward and landward, respectively. The trench axis is marked by a red dashed line. The green lines are the location of the seismic lines. The white dashed line is an anticline. The deformation front is not merely following topographic lows but may be reacting to the incoming structures.



## **2.4. Discussion**

### **2.4.1. Fault development**

Earthquakes and bathymetric trends demonstrate that bending-related faults form at a maximum of approximately 120 km east of the Japan Trench axis (Obana et al. 2012; Nakanishi 2011). A simple subduction calculation with the Pacific Plate subducting at a rate of approximately 8 to 10 cm/year (DeMets et al. 2010; Apel et al. 2006; Argus et al. 2011; Niitsuma 2004) nearly orthogonally under Honshu, predicts the oldest normal faults about to be subducted to be approximately 1.2 to 1.5 Ma. Assuming steady slip on the normal faults, maximum throws of 500 m divided by the age of the oldest faults gives a maximum throw rate of 333 to 417 m/Ma. Faults with smaller offsets must be much younger or less active. The increase in the density of the faults westward, towards the trench, indicates that new faults continue to form as the plate nears the trench, which indicates that the assumption of steady-state deformation is incorrect. This overall pattern is similar to normal fault development in other trenches, such as the Middle America Trench (Ranero et al. 2003). Furthermore, average fault spacing of 2 km is on the same order as predicted in some modeling studies (Faccenda et al. 2009), although other models generate larger fault spacing of up to 10 km (Naliboff et al. 2013), which is the maximum fault spacing we observe. The increase in the number of faults towards the trench and the range of fault spacing suggests continuous formation of new faults occurs as the Pacific Plate approaches the trench rather than apportioning strain to only major, more widely spaced faults.

The fault traces in our survey area is similar to patterns developed in other locations and in analog models. Onshore three-dimensional (3D) normal fault propagation through basalt shows linkage of surface fractures that produce a fault with an irregular trace (Kaven and Martel 2007). Similar zig-zag fault traces have been generated in analog fault experiments where

different stress directions were applied to the sediments (e.g., Henza et al. 2011). The 3D stress field of the Japan Trench outer rise is poorly known. A bend in the Japan Trench trend at 38° N will create 3D effects not accounted for in 2D models. Furthermore, coseismic rupture of thrust segments south and north of 38° N will create a heterogeneous stress field on the outer rise. This is the only region along the Japan Trench where topographic structures on the subducting plate lie collinear with the fracture zone strike (Nakanishi 2011). At approximately 30° from the trend of the northern part of the trench (Figure 2.1), the fracture zone trend is slightly more than the approximately 25° reactivation cutoff determined by Billen et al. (2007). However, that study considered only reactivation of abyssal hill trends, but this may still imply that fracture zones are still weak with a lower coefficient of friction than the surrounding rock. Following initial surface breaks parallel to the trench, large fault-tip stress concentrations may help reactivate the pre-existing fabrics to develop the fault trace geometry found in the survey area (Figure 2.1).

Branches, relays, and conjugate faults are found in many normal fault populations (Peacock 2002; Morley et al. 2007; Nicol et al. 1995; Walsh et al. 1999). The presence of such features in our study area indicates poor lateral fault connectivity. Regional north to south differences in cumulative throw (Figure 2.4) may be related to such lateral effects. Fault interactions, especially in areas with closely spaced faults, may also contribute to variations in slip distributions along a single fault (Martel and Shacat 2006). Therefore, our throw analysis should be viewed cautiously due to effects of nearby faults and location of our MCS lines within individual fault segments.

#### **2.4.2. Incoming plate sediment thickness**

Sediment thickness and lithology of the incoming plate plays a dominant role in development and growth of accretionary prisms. Accurate understanding of the geometry of the

TIC and overlying sediments is vital to measuring sediment influx and fault throw. Although basement-cutting faults offset the TIC, the TIC is not always a continuous, strong reflector in between basement-cutting faults within the study area, as seen on the eastern section of line D02 (Figure 2.5A). This discontinuous nature of the TIC in our seismic lines is due to several factors:

- 1) seismic imaging through complex geology scatters ray paths, resulting in an inadequately imaged subsurface. In our study area, this is largely caused by to the rough seafloor and the chert layer overlying the TIC. The high-resolution survey data likely show greater scattering (due to the higher frequency content), as the regional lines image the TIC more consistently.
- 2) The velocity of the overlying chert creates little impedance contrast with the TIC. Although no formation velocity for DSDP Site 436 was measured for the chert unit, velocities of porcellanite and chert samples generally range from 2.6 to 4.8 km/s (Shipboard Scientific Party 1980), which may be near the velocity of the TIC.
- 3) Drilling at Site 436 did not reach the igneous basement, leaving the composition and alteration of the basement unknown near our survey location. Mineralogic analysis of oceanic basalts elsewhere reveals significant alteration with a large potential for fluid incorporation (Kameda et al. 2011), which may lower the acoustic impedance across the TIC.
- 4) The igneous basement may differ compositionally throughout the survey area. The seismic character of a sill or sheet flow may produce a smoother and stronger reflector than pillows and flows (Abrams et al. 1993), creating variations in reflector strength for the TIC.
- 5) Continued faulting along the outer rise will further reduce continuous reflections from the TIC. This can be from development of a new fault breach through the TIC, secondary faulting, or off-fault, nonelastic deformation, including fissure and cavity formation, as the fault tip propagates towards the surface (Holland et al. 2006; Martel and Langley 2006). Even with sections of discontinuous TIC, we are confident in our interpretation because we observe relative amplitude

and frequency differences between the sediment and underlying basalt along with regions of a prominent TIC horizon.

Our results reveal variations of as much as 600 m in thickness of the sediments overlying the TIC (Figure 2.1B). Correlation of sediment thickness between regional lines was not possible because the seismic line spacing is too wide and there are complications imposed by variation in fault strikes. Basement topography is a dominant factor in variation of sediment thickness in two ways. 1) Older structures contribute to sediment variations. For example, the abyssal hill imaged in line D19 (Figure 2.2) has thinner sediments above it than on its flanks (Figures 2.1 and 2.2). Interpreted petite spot volcanic fields found in the southeast of the survey (Figure 2.1) have little to no sediment cover owing to their likely young age, based on ages of nearby fields (Hirano et al. 2008). Similarly, sediment overlying the tops of seamounts is generally much thinner than on the seamounts' flanks. 2) Basement-cutting normal faults influence sediment thickness. This may be caused by erosion of topographic highs by bottom currents or by mass wasting (Figure 2.6) and filling of topographic lows, such as along graben systems (Figure 2.5). Sediment thickness generally increases towards the trench but with fluctuations as large as approximately 400 m on individual lines. No regional trends in sediment thickness are found in other directions. However, the large grid spacing between regional lines will mask small-scale trends. Because the Japan Trench accretes a large portion of sediment at the toe (Figure 2.7; Kodaira et al. 2012; Nakamura et al. 2013), sediment variations of 600 m may still affect prism morphology because they are a large percentage of the total sediment thickness. However, due to the fluctuations in sediment thickness and lack of regional trends, prism morphology and growth in our survey area owing to the incoming sediments is difficult to constrain.

### **2.4.3. Décollement propagation**

Seismic sections of a near-trench subducting graben (Figure 2.7; Kodaira et al. 2012; Nakamura et al. 2013) reveal a low-angle, seaward-dipping reflector descending into the graben from the adjacent horst block. Imbricate structures sole into the same plane, which is thus interpreted to be the décollement. The mechanism for this décollement step-down into a local trench graben is poorly understood. Although landslides are a potential mechanism for creating the step-down (Strasser et al. 2013), we propose additional mechanisms for the step-down that involves the subduction and burial of an active normal fault (Figure 2.10). Surface breaching normal faults, like the majority of incoming faults, have a very different stress field than that of buried faults. Large horizontal and vertical tensile stresses occur at the fault tip and footwall of buried faults (Martel and Langley 2006). As the décollement propagates over a breached normal fault, it buries this fault under the prism. We propose the following situations may occur as a result:

- 1) As a graben passes beneath the near-trench edge of the overriding plate, the tensile stress from the buried normal fault may increase. The stress field of a fault tip breaching the seafloor versus being buried differs drastically (e.g., Martel and Langley 2006). This increase in tensile stress may promote the décollement to step-down into the graben.

- 2) Subduction of horst-graben structures may be similar to seamount subduction. Coulomb wedge mechanics argues that the change in basement slopes due to subducting a seamount promote both overcritical and undercritical wedge deformation (Lallemand and Le Pichon 1987). For an incoming horst block, the increase in basement slope could promote undercritical wedge deformation and affected by shortening. For an incoming graben, the decrease in the basement slope could promote overcritical deformation within the prism, creating listric faulting or slumps into the graben. There are three morphologic differences between

subducting seamounts and normal faults: their vertical scales, slopes, and associated sediment. Seamounts studied near active margins tend to be greater than 16-km-wide and more than 1.5 km above the seafloor with slopes less than  $20^\circ$  (Dominguez et al. 1998). They also have significantly less sediment cover than their surroundings. However, horst-graben structures entering the Japan Trench are much smaller, lower-relief features (average throw of approximately 122 m and fault spacing of approximately 2 km), have steeper flanks (approximately  $50^\circ$  to  $80^\circ$  fault dips) and have smaller variations in sediment thickness. The large broad change in both sediment type and thickness, may play an important role for seamount subduction as a mechanically distinctive zone, but the horst-graben lithology varies little. These differences may create a different upper plate deformation for a horst-graben than a seamount.

3) Normal faults restricted to sedimentary units 1 and 2 (Figure 2.6) may become more active, with increasing offsets, as the plate moves closer to the trench. By breaking through the layered sediments, these sediment-restricted faults could act as a pathway for the décollement step-down from the top of the horst blocks into the adjacent graben.

4) As the décollement propagates seaward, either on top of the graben or within the graben sediments, the buried active basement-cutting normal fault will continue propagating upward, and the décollement will eventually be offset by the basement-cutting fault. These two intersecting faults may continue to offset the fault plane of the other if they remain active. The effects of active normal faults further landward, beneath the prism, are less easily resolved. However, such basement-cutting faults may continue to influence the décollement geometry, as OBS data reveal, they remain active under the prism (Obana et al. 2013).

Horst block subduction also affects the up-dip geometry of the décollement (Kimura et al. 2012) and potentially lateral décollement connectivity. Our regional lines image subducted horsts

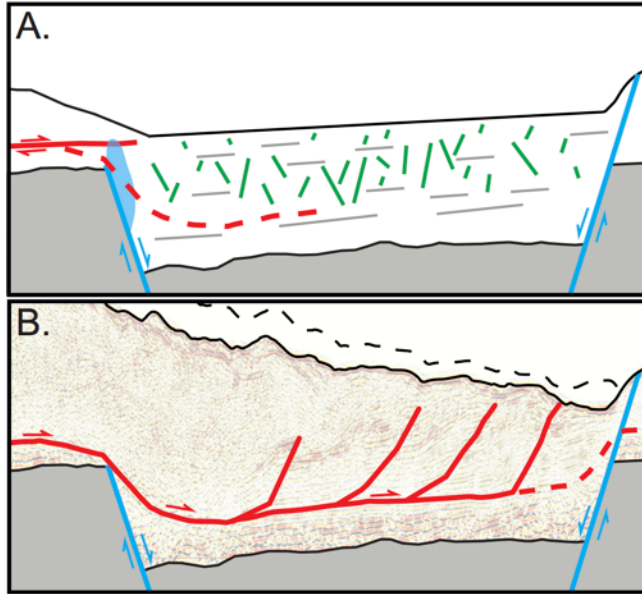


**Figure 2.10.** A schematic model for near-trench décollement propagation. Model uses seismic line HD34B (Figure 2.7) with the western basement-cutting normal faults simplified to just one. **(A)** Early stages of the décollement step-down into a trench graben. This model is based on two fault tips and their associated tensional stress fields, both of which are found in the trench graben (décollement in red, normal faults in blue, sedimentary faults in green). Blue region is the area of vertical tension based on a 100-m buried normal fault (modified from Martel and Langley, 2006). Red dashed line is the future path of the décollement into the trench graben. **(B)** The future décollement step-up out of the graben. The red solid line is the current location of the décollement (Figure 2.7) with the red dashed section being a potential future pathway. The future ramp-up may develop from a frontal thrust. The seafloor will likely steepen (black dashed line) as the wedge advances seaward.

near the trench and show that the décollement ascends over the subducting horst along a fault ramp (Figure 2.5B). A seafloor bathymetric high above the ramp is an anticline caused by sediments being folded over the fault bend (Figure 2.9). Fault slip over this 20° dipping décollement fault ramp will create greater seafloor uplift than in sections of shallow dips. Furthermore, the sediment column overlying the décollement ramp shows no continuous reflections, thus indicates internal deformation (Figure 2.5). In the high-resolution lines, the décollement stops within a graben near the incoming horst block (Figure 2.7). Seafloor topography within this graben deepens to the south. This morphology change can be attributed to varying internal deformation and uplift along strike, in that the décollement propagates seaward to a horst where the prism

topography steepens before creating a ramp over the horst. If décollement propagation does vary in horst-graben systems, subduction of intersecting or linked normal fault sections would create lateral décollement segments that are linked at depth.

Faults within the sediment column may play an additional role in décollement propagation. DSDP Site 436 (Figure 2.1C) is the only nearby site where sediments on the Japan Trench's outer rise have been sampled; drilling there only penetrated to the chert layer (Shipboard Scientific Party 1980). At Site 436, a small layer of pelagic clay overlies the chert. In this deep water setting, the overall lithology is not expected to vary much laterally, allowing for a general correlation among our seismic lines. Ogawa et al. (1997) discovered cracks in the seafloor along the outer rise and proposed that a combination of gravitational slope instability and earthquake shaking for the cracks formation. These surface cracks may be from the early stages of sediment-restricted normal faulting at depth, imaged in the high-resolution survey (Figure 2.6). These sediment-restricted faults may have a basal sliding plane between the basement-chert, chert-clay boundaries, and/or within the upper unit, deforming the sediment along strata. The creation of these sliding surfaces before subduction may play a role during seismic rupture to the trench. The Japan Trench Fast Drilling Project (Integrated Ocean Drilling Program Expedition 343 and 343 T) drilled to the chert layer further landward (Figure 2.1) and found that the décollement is located within a thin band of pelagic clay (Chester et al. 2012), with localized deformation occurring within 5 m of this pelagic clay. Thus, this lithological unit may be a regional control on rupture to the trench (Chester et al. 2013), as the low coseismic shear stress and low coseismic friction of the clay may have allowed the 2011 Tohoku earthquake to rupture to the trench (Fulton et al. 2013; Ujiie et al. 2013). However, Expedition 343 drilled only above a horst block. Seismic results agree with the décollement's location above the horst. However, within the graben, the décollement located higher in the sediment column (Figure 2.7). The pelagic clay within a graben may have a more dominant role in sediment sliding and sediment-restricted faulting (Figure 2.6) than for décollement propagation. Near-

trench faults in sediment may play an important role in weakening the sediment before subduction.

The accretionary prism at the toe of the Japan Trench initially accumulates a major proportion of incoming sediment. Previous models indicated that all of the sediments within a graben were subducted, as the décollement propagated over the top of the entire graben sediment column (e.g., Hilde 1983). This would allow for significant sediment subduction. However, the décollement appears to initially scoop out the majority of sediments within a graben (Figure 2.7). Furthermore, both seismic and drilling (e.g., Chester et al. 2013) indicate that the décollement is near the base of the sediment column when located above a horst. These results reduce the amount of sediment available for subduction under the toe of the frontal prism. Variations in both the incoming sediment column thickness (Figure 2.1) and the amount of long-term sediment accretion cause potential difficulties in calculating the amount of sediment subducted (e.g., Clift and Vannucchi 2004). Additionally, instead of underthrust sediment-filled graben blocks being only vertically loaded, initial sediment accretion may affect overall sediment porosity due to the addition of both vertical and horizontal strains on the subducting sediment (e.g., Moore et al. 2011). This may affect the sediment dehydration further landward and, as a result, whether or not subduction erosion might occur at depth. Other water-rich sources may contribute more to the fluid budget including both the igneous basement and chert, where the dehydration range for siliceous sediments starts at approximately 40 km landward of the Japan Trench (Kimura et al. 2012). Sediment cracks and faults along with basement faults may provide necessary pathways for fluid transport and may play a vital role in hydration below the sediment column. These near-trench processes may influence different subduction processes occurring at depth at the Japan Trench subduction zone.

## 2.5. Conclusions

Although generally included in discussion of subducting topography (e.g., Bilek 2007), bending-related normal faults are typically not considered to directly deform the overriding plate at the toe of the landward trench slope. Our depth-migrated regional and high-resolution seismic lines that image the incoming Pacific Plate along the Japan Trench off Tohoku show trench-parallel faults that offset the igneous crust on the outer-rise seaward of the trench. As the plate moves landward, reactivation of pre-existing seafloor structures, due to either increasing bending stresses or interaction with trench-parallel faults, further deforms the plate. Throw analysis indicates more offset in the north than south of our survey area with continuing formation of faults towards the trench. Sediment thickness of the Pacific Plate is not uniform but fluctuates between 0 and 600 m with a general increase in thickness towards the trench. Recent sediment deposits are present in some normal fault footwalls and near-trench topographic lows. Furthermore, the sediment column contains densely spaced fault populations with only a few meters of offset. We expand on previous studies (e.g., Kodaira et al. 2012; Nakamura et al. 2013) to document up-dip décollement propagation over both horst and graben systems along the Japan Trench and found the deformation front located further landward during initial subduction of a horst block compared to graben subduction. We propose a relationship between the décollement seaward propagation and normal faults that reflect stresses and displacements at the tips of actively subducting active normal faults. Other margins where horst blocks are subducting, such as the Middle America Trench off Costa Rica (Moore et al. 1986; Moore and Shipley 1988) should also be considered for anomalous seafloor displacement during coseismic rupture to the trench axis. Furthermore, our results have additional implications for the hydration of the plate and upper mantle (Ranero et al. 2003; Garth and Rietbrock 2014) from both large- and small-

scale faulting, prism development (Underwood 2007; Ike et al. 2008), and coseismic near-trench anomalous vertical displacement (e.g., Kodaira et al. 2012). Thus, bending-related normal faults may play an integral role in near-trench subduction zone processes.

### **Acknowledgements**

Funding for this project was through the National Science Foundation (grant numbers OCE-1260718 and OCE-1138051). The authors are grateful to S. Martel, P. Fryer, and C. Conrad for their piercing comments that greatly improved the manuscript. We thank Paradigm Geophysical and Landmark Graphics (Halliburton) for their academic software licenses. The authors would like to thank the scientists and crews of KR11-05 Leg 2, KR11-E03, KR11-E05, and KY11-E05.

### **References**

- Abrams LJ, Larson RL, Shipley TH, Lancelot Y (1993) Cretaceous volcanic sequences and Jurassic oceanic crust in the East Mariana and Pigafetta basins of the western Pacific. In: Pringle MS, Sager WW, Sliter WV, Stein S (eds) *The Mesozoic Pacific: geology, tectonics, and volcanism*, Geophys Monogr 77. AGU, Washington, D.C., pp 77–101
- Apel EV, Bürgmann R, Steblov G, Vasilenko N, King R, Prytkov A (2006) Independent active microplate tectonics of northeast Asia from GPS velocities and block modeling. *Geophys Res Lett* 33(11), L11303, doi:10.1029/2006gl026077
- Argus DF, Gordon RG, DeMets C (2011) Geologically current motion of 56 plates relative to the no-net-rotation reference frame. *Geochem Geophys Geosyst* 12(11), Q11001, doi:10.1029/2011gc003751
- Bilek SL (2007) Influence of subducting topography on earthquake rupture. In: Dixon T, Moore C (eds) *The seismogenic zone of subduction thrust faults*. Columbia University Press, New York, pp 123–146
- Billen M, Cowgill E, Buer E (2007) Determination of fault friction from reactivation of abyssal-hill faults in subduction zones. *Geology* 35(9):819–822, doi:10.1130/G23847a.1
- Bodine JH, Steckler MS, Watts AB (1981) Observations of flexure and the rheology of the oceanic lithosphere. *J Geophys Res* 86(Nb5):3695–3707, doi:10.1029/Jb086ib05p03695
- Chester FM, Mori JJ, Toczko S, Eguchi N, Expedition 343/343T Scientists (2012) Japan Trench Fast Drilling Project (JFAST). IODP Prel Rept 343/343T, doi:10.2204/iodp.pr.343343T

- Chester FM, Rowe C, Ujiie K, Kirkpatrick J, Regalla C, Remitti F, Moore JC, Toy V, Wolfson-Schwehr M, Bose S, Kameda J, Mori JJ, Brodsky EE, Eguchi N, Toczko S, Expedition 343 and 343 T Scientists (2013) Structure and composition of the plate-boundary slip zone for the 2011 Tohoku-Oki earthquake. *Science* 342(6163):1208–1211, doi:10.1126/science.1243719
- Christensen DH, Ruff LJ (1988) Seismic coupling and outer rise earthquakes. *J Geophys Res* 93(B11):13421–13444, doi:10.1029/JB093iB11p13421
- Clift P, Vannucchi P (2004) Controls on tectonic accretion versus erosion in subduction zones: implications for the origin and recycling of the continental crust. *Rev Geophys* 42(2), RG2001, doi:10.1029/2003rg000127
- Costa Pisani P, Reshef M, Moore GF (2005) Targeted 3-D prestack depth imaging at Legs 190–196 ODP drill sites (Nankai Trough, Japan). *Geophys Res Lett* 32(20), L20309, doi:10.1029/2005GL024191
- DeMets C, Gordon RG, Argus DF (2010) Geologically current plate motions. *Geophys J Int* 181(1):1–80, doi:10.1111/j.1365-246X.2009.04491.x
- Dominguez S, Lallemand SE, Malavieille J, von Huene R (1998) Upper plate deformation associated with seamount subduction. *Tectonophysics* 293(3):207–224
- Faccenda M, Gerya TV, Burlini L (2009) Deep slab hydration induced by bending-related variations in tectonic pressure. *Nat Geosci* 2(11):790–793, doi:10.1038/Ngeo656
- Fujii Y, Satake K, Sakai S, Shinohara M, Kanazawa T (2011) Tsunami source of the 2011 off the Pacific coast of Tohoku earthquake. *Earth Planets Space* 63(7):815–820, doi:10.5047/Eps.2011.06.010
- Fujiwara T, Kodaira S, No T, Kaiho Y, Takahashi N, Kaneda Y (2011) The 2011 Tohoku-Oki earthquake: displacement reaching the trench axis. *Science* 334(6060):1240, doi:10.1126/science.1211554
- Fulton PM, Brodsky EE, Kano Y, Mori J, Chester F, Ishikawa T, Harris RN, Lin W, Eguchi N, Toczko S, Expedition 343, 343 T, and KR13–08 Scientists (2013) Low coseismic friction on the Tohoku-Oki fault determined from temperature measurements. *Science* 342(6163):1214–1217, doi:10.1126/science.1243641
- Garth T, Rietbrock A (2014) Order of magnitude increase in subducted H<sub>2</sub>O due to hydrated normal faults within the Wadati-Benioff zone. *Geology* 42(3):207–210, doi:10.1130/g34730.1
- Grevemeyer I, Ranero CR, Flueh ER, Kläschen D, Bialas J (2007) Passive and active seismological study of bending-related faulting and mantle serpentinization at the Middle America Trench. *Earth Planet Sci Lett* 258(3–4):528–542, doi:10.1016/j.epsl.2007.04.013

- Groshong RH (2006) 3-D Structural geology: a practical guide to quantitative surface and subsurface map interpretation. Springer, New York
- Henza AA, Withjack MO, Schlische RW (2011) How do the properties of a pre-existing normal-fault population influence fault development during a subsequent phase of extension? *J Struct Geol* 33(9):1312–1324, doi:10.1016/j.jsg.2011.06.010
- Hilde TWC (1983) Sediment subduction versus accretion around the Pacific. *Tectonophysics* 99(2–4):381–397
- Hino R, Azuma R, Ito Y, Yamamoto Y, Suzuki K, Tsushima H, Suzuki S, Miyashita M, Tomori T, Arizono M, Tange G (2009) Insight into complex rupturing of the immature bending normal fault in the outer slope of the Japan Trench from aftershocks of the 2005 Sanriku earthquake (Mw =7.0) located by ocean bottom seismometry. *Geochem Geophys Geosys* 10(7):Q07O18, doi:10.1029/2009gc002415
- Hirano N, Koppers AAP, Takahashi A, Fujiwara T, Nakanishi M (2008) Seamounts, knolls and petit-spot monogenetic volcanoes on the subducting Pacific Plate. *Basin Res* 20(4):543–553, doi:10.1111/j.1365-2117.2008.00363.x
- Holland M, Urai JL, Martel S (2006) The internal structure of fault zones in basaltic sequences. *Earth Planet Sci Lett* 248:301–315
- Ide S, Baltay A, Beroza GC (2011) Shallow dynamic overshoot and energetic deep rupture in the 2011 Mw 9.0 Tohoku-Oki earthquake. *Science* 332(6036): 1426–1429, doi:10.1126/science.1207020
- Ike T, Moore GF, Kuramoto S, Park J-O, Kaneda Y, Taira A (2008) Variations in sediment thickness and type along the northern Philippine Sea Plate at the Nankai Trough. *Isl Arc* 17(3):342–357, doi:10.1111/j.1440-1738.2008.00624.x
- Ito Y, Tsuji T, Osada Y, Kido M, Inazu D, Hayashi Y, Tsushima H, Hino R, Fujimoto H (2011) Frontal wedge deformation near the source region of the 2011 Tohoku-Oki earthquake. *Geophys Res Lett* 38(7):L00G05, doi:10.1029/ 2011gl048355
- Iwabuchi Y (2012) Extension rates in the outer slope of Japan Trench derived from precise sea bottom topographies. *Zisin* 65:9–19, doi:10.4294/zisin.65.9
- Iwabuchi Y (2013) Developed tectonic relief and frequency of great earthquakes caused by normal faults in the outer slope of the Japan Trench. *Report of Hydrographic and Oceanographic Researches* 50:1–24
- Kameda J, Yamaguchi A, Saito S, Sakuma H, Kawamura K, Kimura G (2011) A new source of water in seismogenic subduction zones. *Geophys Res Lett* 38(22), L22306, doi:10.1029/2011gl048883
- Kanamori H (1971) Seismological evidence for a lithospheric normal faulting - the Sanriku earthquake of 1933. *Phys Earth Planet Inter* 4:289–300

- Kaven JO, Martel SJ (2007) Growth of surface-breaching normal faults as a three-dimensional fracturing process. *J Struct Geol* 29(9):1463–1476, doi:10.1016/J.Jsg.2007.05.007
- Kimura G, Hina S, Hamada Y, Kameda J, Tsuji T, Kinoshita M, Yamaguchi A (2012) Runaway slip to the trench due to rupture of highly pressurized megathrust beneath the middle trench slope: the tsunamigenesis of the 2011 Tohoku earthquake off the east coast of northern Japan. *Earth Planet Sci Lett* 339–340:32–45, doi:10.1016/j.epsl.2012.04.002
- Kodaira S, No T, Nakamura Y, Fujiwara T, Kaiho Y, Miura S, Takahashi N, Kaneda Y, Taira A (2012) Coseismic fault rupture at the trench axis during the 2011 Tohoku-Oki earthquake. *Nat Geosci* 5(9):646–650, doi:10.1038/Ngeo1547
- Lallemand S, Le Pichon X (1987) Coulomb wedge model applied to the subduction of seamounts in the Japan Trench. *Geology* 15(11):1065–1069, doi:10.1130/0091-7613(1987)15<1065:CWMATT>2.0.CO;2
- Lay T, Ammon CJ, Kanamori H, Kim MJ, Xue L (2011) Outer trench-slope faulting and the 2011 Mw 9.0 off the Pacific coast of Tohoku earthquake. *Earth Planets Space* 63(7):713–718, doi:10.5047/eps.2011.05.006
- Ludwig WJ, Ewing JI, Ewing M, Murauchi S, Den N, Asano S, Hotta H, Hayakawa M, Asanuma T, Ichikawa K (1966) Sediments and structure of the Japan Trench. *J Geophys Res* 71(8):2121–2137
- Martel SJ, Langley JS (2006) Propagation of normal faults to the surface in basalt, Koaie fault system, Hawaii. *J Struct Geol* 28(12):2123–2143, doi:10.1016/j.jsg.2005.12.004
- Martel SJ, Shacat C (2006) Mechanics and interpretations of fault slip. In: Abercrombie G, Di Toro G, Kanamori H, McGarr A (eds) *Radiated energy and the physics of earthquake faulting*, *Geophys Monogr* 170. AGU, Washington, D.C, pp 207–216
- Masson DG (1991) Fault patterns at outer trench walls. *Mar Geophys Res* 13:209–225 McCann WR, Sykes LR (1984) Subduction of aseismic ridges beneath the Caribbean plate: implications for the tectonics and seismic potential of the northeastern Caribbean. *J Geophys Res* 89:4493–4519
- Moore GF, Shipley TH (1988) Behavior of the decollement at the Toe of the Middle America Trench. *Geol Rundsch* 77:275–284
- Moore GF, Shipley TH, Lonsdale PF (1986) Subduction erosion versus sediment offscraping at the toe of the Middle America Trench off Guatemala. *Tectonics* 5:513–523
- Moore GF, Saffer D, Studer M, Costa Pisani P (2011) Structural restoration of thrusts at the toe of the Nankai Trough accretionary prism off Shikoku Island, Japan: implications for dewatering processes. *Geochem Geophys Geosyst* 12(5):Q0AD12, doi:10.1029/2010gc003453

- Morley CK, Gabdi S, Seusutthiya K (2007) Fault superimposition and linkage resulting from stress changes during rifting: examples from 3D seismic data, Phitsanulok Basin, Thailand. *J Struct Geol* 29(4):646–663, doi:10.1016/j.jsg.2006.11.005
- Nakamura Y, Kodaira S, Miura S, Regalla C, Takahashi N (2013) High-resolution seismic imaging in the Japan Trench axis area off Miyagi, northeastern Japan. *Geophys Res Lett* 40(9):1713–1718, doi:10.1002/grl.50364
- Nakanishi M (2011) Bending-related topographic structures of the subducting plate in the northwestern Pacific Ocean: accretionary prisms and convergent margin tectonics in the northwest Pacific basin. In: Ogawa Y, Anma R, Dilek Y (eds) *Modern Approaches in Solid Earth Sciences*, vol 8. Springer, Netherlands, pp 1–38
- Naliboff JB, Billen MI, Gerya T, Saunders J (2013) Dynamics of outer-rise faulting in oceanic-continental subduction systems. *Geochem Geophys Geosyst* 14(7):2310–2327, doi:10.1002/ggge.20155
- Nicol A, Walsh JJ, Watterson J, Bretan PG (1995) Three-dimensional geometry and growth of conjugate normal faults. *J Struct Geol* 17(6):847–862, doi:10.1016/0191-8141(94)00109-D
- Niitsuma N (2004) Japan Trench and tectonics of the Japanese Island Arcs. *Isl Arc* 13(1):306–317, doi:10.1111/J.1440-1738.2003.00427.X
- Obana K, Fujie G, Takahashi T, Yamamoto Y, Nakamura Y, Kodaira S, Takahashi N, Kaneda Y, Shinohara M (2012) Normal-faulting earthquakes beneath the outer slope of the Japan Trench after the 2011 Tohoku earthquake: implications for the stress regime in the incoming Pacific plate. *Geophys Res Lett* 39(7):L00G24, doi:10.1029/2011gl050399
- Obana K, Kodaira S, Shinohara M, Hino R, Uehira K, Shiobara H, Nakahigashi K, Yamada T, Sugioka H, Ito A, Nakamura Y, Miura S, No T, Takahashi N (2013) Aftershocks near the updip end of the 2011 Tohoku-Oki earthquake. *Earth Planet Sci Lett* 382:111–116, doi:10.1016/j.epsl.2013.09.007
- Obana K, Kodaira S, Nakamura Y, Sato T, Fujie G, Takahashi T, Yamamoto Y (2014) Aftershocks of the December 7, 2012 intraplate doublet near the Japan Trench axis. *Earth Planets Space* 66:24, doi:10.1186/1880-5981-66-24
- Ogawa Y, Kobayashi K, Hotta H, Fujioka K (1997) Tension cracks on the oceanward slopes of the northern Japan and Mariana Trenches. *Mar Geol* 141(1–4):111–123, doi:10.1016/S0025-3227(97)00059-5
- Peacock DCP (2002) Propagation, interaction and linkage in normal fault systems. *Earth-Sci Rev* 58(1–2):121–142, doi:10.1016/S0012-8252(01)00085-X
- Ranero CR, Morgan JP, McIntosh K, Reichert C (2003) Bending-related faulting and mantle serpentinization at the Middle America Trench. *Nature* 425(6956):367–373, doi:10.1038/Nature01961

- Sato T, Hiratsuka S, Mori J (2013) Coulomb stress change for the normal-fault aftershocks triggered near the Japan Trench by the 2011 Mw 9.0 Tohoku-Oki earthquake. *Earth Planets Space* 64(12):1239–1243, doi:10.5047/eps.2012.04.003
- Shipboard Scientific Party (1980) Site 436: Japan Trench outer rise, Leg 56. In: *Initial reports of the Deep Sea Drilling Project*, vol 56, 57, Pt. 1. U.S. Govt. Printing Office, Washington, pp 399–446, doi:10.2973/dsdp.proc.5657.107
- Strasser M, Kolling M, dos Santos FC, Fink HG, Fujiwara T, Henkel S, Ikehara K, Kanamatsu T, Kawamura K, Kodaira S, Romer M, Wefer G, R/V Sonne Cruise SO219A, JAMSTEC Cruise MR12–E01 Scientists (2013) A slump in the trench: tracking the impact of the 2011 Tohoku-Oki earthquake. *Geology* 41(8):935–938, doi:10.1130/G34477.1
- Taylor FW, Mann P, Bevis MG, Edwards RL, Cheng H, Cutler KB, Gray SC, Burr GS, Beck JW, Phillips DA, Cabioch G, Recy J (2005) Rapid forearc uplift and subsidence caused by impinging bathymetric features: examples from the New Hebrides and Solomon arcs. *Tectonics* 24(6), TC6005, doi:10.1029/2004tc001650
- Tsuru T, Park JO, Takahashi N, Kodaira S, Kido Y, Kaneda Y, Kono Y (2000) Tectonic features of the Japan Trench convergent margin off Sanriku, northeastern Japan, revealed by multichannel seismic reflection data. *J Geophys Res* 105(B7):16403–16413, doi:10.1029/2000jb900132
- Ujiie K, Tanaka H, Saito T, Tsutsumi A, Mori JJ, Kameda J, Brodsky EE, Chester FM, Eguchi N, Toczko S, Expedition 343 and 343 T Scientists (2013) Low coseismic shear stress on the Tohoku-Oki megathrust determined from laboratory experiments. *Science* 342(6163):1211–1214, doi:10.1126/science.1243485
- Underwood MB (2007) Sediment inputs to subduction zones: why lithostratigraphy and clay mineralogy matter. In: Dixon TH, Moore JC (eds) *The Seismogenic Zone of Subduction Thrust Faults*. Columbia University Press, New York, pp 42–85
- von Huene R, Culotta R (1989) Tectonic erosion at the front of the Japan Trench convergent margin. *Tectonophysics* 160(1):75–90
- von Huene R, Ranero CR, Vannucchi P (2004) Generic model of subduction erosion. *Geology* 32(10):913–916, doi:10.1130/g20563.1
- Walsh JJ, Watterson J, Bailey WR, Childs C (1999) Fault relays, bends and branch- lines. *J Struct Geol* 21(8):1019–1026
- Yilmaz O (2001) *Seismic data analysis: processing, inversion, and interpretation of seismic data*. SEG, Tulsa, OK

## Chapter 3

### The Outer to Inner Accretionary Prism Transition of the Nankai Trough, Southwest Japan

In preparation for publication as:

Boston, B., Moore, G. F., Jurado, M. J., Sone, H. The Outer to Inner Accretionary Prism Transition of the Nankai Trough, Southwest Japan.

*Abstract*— As an accretionary prism grows seaward, rocks of the outer prism transition to the inner prism and become buried and hidden under thick forearc basins. This project focuses on studying this transition at the Nankai Trough inner accretionary prism using deep scientific drilling and a three-dimensional (3D) seismic volume. We update the 3D seismic volume using well velocity data to better constrain interpretations of deeper horizons that are key to understanding the inner accretionary prism. 3D interpretation of these horizons reveals multiple folds with axial surfaces that strike near parallel to modern outer prism thrust faults, and we interpret that these folds formed as a result of thrust faulting. Reactivation of one inner prism thrust fault continued until at least ~0.44 Ma, after the modern forearc basin formed, indicating that the inner prism had continued deformation until that time. Structural reconstructions of folded seismic horizons validate our interpretation that slip on an old thrust yielded fault-related folds within the modern forearc basin. We find that ~580 m of slip from this steeply dipping deep thrust occurred between ~0.44-1.04 Ma. Logging-while-drilling analysis of the deep inner prism revealed intense deformation of a generally homogenous lithology characterized by bedding that dips steeply (60-90°) to the NW, intersected by faults and fractures, with a range of dips and densities. Our detailed seismic interpretation of the deep Kumano Basin provides new

insights into the poorly studied inner to outer prism transition and reveals that although inner prisms do partially preserve outer prism structures, they become heavily deformed during the dynamic transition from the outer prism.

### **3.1. Introduction**

In sediment-dominated subduction zones, kilometers-wide accretionary prisms form by off-scraping marine sediments from the down going plate. These outer accretionary prisms grow from large sediment input, underplating, and frontal accretion. In contrast, inner accretionary prism growth is not fully understood but they likely do not grow steadily. They tend to be located under shallow forearc basins and at strongly negative gravity anomalies where coseismic slip produces some of the world's largest earthquakes [*Wells et al.*, 2003; *Song and Simons*, 2003; *Fuller et al.*, 2006]. However, because thick forearc basin sediments often overlie them, inner accretionary prisms are poorly understood and lack *in situ* exploration in the marine setting, whereas most land studies have additional deformation resulting from the exhumation of the deep prism [e.g., *Hasebe and Tagami*, 2001].

The framework typically used to understand accretionary systems is Coulomb wedge theory. The outer accretionary prisms thicken and grow outward through in-sequence thrust faulting, in which thrust faulting scrapes packets of sediments from the incoming plate, forming a wedge [*Davis et al.*, 1983], and underplating, which takes place at the base of the prism where sediment from the subducting plate is scraped off and underplated beneath the prism [*Stockmal*, 1983; *von Huene and Scholl*, 1991; *Platt*, 1986; *Moore and Biju-Duval*, 1984]. Coulomb wedge theory associates the stability of the accretionary prism to a wedge of soil in front of a bulldozer where frictional and fluid dynamic properties along with the dip angle of the décollement and slope of the seafloor play a critical role in the stability and shape of the wedge [*Davis et al.*,

1983; *Dahlen, 1990; Suppe, 2007*]. This means that if the wedge is not at the critical taper angle it will become more stable by internal wedge deformation, most easily achieved by flattening or steepening of the topography [*Davis et al., 1983; Lallemand and Lepichon, 1987; Kukowski et al., 2010*]. If the prism grows too wide too rapidly, the surface slope decreases, which in turn decreases the wedge taper, and in order for this wedge to restore its equilibrium taper, thrusts may cut the wedge landward of the deformation front and not follow a in-sequence deformation style (out-of-sequence thrusts, OOSTs) to increase the surface slope and wedge taper. These OOSTs may also reactivate older in-sequence thrusts [*Morley, 1988*]. Coulomb wedge theory generally assumes a strong static backstop (a region within the forearc with a greater shear strength than the seaward region [*Byrne et al., 1993*]). However, a dynamic backstop consisting of older accreted sediments can develop further seaward [*Kopp and Kukowski, 2003*], with this new inner accretionary prism remaining stable throughout the earthquake cycle, in contrast to the outer accretionary prism that deforms during the cycle [*Wang and Hu, 2006*].

In addition to providing a mechanism for wedge thickening and defining the slope of the wedge, OOSTs can lead to the formation of an outer ridge, creating a backstop for sediment deposition on top of the older accretionary prism [*Park et al., 2002; Moore et al., 2007; Gulick et al., 2010*]. This shortening may be recorded by deformation patterns seen in the forearc basin by landward tilted sediments, demonstrating that the creation of OOST faults can influence the formation and growth of the basin [*Gulick et al., 2010; Moore et al., 2015*]. Because the inner prism remains stable throughout the earthquake cycle, this new setting provides a favorable environment for an overlying forearc basin to form and develop [*Wang and Hu, 2006*].

The growth and dynamics of the inner accretionary prism are less well understood than those of the juxtaposed outer prism. In contrast to the outer prism that grows seaward through

constant accretion of sediments from in-sequence-faulting, the inner prism grows through rapid addition of large sections of outer prism material as a result of the formation of OOSTs or megasplay faults [Park *et al.*, 2002; Moore *et al.*, 2007]. In between these OOST faulting events, the inner prism does not grow seaward. Whereas outer prisms commonly have high fluid flow along fault systems [Moore and Vrolijk, 1992], the role of inner prism faults in the hydrologic system of the margin is less well understood. The inner prism tectonic setting is clearly distinct from that of the outer prism but with a less clear role in regional subduction zone dynamics.

This paper focuses on the inner accretionary prism of the central Nankai Trough. This region has been the focus of multiple seismic cruises and Integrated Ocean Drilling Program (IODP) drill sites. IODP Expedition 338 and 348 drilled deep into the inner accretionary prism south of the Kii Peninsula [Strasser *et al.*, 2014; Tobin *et al.*, 2015a], providing direct measurements to anchor the seismic interpretations. In this paper, we update the 3D seismic depth volume, make new and updated interpretations from the seismic volume and logging data, and model fault-related folds. Our goal is to provide new structural constraints on this setting and identify the processes involved in the transition of the outer to inner prism.

### **3.2. Tectonic Setting**

Located south of central Honshu, Japan (Figure 3.1), the Nankai Trough is located where the Philippine Sea Plate (PSP) subducts beneath the Eurasian Plate at an estimated convergence rate of ~40-60 mm/yr [Seno *et al.*, 1993; DeMets *et al.*, 2010; Loveless and Meade, 2010]. Evidence of long-term accretion extends landward from the trench where Cretaceous and Tertiary accretionary prism units have formed sub-parallel to the trench axis with imbricated thrust slices analogous to the modern subduction zone there [Taira *et al.*, 1988]. This margin has one of the longest historical records (~1,300 years) of regularly recurring great earthquakes (M

>8) at approximately 100-200 year intervals [Ando, 1975], including the instrumentally recorded 1944 Tonankai and 1946 Nankaido earthquakes [Kanamori, 1972]. Both of these events involved slip on a splay fault [Baba et al., 2006; Baba et al., 2002] that likely played a role in tsunamigenesis [Wendt et al., 2009].

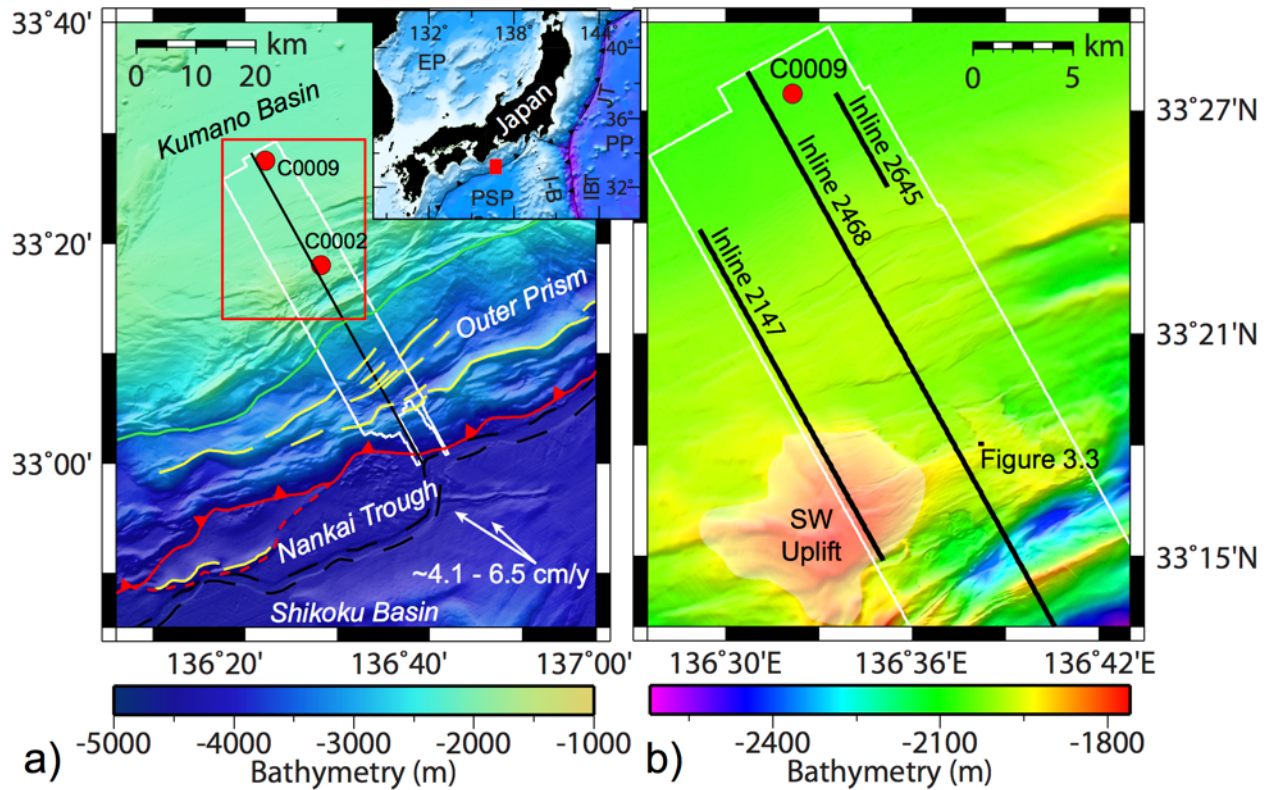


**Figure 3.1.** Bathymetric map of the Kumano section of the Nankai Trough. The map shows the locations of IODP drill sites (red dots), the outline of the 3D seismic volume (white box), and seismic inline (black line). **(a)** Tectonic interpretation of the Nankai region (modified from Moore et al. [2009]). Red solid and dashed lines are the frontal thrust fault and the new frontal thrust fault, respectively. Yellow lines mark the crests of anticlines or ridges. Green line is the out-of-sequence thrust fault. Black dashed lines mark the trench axis channel. Red box is location of Figure 3.1b. Black line is seismic inline 2468. Inset in the upper right shows the regional tectonic setting of the Nankai Trough with the red box showing the location of the main map – EP= Eurasian Plate; PSP= Philippine Sea Plate; I-B= Izu-Bonin arc; IBT= Izu-Bonin Trench; PP= Pacific Plate; JT= Japan Trench. **(b)** Study region for this paper. Black lines are seismic inlines shown. Black box is Site C0002 region in Figure 3.3.

The shape and development of both the Nankai inner and outer accretionary prisms (Figure 3.2) are highly influenced by the incoming sediments. The Shikoku Basin, located on the incoming plate (Figure 3.1), defines the basaltic basement and sediment structure of northern margin of the PSP and was produced by rifting and back-arc spreading from the Izu-Bonin island arc system ~25-15 Ma [Kobayashi and Nakada, 1978; Okino *et al.*, 1994; Okino *et al.*, 1999]. Clockwise rotation of the spreading axis occurred during the early to mid-Miocene with late-stage volcanism continuing until the late Miocene when large variations in the basement morphology formed, such as the Kinan seamount chain [Okino *et al.*, 1994; Okino *et al.*, 1999]. Farther east, the Izu Bonin Mariana volcanic arc collided against the Honshu arc ~15 Ma leading to rapid erosion of the uplifted region and increase of sediment transport and deposition down through the Nankai trench axis [Itoh, 1988; Underwood *et al.*, 1993]. Variations in the igneous basement relief channeled terrigenous Miocene turbidites into graben and low-lying areas while leaving basement highs with thin hemipelagic sediments [Ike *et al.*, 2008a; b]. These sediments filled the trenchward part of the Shikoku Basin, leaving little evidence of basement relief, and the large increase in sediment led to the accretionary prism growing ~40 km perpendicular to the trench over the last 2 Ma [Moore *et al.*, 2001]. The influx of sediment changed the structure of the wedge to that of the present day. Based on Coulomb wedge theory, the prism flattened from the increased growth from high input at the trench, and in turn resulted in an OOST that thickened and maintained a critical taper in a self-similar geometry [Davis *et al.*, 1983]. This tectonic history likely influenced the OOST system throughout the Nankai Trough.

The Kumano Basin is located landward of a backstop boundary marked by OOSTs and overlies deeper inner prism thrusts and slope fill (Figure 3.2). The seaward edge of this forearc basin has been interpreted to be a strike-slip fault zone [Martin *et al.*, 2010; Tsuji *et al.*, 2014a].

The distal portion of the Kumano Basin is largely defined by landward tilted horizons [Gulick *et al.*, 2010; Moore *et al.*, 2007] and multiple sets of normal fault populations [Moore *et al.*, 2013; Sacks *et al.*, 2013]. The evolution of Kumano forearc basin is directly interwoven with OOST formation and uplift, developing from an interplay between tectonics and sedimentation [Moore *et al.*, 2015]. The distal edge of the Kumano Basin and underlying accretionary prism has been divided into five units, based on cores, cuttings, and logs from IODP Sites C0002 and C0009 [Expedition 314 Scientists, 2009; Expedition 319 Scientists, 2010; Strasser *et al.*, 2014]. The upper units (I and II) are considered to be modern Kumano Basin sediments consisting largely of hemipelagic deposits with fine-grained turbiditic sediments [Expedition 314 Scientists, 2009; Expedition 315 Scientists, 2009]. Unit III contains slope basin deposits that overlie an older accretionary prism (Unit IV) [Expedition 319 Scientists, 2010]. Unit IV is generally exhibits a chaotic seismic reflection pattern. Unit V is thought to be older Shikoku basin sediments with the oldest sediments dated at Site C0002 [Strasser *et al.*, 2014; Tobin *et al.*, 2015a]. Additionally, 12 seismic sequences have also been defined based on major unconformities within Unit I/II [Gulick *et al.*, 2010] and three seismic sequences within Unit III [Ramirez *et al.*, 2015]

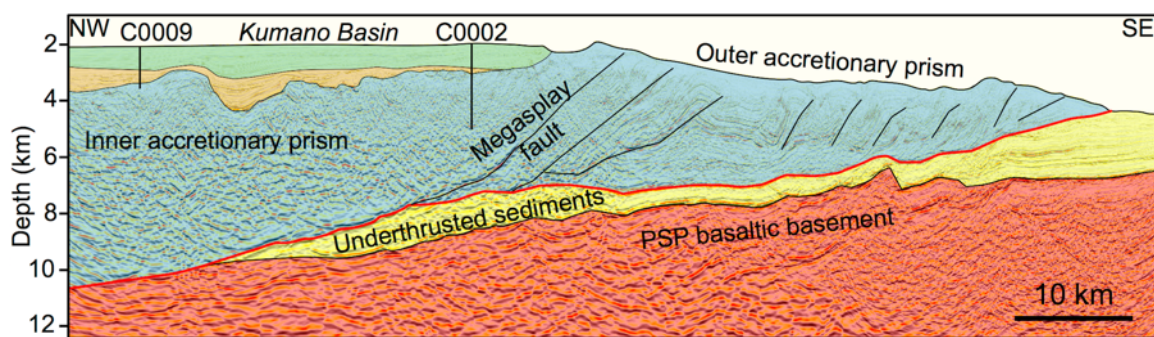


**Figure 3.2.** Seismic inline 2468 across the outer and inner accretionary prism. Interpretation based on Moore *et al.* [2014]. PSP = Philippine Sea Plate. Projected drill Sites C0002 and C0009 are also shown. The green and orange units are forearc basin fill and slope fill, respectively. The red line is the plate boundary fault.

### 3.3. Data and Methods

#### 3.3.1. Seismic Data

In 2006, a three-dimensional (3D) seismic reflection volume was collected aboard the M/V *Nordic Explorer* by Petroleum GeoServices (PGS) off southwest Japan (Figure 3.1). Acquisition was performed with a two-source array, each consisting of 28 airguns fired alternately at 37.5 m intervals. Four 4500 m long streamer cables were spaced 150 m apart, with 12.5 m spacing of receiver groups for each cable. The resulting seismic volume has an inline spacing of 12.5 m, a crossline spacing of 18.75 m, and a nominal fold of 30. Compagnie Générale de Géophysique (CGG) processed the data through 3D pre-stack time migration (PSTM) using traditional data conditioning and multiple reduction, and later, the Japan Agency for Marine Earth Science and Technology (JAMSTEC) performed a 3D pre-stack depth migration (PSDM). Due to the relatively short streamer length and strong feathering by the Kuroshio Current, velocity resolution at depth is less accurate than in the shallow section [Moore *et al.*, 2009]. Depth processing produced clear images (Figure 3.2) with a resolution of ~5-20 m for the Kumano Basin sediments [Moore *et al.*, 2009]. This dataset extends into the Kumano Basin landward of the OOST (Figure 3.1) covering a ~12 km x 25 km area within the basin. Using the 3D PSDM seismic volume, we mapped individual horizons throughout the basin. Two main boundaries, seismic horizons KL and UC2, were mapped based on onlapping relationships, seismic character, and well data. Additional Kumano Basin horizons were also mapped in 3D with horizon names following previous labeling schemes [e.g., Moore *et al.*, 2015].

#### 3.3.2. Well Data

IODP has extensively used the D/V *Chikyu* to drill the Kumano portion of the Nankai Trough, including two well sites within the Kumano Basin (Figure 3.1). Site C0002 is located

near the seaward side of the basin, whereas C0009 is near the landward extent of the 3D survey. Expedition 314 drilled Hole C0002A to 1401 meters below seafloor (mbsf) with logging-while-drilling (LWD) data [Expedition 314 Scientists, 2009]. Hole C0009A on Expedition 319 collected LWD data and cores [Expedition 319 Scientists, 2010]. Expedition 338 extended C0002F to 2005.5 mbsf and also collected LWD data and cores, while Expedition 348 extended Site C0002 to 3058.5 mbsf using sidetracked hole C0002P collecting a suite of LWD data, including natural gamma ray, electrical resistivity logs and images, sonic velocity, and sonic caliper logs [Tobin *et al.*, 2015b].

The focus here is on a subset of Hole C0002P data: the gamma ray log, the resistivity log, resistivity image, and the sonic log. The RH48PC resistivity log is a phase shift resistivity log with a 48-inch sensor spacing collected at 2 MHz frequency [Tobin *et al.*, 2015b]. The azimuthal focused resistivity (AFR) produces a high-resolution resistivity image acquired in 128 discrete azimuthal bins with an ideal 10 mm image resolution [Tobin *et al.*, 2015b]. The AFR image was filtered with a median 5x5 filter to reduce noise. Picks of bedding, faults, and fractures were interpreted from the AFR static image. The sonic log used both a monopole and dipole mode source with a frequency between 2 and 25 kHz and recorded the full waveform signal [Tobin *et al.*, 2015b]. We reprocessed the sonic compressional velocity data based on the original raw waveforms.

### **3.3.3. Velocity-Corrected Seismic Volume**

We created a new 3D velocity model at Site C0002 using the PSDM water interval velocity, a seismic check-shot survey at C0002A, and LWD sonic data at C0002F/C0002P. The model is based on the smoothed interval velocity data for C0002A [Expedition 314 Scientists, 2009]. Velocity data were combined into a one-dimensional (1D) profile that was then gridded

and smoothed into a 3D velocity cube covering seismic inlines 2527-2536 and crosslines 6220-6228, bounding the location of all the holes at Site C0002 (Figure 3.3). Seismic scaling of the PSDM seismic data updated with the well-based velocity cube created the updated depth seismic section. We converted the PSDM volume to time using the original PSDM velocity volume, and then re-converted the time volume back to depth using our updated velocity volume at Site C0002.

#### **3.3.4. Trishear Model**

Due to (1) a seafloor multiple reflection that obscures reflections within the older prism section under the forearc basin and (2) high angle dips of the strata, interpretations of the deep thrust faults are poorly constrained. We utilize structural reconstructions to test and verify our interpretations of the seismic reflection data. Our model in this study uses a forward trishear modeling program, LithoTect<sup>®</sup>, a graphical structural modeling software that uses our interpreted seismic horizons. Trishear is a kinematic model that deforms a triangular zone ahead of the propagating fault tip based on simple shear with a fixed footwall and a constant-velocity hanging wall [Erslev, 1991; Allmendinger, 1998]. This model assumes two-dimensional (2D) deformation within the shear zone based on a velocity field solution by Zehnder and Allmendinger [2000]. Following a forward modeling approach, we estimate trishear parameters, fault geometry, and fault slip by restoring each seismic horizon to a planar footwall slope extended with the same dip as the undeformed seaward part of the same horizon.

#### **3.4. Results**

We focus on a regional to borehole scale study of the deep inner accretionary prism. This tectonic setting has generally been difficult to study. We present results of 3D seismic

interpretation, structural interpretation, modeling that tests our interpretation, and deep borehole structural data from the inner prism at the Nankai Trough to illuminate margin processes.

### 3.4.1. Top of the Miocene Prism

Because velocities in the updated seismic volume are slightly lower than those of the original PSDM, the new depths for seismic reflections at the base of the forearc basin are ~100 m shallower than in the original PSDM volume (Figure 3.3). The depth at the top of Unit IV at Hole C0002A is 2871.6 meters below sea level (mbsl) from previous LWD results [*Expedition 314 Scientists*, 2009]. The updated seismic volume has the LWD based top of Unit IV clearly correlated to a positive (black) seismic reflection, with the previous PSDM being a negative (white) reflection. Using the updated seismic volume and LWD well tie, we can make a confident and precise seismic interpretation of the top of Unit IV, labeled seismic horizon UC2. Because our updated velocity model is limited to the well site, we use the PSDM volume to extrapolate an interpretation of seismic horizon UC2 throughout the full volume (Figure 3.4). Additionally, we use Site C0009 to help constrain the landward portion of UC2.

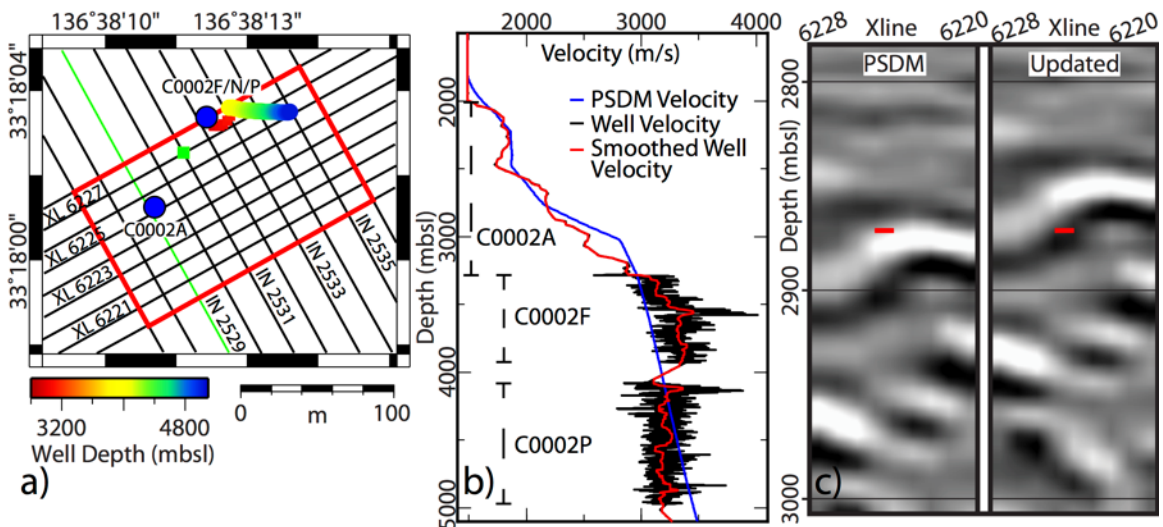


**Figure 3.3.** Well compressional velocity and velocity-corrected seismic data. **(a)** Location of Site C0002 holes (blue circles) and well paths (depth color coded). Red box is region of the

seismic update. Green box is the location of PSDM velocity profile shown in Figure 3.3b. Green line is seismic inline for Figure 3.3c. **(b)** Well velocities and PSDM velocity. **(c)** Original PSDM seismic reflectors (left) compared to the updated seismic reflectors (right) of seismic inline 2529. Red line marks the depth of to the top of Unit IV [*Expedition 314 Scientists, 2009*]. Note that our new velocity model shifts all reflections shallower.

UC2 overlies generally discontinuous seismic returns. Because this horizon is an unconformity, in regions where the horizon amplitude is weak, we also use the seismic character, of continuous slope basin reflectors onlap or truncate onto a discontinuous seismic basement to define the boundary. Where a seismic reflection defines the boundary, the reflection is positive, in agreement with the updated seismic volume at Site C0002. This adds confidence to our interpretation of seismic horizon UC2. The final horizon map is smoothed using a 100 m Gaussian filter.

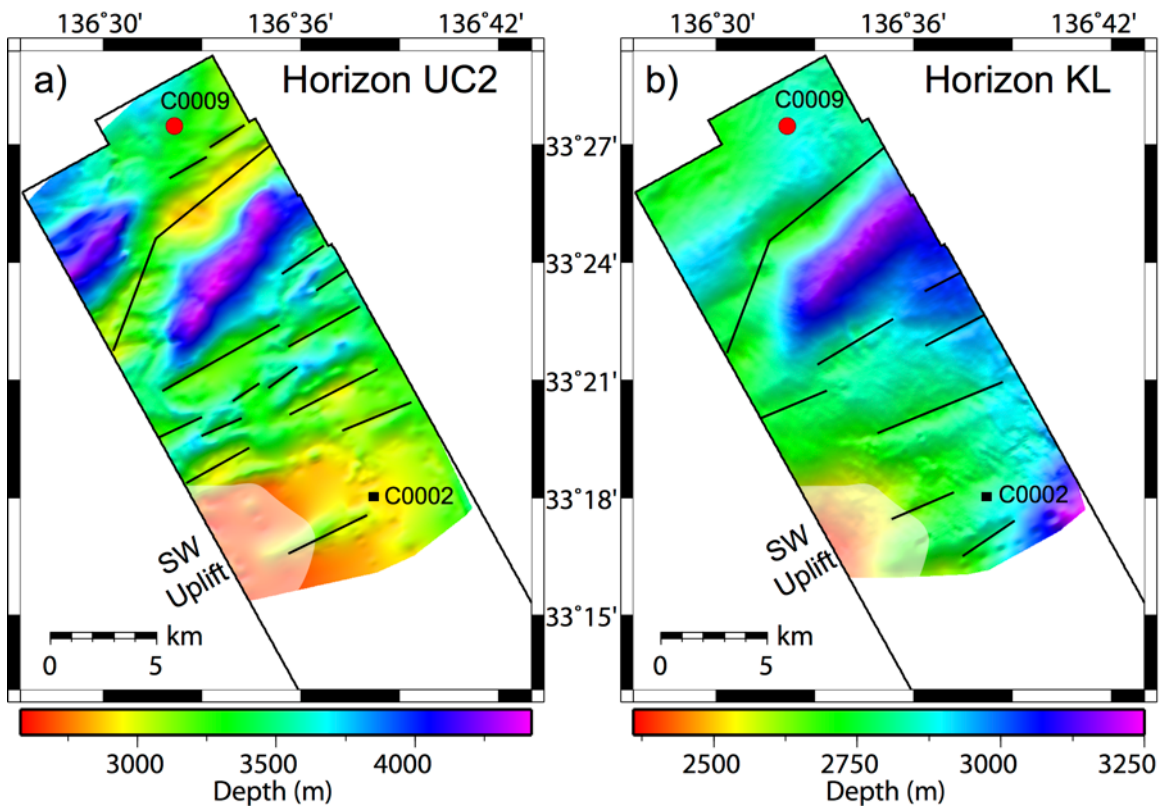


**Figure 3.4.** Map view of deep seismic horizons. **(a)** Horizon UC2 interpreted to be the top of Unit IV. **(b)** Horizon KL interpreted to be the basal boundary of the modern forearc basin. Black

box is the limit of the 3D seismic volume. Black lines mark the main anticlines. The SW uplift mapped is from bathymetry (Figure 3.1b).

Horizon UC2's morphology is one of the most irregular within the Kumano Basin, with its depth varying by ~2000 m (Figure 3.4a). The southwestern section of UC2 is the shallowest and corresponds to an area of local uplift documented within the upper sections and seafloor (Figure 3.1) [Gulick *et al.*, 2010; Moore *et al.*, 2015]. However, UC2 contains higher frequency components (folds) than the seafloor, indicating these subsurface components existed before the local uplift event. Multiple small-scale folds with wavelengths of ~1-2 km and amplitudes as great as ~500 m are abundant in the southern section. The axial surfaces of these folds strike ~50°-70°, similar to the strike of the outer prism's thrusts faults and the local trend of the Nankai Trough. In the northwestern section of the survey, the largest anticline occurs, with more than 1 km of relief; it is marked in Figure 3.4 by the angular trace of the axial surface. The northeast portion of its crest trends ~050° and the southwest portion trends ~020°. Two main synclines flank this anticline, with one south and one northwest of the anticline crest. Horizon UC2 shows clear similarities to the modern outer prism seafloor, indicating that these folds are from imbricate thrusts.

We also map the top of Unit III (slope fill), seismic horizon KL (Figure 3.4b). This horizon, which marks the top of the slope basin and early Kumano Basin deposits [Ramirez *et al.*, 2015], is overlapped by the tilted Kumano Basin fill; it is not horizontal but exhibits ~1000 m of relief. Similar folds are found at the same positions in map view for both horizons KL and UC2. Although horizon KL was tilted during Kumano Basin formation [Moore *et al.*, 2015], these folds indicate that the same basement structures that deformed horizon UC2 were active

before forearc basin deposition. This horizon no longer follows a wedge morphology, indicating uplift and tilting occurred during the transition from outer to inner prism.

Drilling at Site C0002 revealed increasing depositional ages with depth. The forearc basin fill are all Quaternary (<2 Ma) in age [*Expedition 315 Scientists*, 2009; *Strasser et al.*, 2014; *Tobin et al.*, 2015a]. Trench slope sediments are Pliocene in age and have a basal unconformity with a deformed upper Miocene accretionary prism basement [*Expedition 315 Scientists*, 2009; *Strasser et al.*, 2014]. This Miocene prism also reveals increasing ages with depth with the bottom of Hole C0002P containing depositional ages of ~10 Ma [*Tobin et al.*, 2015a; *Strasser et al.*, 2014]. Biostratigraphic analyses of nearby Site C0009 also indicate sediments below UC2 are Miocene in age [*Expedition 319 Scientists*, 2010].

### **3.4.2. Inner Prism Thrusts**

#### **3.4.2.1. Inferring Inner Prism Thrusts**

We find similar fold-and-thrust structures within the inner prism the outer prism. However, no thrust fault is directly imaged within the inner prism. Whereas the megasplay fault and décollement associated with the outer prism have prominent returns (Figure 3.2) [*Bangs et al.*, 2009; *Moore et al.*, 2007], only tilted and folded horizons are preserved within the inner prism on the western portion of the 3D seismic volume (Figure 3.5), which is typical of imbricate thrusts at the outer prism. However, these folds are not continuous throughout the volume, with most of the Miocene prism containing chaotic reflections. These deformed horizons correlate with UC2 folds. We interpret these folded packages to be bounded by thrust faults formed at the outer accretionary prism.

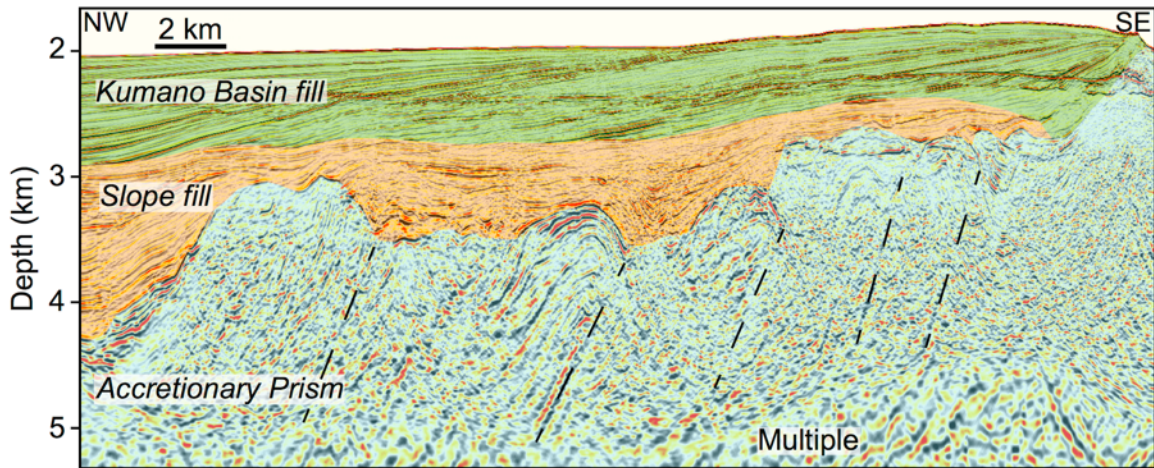


**Figure 3.5.** Seismic inline 2147 through the Kumano Basin. Location shown in Figure 3.1b. Buried anticlines are still preserved in some locations and slope fill shows local deformation. Dashed lines are inferred faults based on folded horizons and slope fill deformation.

### 3.4.2.2. Recent Uplift within the Kumano Basin

On the landward side of the 3D seismic volume, the beds show a more complex structure than just tilting. The KL unconformity surface and underlying slope fill sediments are warped over a basement fault block of accretionary prism sediments (Figure 3.6). Slope fill strata thins over the top of the fault block, where the strata is deformed into an anticline. Deep slope fill horizons are continuous on the southeastern side of the anticline but terminate next to the chaotic horizons of the accretionary prism (Figure 3.6b). Above these deep horizons, the slope fill shows clear signs of growth strata, indicating this structure is a thrust fault. Dip variations in these growth strata indicate syndepositional deformation of the early slope basin. Late stage slope basin filling [Ramirez *et al.*, 2015] also shows signs on tilting. Slip along this buried thrust fault has deformed strata seaward of the fault into a syncline that is continuous for ~10 km along strike, with slope fill being the thickest in the survey at >1000 m thick. From slope fill deformational and depositional patterns, we interpret a deep inner prism thrust fault that initially formed at the outer prism and was active during slope basin formation.

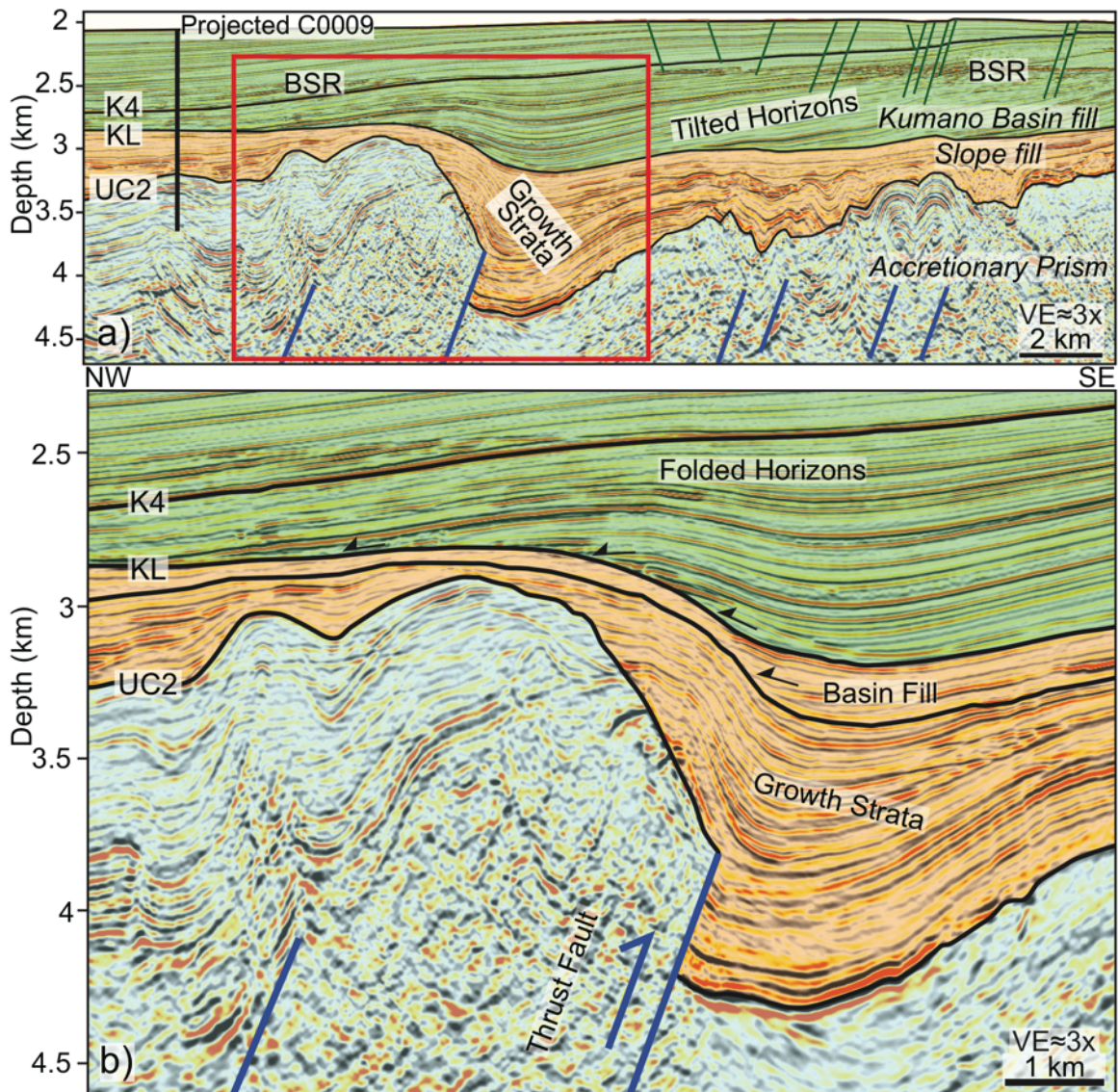


**Figure 3.6.** Reactivated buried thrusts within the inner prism. Thin black lines are normal faults and thick blue lines are thrust faults. **(a)** Seismic inline 2645 across northern anticline and interpretation. Red box is location of Figure 3.6b. **(b)** Seismic section shows clear growth strata from paleo-thrust uplift onlapping onto the inner accretionary prism. Black arrows indicate onlap.

This type of deformation is expected in the outer accretionary prism; however, continued thrusting beneath the modern forearc basin is not, as the inner prism is thought to remain stable [Wang and Hu, 2006]. Forearc basin fill is tilted landward as a result of slip on splay faults [Park

*et al.*, 2002] but is also folded above the buried thrust (Figure 3.6). The deeper Kumano Basin fill horizons show the greatest folding, with shallow horizons only being tilted (Figure 3.6). Horizon K4 extends to Site C0002 where it correlates with sediments dated to ~0.44 Ma [Moore *et al.*, 2015]. This indicates the reactivated fault persisted until at least ~0.44 Ma.

### **3.4.2.3. Kinematic Model of Uplift**

We performed multiple iterations of trishear structural reconstructions with Lithotect [Zehnder and Allmendinger, 2000] to test our interpretation of a reactivated thrust fault and to obtain slip and dip information for the fault (Figure 3.7). The model that performed best used a steeply dipping thrust fault of ~70°, a concentric slip line model for hanging wall deformation, a trishear apical angle of 50°, and a P/S (propagation of fault tip to slip) ratio of 1.25. We added a fault kink to include both the interpretations within the slope basin and reactivated fault tip and geometry. The modern basin formed rapidly, and only three seismic horizons were previously correlated to dated samples from Site C0002: K4 (~0.44 Ma), K5 (~0.9 Ma), and K5b (~1.04 Ma) [Moore *et al.*, 2015]. No samples of the upper basin at Site C0009 are available to provide additional age constraints in this region. We find that the fault is currently not active because horizons between K2 and the seafloor are not discernibly folded. For horizons dated <0.44 Ma, we estimate a total slip of ~90 m using our trishear model. Horizons dated between ~0.44-1.04 Ma have a total slip of ~490 m. For the restoration of the slope fill and UC2, we used a higher P/S ratio of 5 with an apical angle of 60°, for the best modeled results, and found slip of ~660 m and ~1000 m, respectively. Finally, we block-rotated the restored UC2 20° counter clockwise around a vertical axis to remove regional tilting and to estimate the fault geometry when located at the outer prism. Our model indicates that during fault reactivation the fault tip did not propagate into the slope sediments, which is different from the modern OOST fault zone.

However, our interpreted fault geometry is still similar to the modern fault-bend folds of the outer prism [e.g., Moore *et al.*, 1991].

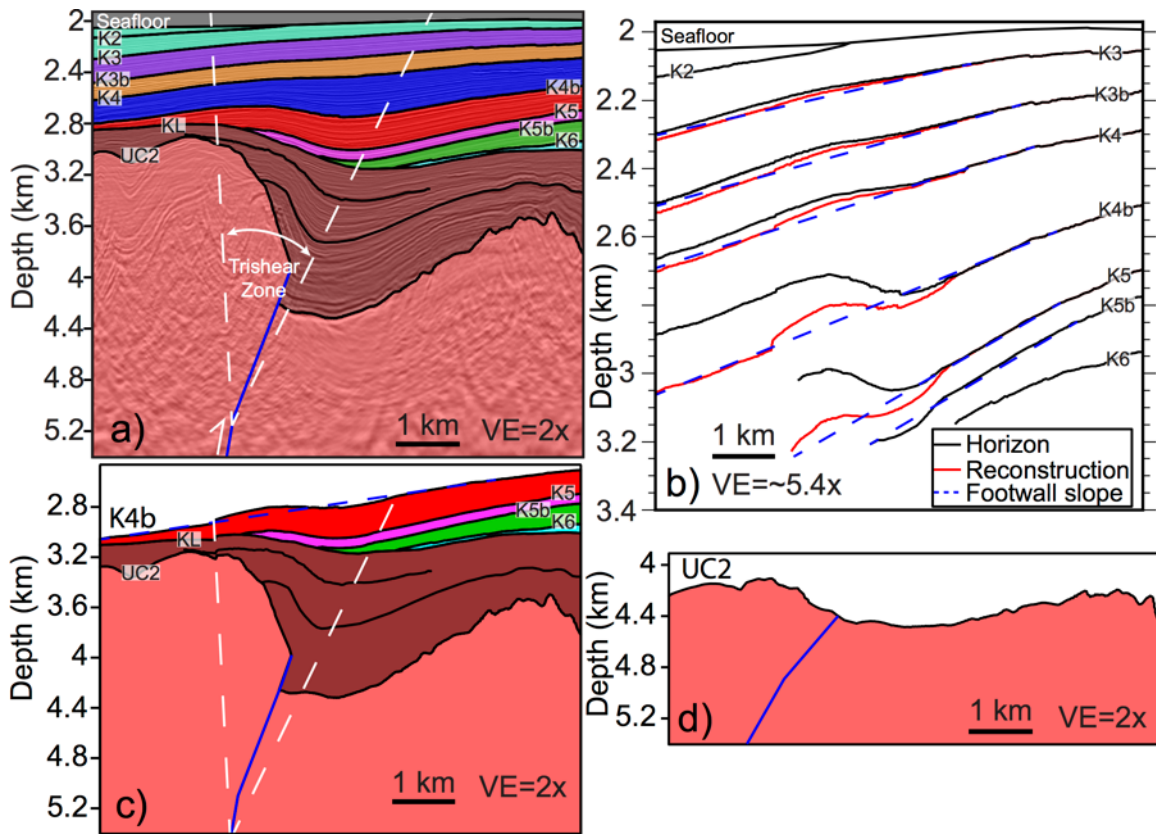


**Figure 3.7.** Structural reconstruction on seismic inline 2645 (Figure 3.6) using a kinematic trishear model. **(a)** Interpretation of thrust (blue solid line) and horizons (black lines). Three horizons are dated: K4 (~0.44 Ma), K5 (~0.9 Ma), and K5b (~1.04 Ma). **(b)** Trishear reconstruction of each horizon. The amount of restored slip for each horizon was: K3: 20 m; K3b: 30 m; K4: 40 m; K4b: 180 m; K5: 310 m. The seafloor, K2, K5b, and K6 did not need to be restored. **(c)** Model view of the restoration of horizon K4b. **(d)** Restoration of UC2, with a 20° block rotation applied.

### 3.4.3. Interior of the Inner Prism

The seismic data do not properly image the deep inner prism, so to better understand the deep prism processes, we focus on borehole-scale data from Hole C0002P. The small range in data values the gamma ray, resistivity, and sonic logs indicate a fairly homogenous logged interval (Figure 3.8), and this hole was previously interpreted to be apart of three subunits [Tobin *et al.*, 2015a]. We reinterpreted bedding and structural data in Hole C0002P from the resistivity

image log (Figures 3.8 and 3.9). We find steeply dipping beds with an average dip of  $\sim 70^\circ$ , and a range from  $\sim 30^\circ$ - $90^\circ$ , with bedding strike perpendicular to the convergence direction (Figures 3.8d and 3.9a). Faults were picked where offsets were observed, whereas fractures show a break in the bedding with no offsets. Fault and fracture attitudes are more variable than bedding attitudes (Figures 3.8e and 3.9b), indicating that there were multiple phases of deformation instead of just tilting. We separately mark additional inferred structures based on variations between interpreted bedding (Figure 3.9c). These structures are identified where bedding strike exhibits a change in azimuth of  $>90^\circ$  and bedding dip changes of  $\geq 10^\circ$  with no fracture or fault interpreted between beds. These inferred structures do not have an exact depth, since they occur between interpreted beds, and they do not have known dip or azimuth, but are plotted to show general locations in the hole. Whereas changes in bedding orientation could be related to stratigraphy, based on the local geology, we assume that they reflect structural features. These inferred structures are thought to be from folding or faulting between interpreted beds, and help fill gaps in lower quality sections of the image log. The highest density of structures is found at  $\sim 2700$  mbsf (Figure 3.9). This corresponds with both a spike and change in trend in the resistivity log. Two large groups of structural features are found from  $\sim 2575$ - $2625$  mbsf and  $\sim 2675$ - $2800$  mbsf. These results indicate that the deep interior of the inner prism has been subsequently deformed since the transition from the outer prism.

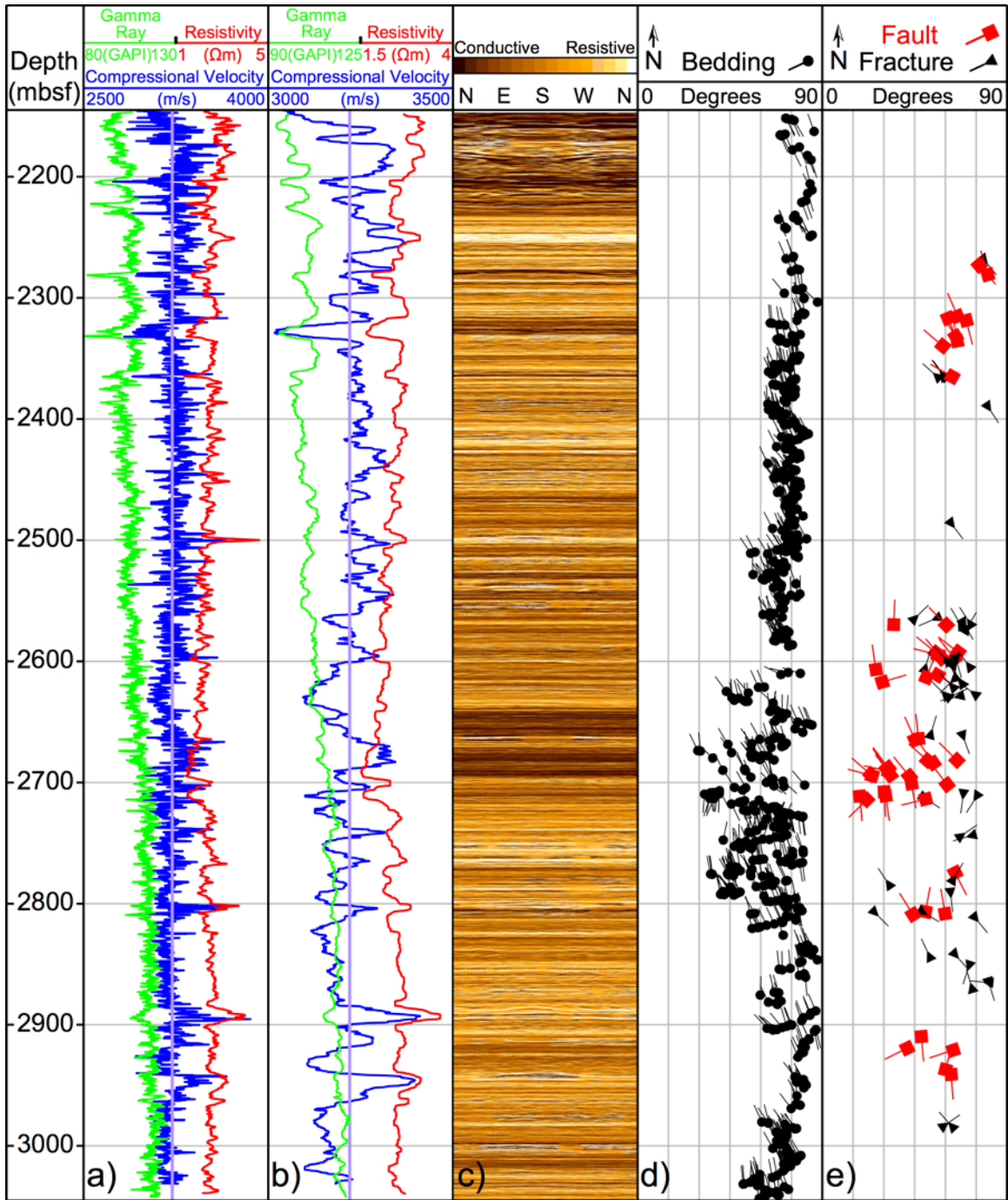


**Figure 3.8.** LWD logs from Hole C0002P. (a) Gamma ray in green (left half), resistivity in red (right half), and compressional velocity in blue (full width) with (b) being a smoothed version of the logs using a ~15 m median filter, note the smaller scales. Light blue line in a) and b) is a constant velocity of 3220 m/s (c) Static resistivity image log. Interpretation of (d) bedding and (e) faults and fractures from the resistivity image plotted as a tadpole diagram.

To better understand the log characteristics of the inner prism, we estimate the true stratigraphic thickness for bedding at C0002P. We use the Setchell equation to do this:

$$TST = MT (\cos\psi - \sin\psi \cos\alpha \tan\phi)\cos\phi,$$

where TST is true stratigraphic thickness, MT is the measured thickness,  $\psi$  is borehole inclination,  $\alpha$  is the difference between borehole azimuth and dip azimuth, and  $\phi$  is the bed dip [Tearpock and Bischke, 1991]. Using the interpreted bedding geometry (Figure 3.8d) and the minimum curvature well path for C0002P (Figure 3.3a), we applied this equation to each bed interval. Our measured section is 892 m, from the first interpreted bed to the last, with a calculated total true stratigraphic thickness for this same interval of 285 m. This stratigraphic thickness is significantly smaller than the measured interval and may explain the fairly homogenous lithological character from both the logs and the cuttings as the well path penetrated this stratigraphic section for an additional 607 m due to the steeply dipping beds.

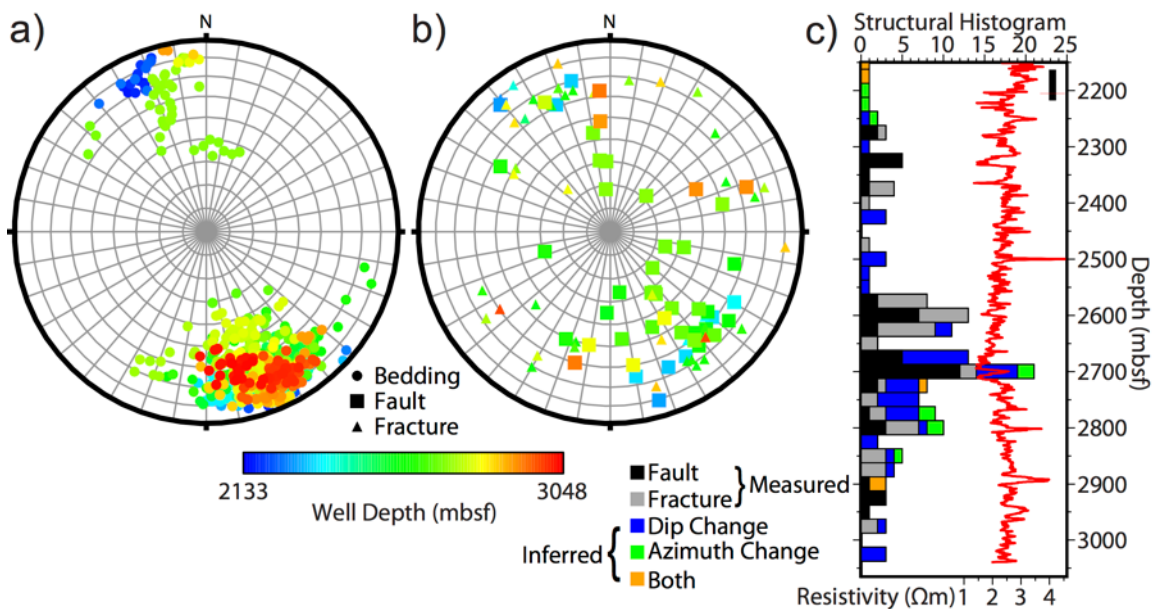


**Figure 3.9.** Structure data from Hole C0002P resistivity image log. (a) and (b) are equal area lower hemisphere stereonet plots with poles to bedding planes, fault planes, and fracture planes plotted with depth color coded. (c) Bar plot is a 25 m bin histogram of measured faults and fractures in addition to inferred structures from bedding that are based on bedding dip changes

>10°, bedding azimuth changes >90°, or both. RH48PC resistivity is plotted as red line. Black line is the cored interval.

### **3.5. Discussion**

#### **3.5.1. Development and Stability of the Inner Accretionary Prism**

The folded and thrust rocks that form the basement of the Kumano Basin form the majority of the inner accretionary prism (Figure 3.2). Seismic imaging of folds and horizons in the Miocene inner prism is poor but with some clearly present. The preservation pattern suggests that deformation within the inner prism is not uniform. Based on our interpretation of the resistivity image (Figure 3.8) and from cores in this section [Tobin *et al.*, 2015a], seismic returns within much of the deep inner prism are low due to steeply dipping beds. Additionally, at greater depths, the seismic resolution is lower, and multiple removal techniques performed on the seismic volume eliminated high frequency data below ~5000 mbsl [Moore *et al.*, 2009] leading to poor seismic interpretations at depth. However, the present of some inner prism folds indicates this preservation pattern is not just the work of data processing but is predominately caused from the local geology.

Reactivation of a buried thrust fault (Figure 3.7) indicates compressional stresses within the inner prism. Previously collected data from the inner accretionary prism at Sites C0009 and C0002 show a change in the trend of the maximum principal horizontal stress orientation of nearly 90° between the sites [Lin *et al.*, 2010; Lin *et al.*, in Press]. Numerical models have also shown multiple spatial stress orientations within the inner prism as a consequence of slip on splay faults [Conin *et al.*, 2012]. The location of the reactivated thrust (Figure 3.4) is consistent with the near-by stress orientation of Site C0009 [Lin *et al.*, in Press; Lin *et al.*, 2010] where the maximum principal horizontal stress orientation at depth is nearly perpendicular to the fault

strike. The lack of other reactivated thrusts near C0002 is also in agreement with the local stress field at the borehole [Lin *et al.*, in Press]. However, this region is complicated by both normal faults within the Kumano Basin fill and western uplift, making interpretation of fault-related folds difficult. The location of the reactivated thrust fault is consistent with stress orientations found at the well sites.

The complexity of the outer prism will affect the complexity of the inner prism as the structures transition from one setting to the other. Similarities in fold locations in horizon UC2 and KL (Figure 3.4) indicates that many of these thrust faults were active until at least forearc basin deposition, but became inactive during forearc basin formation. Reactivation of a buried thrust fault (Figure 3.7) instead of creating new thrusts indicates that outer prism thrusts can still be preserved as they transition into the inner prism. The buried fault tip did not propagate to offset the slope fill during reactivation, in contrast to faults in the modern OOST fault system. The fault geometry of outer prism thrusts will later influence the inner prism thrusts as the reactivated fault maintains the same strike, but the fault dip becomes steeper. Core analysis from Site C0009 suggested that the inner prism rotated  $\sim 15^\circ$  around a vertical axis [Hayman *et al.*, 2012]. The strikes of axial surfaces of many UC2 folds (Figure 3.4) are within the strike range of the outer prism thrusts, with a fold axis near C0009 having a more northerly strike.

The role of bedding geometry in inner prism stability is unknown. Steeply dipping beds found throughout Hole C0002P (Figure 3.8) indicate strong deformation before the overlying Kumano Basin fill developed, as the basin sediments are much less deformed. Bedding dip also follows plate convergence direction, indicating continued rotation of beds since they were located at the outer prism. The steeply dipping prism beds may make for a more stable backstop for outer prism growth. A low seismic attenuation factor of P-waves during a long-offset walk-

away vertical seismic profile at Site C0009 also may reflect the current stability of the inner prism [*Hino et al.*, 2015].

The seaward edge of the forearc basin is still tectonically active with normal faults [*Moore et al.*, 2013], strike-slip faults [*Martin et al.*, 2010], and the OOST zone [*Strasser et al.*, 2009]. Fault and fracture data at Hole C0002P indicate multiple stages of deformation (Figures 3.8 and 3.9). The source of these multiple stages of fracturing may be from the nearby active structures within the proximity of Hole C0002P.

The southwestern uplift of the basin is clearly displayed on the regional bathymetry map (Figure 3.1) and on horizons KL and UC2 (Figure 3.4). Our initial interpretation is that a small seamount subducted underneath this uplifted region, based on the seafloor morphology as the peak of this region is outside of the 3D seismic volume. This is similar to a proposed subducted seamount inferred to be located east of the 3D seismic volume [*Kimura et al.*, 2011]. However, the southwestern uplift event tilted horizons outside of just the seafloor high region [*Gulick et al.*, 2010; *Moore et al.*, 2015], and must be related additional prism processes. Inner prism thrust faults do not appear to have been reactivated during this event and therefore did not contribute to the southwestern uplift.

Rapid sedimentation may influence accretionary prism development [e.g., *Simpson*, 2010]. The onset of the distal Kumano forearc basin sedimentation is estimated at ~1.95-2.0 Ma and restricted to a narrow trough seaward of Site C0002 [*Moore et al.*, 2015]. At ~1.2 Ma, the basin depocenter started to shift landward as rapid tilting of the basin took place [*Moore et al.*, 2015]. By the time of deposition of horizon K5b (~1.04 Ma), reactivation of a buried thrust fault had started (Figure 3.7). Maximum deposition above the buried thrust occurred between K3 and K4 with a depocenter near the buried thrust [*Moore et al.*, 2015]. As the depocenter shifted

landward of the buried thrust, we find a decrease of slip on this fault (Figure 3.7). This correlation between forearc basin filling and the reactivated fault becoming inactive suggests that rapid sedimentation of forearc basins does play a role in the stability of the inner prism.

Overlying the inner prism thrusts and slope fill, the Kumano forearc basin is directly affected by the local tectonics [e.g., *Moore et al.*, 2015]. Long-term subsidence will also influence how the basin evolves. The tectonic subsidence curves for forearc basins have an assortment of trends, with proposals for these variations ranging from a change in subduction rate, variation in impact angle, and change in lithospheric thickness and density due to the age and structure of the subducted plate [*Moxon and Graham*, 1987; *Xie and Heller*, 2009]. For the distal strata of the Kumano Basin, the reactivated thrust fault altered sediment deposition for multiple horizons [*Moore et al.*, 2015]. Additionally, large depth variations of UC2 (Figure 3.4) create an irregular basement for the Kumano forearc basin. Both late stage thrust faulting and the original structure in an outer prism in addition to local tectonics will influence the variability of forearc basin subsidence.

### **3.5.2. Fluid Localization**

Fluid flow is viewed as an important process in accretionary prisms, with fault and fracture networks containing high permeability zones allowing fluids from depths to flow up to the seafloor [e.g., *Moore and Vrolijk*, 1992]. Thrust faults within the inner prism are then potential fluid conduits, but because many of these structures have been inactive since the Kumano Basin formation, processes of cementation and consolidation would reduce their permeability. However, the reactivated thrust fault (Figures 3.6 and 3.7) appears to play a role in fluid migration. The seismic volume shows a strong bottom-simulating reflector (BSR) above the UC2 anticline and thrust fault, indicating a free gas accumulation there, whereas the region

seaward of the anticline that has no BSR (Figure 3.6). This UC2 anticline shows no large seismic amplitude change indicating no large gas buildup at depth, but with fluids migrating above the UC2 anticline. This reactivated fault may serve as a conduit for fluid and mud migration from depth. An estimated high pore pressure zone is located near the reactivated thrust fault [Tsuji *et al.*, 2014b], indicating that this fault had an effect on fluid flow. Similar fluid migration locations have been found on the landward section of the Costa Rica margin [Bangs *et al.*, 2015].

Evidence for fluid flow within the Kumano Basin has been found throughout much of the basin. An estimated 13 mud volcanoes are documented within the center of the Kumano Basin, landward of the 3D seismic volume, with some extending >100 m above the seafloor and having moderate to low activity compared to submarine mud volcanoes fluid discharge intensities in other locations [Pape *et al.*, 2014]. These surface expressions are evidence for deeper fluid migration within the basin. Seismic surveys image anticlines beneath many of these mud volcanoes [Morita *et al.*, 2004], with deep structures similar to the large UC2 anticline and reactivated thrust fault found within the 3D seismic survey (Figure 3.6). Therefore, inner prism structures continue to play a role in fluid migration as the outer prism moves seaward. Hydrocarbons at four mud volcanoes within the Kumano Basin show a range of both thermogenic and microbial gas with potential formation depth ranges of 2300-4300 mbsf [Pape *et al.*, 2014]. Drilling into a Kumano Basin mud volcano found a two-source reservoir based on estimated temperatures derived from a lithium isotope [Nishio *et al.*, 2015]. At Site C0002, mature microbial hydrocarbons were found to a depth of 2325 mbsf, where a change to thermogenic gas occurred [Tobin *et al.*, 2015a]. Mud gas monitoring at Site C0009 indicated low fluid flow north of the reactivated thrust fault [Wiersberg *et al.*, 2015]. Whereas this drill site points to low fluid flow in the Kumano Basin, the reactivated thrust fault correlates with

evidence for channelized fluid migration, and similar deep structures within the central part of the Kumano Basin may also contribute to fluid migration.

### **3.6. Conclusions**

In this study, we find that the inner accretionary prism of the Nankai Trough displays a history of both temporal- and spatial-structural variability. Thrust faults formed at the outer prism play an integral role in shaping the inner prism. We mapped and interpreted multiple inner prism thrust faults, and though these faults are currently inactive, we found that one fault was reactivated at  $\sim 1.04$  Ma, after the OOST formed. Slip along this reactivated fault decreased as the forearc basin depocenter shifted over the thrust fault and it became inactive less than  $\sim 0.44$  Ma. We interpret localized fluid flow around this structure, indicating that reactivated faults may play an integral role in the hydraulic systems of the inner prism. Steeply dipping beds found at depth denote continued tilting of beds during the formation of the megasplay fault, while faults and fractures indicate multiple phases of deformation. Our work reveals that the transition from outer to inner accretionary prism settings maintains some older structures, though additional stages of activity at depth can also heavily deform them.

### **Acknowledgments**

This research used data provided by the Integrated Ocean Drilling Program (IODP). Funding for this research was provided by the National Science Foundation (grant OCE-0451790) and U.S. Science Support Program Post-Expedition Awards. The authors thank the science party of Expedition 348 and are grateful for the support provided by the logging staff scientists (Y. Sanada, Y. Kido, and Y. Hamada), the D/V *Chikyu* crew, and technicians. We thank Paradigm Geophysical and Landmark Graphics (Halliburton) for their academic software grants.

## References

- Allmendinger, R. W. (1998), Inverse and forward numerical modeling of trishear fault-propagation folds, *Tectonics*, 17(4), 640-656. doi:10.1029/98tc01907.
- Ando, M. (1975), Source mechanisms and tectonic significance of historical earthquakes along the Nankai Trough, Japan, *Tectonophysics*, 27(2), 119-140. doi:10.1016/0040-1951(75)90102-x.
- Baba, T., Y. Tanioka, P. R. Cummins, and K. Uhira (2002), The slip distribution of the 1946 Nankai earthquake estimated from tsunami inversion using a new plate model, *Phys. Earth Planet. Inter.*, 132(1-3), 59-73. doi:10.1016/S0031-9201(02)00044-4.
- Baba, T., P. R. Cummins, T. Hori, and Y. Kaneda (2006), High precision slip distribution of the 1944 Tonankai earthquake inferred from tsunami waveforms: Possible slip on a splay fault, *Tectonophysics*, 426(1-2), 119-134. doi:10.1016/j.tecto.2006.02.015.
- Bangs, N. L., K. D. McIntosh, E. A. Silver, J. W. Kluesner, and C. R. Ranero (2015), Fluid accumulation along the Costa Rica subduction thrust and development of the seismogenic zone, *J. Geophys. Res.*, 120(1), 67-86. doi:10.1002/2014jb011265.
- Bangs, N. L. B., G. F. Moore, S. P. S. Gulick, E. M. Pangborn, H. J. Tobin, S. Kuramoto, and A. Taira (2009), Broad, weak regions of the Nankai Megathrust and implications for shallow coseismic slip, *Earth Planet. Sci. Lett.*, 284(1-2), 44-49. doi:10.1016/J.Epsl.2009.04.026.
- Byrne, D. E., W. Wang, and D. M. Davis (1993), Mechanical role of backstops in the growth of forearcs, *Tectonics*, 12(1), 123-144.
- Conin, M., P. Henry, V. Godard, and S. Bourlange (2012), Splay fault slip in a subduction margin, a new model of evolution, *Earth Planet. Sci. Lett.*, 341-344, 170-175. doi:10.1016/j.epsl.2012.06.003.
- Dahlen, F. A. (1990), Critical Taper Model of Fold-and-Thrust Belts and Accretionary Wedges, *Annu. Rev. Earth Planet. Sci.*, 18, 55-99. doi:10.1146/Annurev.Earth.18.1.55.
- Davis, D., J. Suppe, and F. A. Dahlen (1983), Mechanics of Fold-and-Thrust Belts and Accretionary Wedges, *J. Geophys. Res.*, 88(Nb2), 1153-1172. doi:10.1029/Jb088ib02p01153.
- DeMets, C., R. G. Gordon, and D. F. Argus (2010), Geologically current plate motions, *Geophys. J. Int.*, 181(1), 1-80. doi:10.1111/J.1365-246x.2009.04491.X.
- Erslev, E. A. (1991), Trishear Fault-Propagation Folding, *Geology*, 19(6), 617-620. doi:10.1130/0091-7613(1991)019<0617:Tfpf>2.3.Co;2.
- Expedition 314 Scientists (2009), Expedition 314 Site C0002, In: *Proc. IODP*, 314/315/316, M. Kinoshita, H. Tobin, J. Ashi, G. Kimura, S. Lallement, E. J. Screaton, D. Curewitz, H. Masago, K. T. Moe and Expedition 314/315/316 Scientists (Eds.), Integrated Ocean Drilling Program, Washington, DC. doi:10.2204/iodp.proc.314315316.114.2009.

- Expedition 315 Scientists (2009), Expedition 315 Site C0002, In: *Proc. IODP*, 314/315/316, M. Kinoshita, Tobin, H., Ashi, J., Kimura, G., Lallemand, S., Screaton, E.J., Curewitz, D., Masago, H., Moe, K.T., and the Expedition 314/315/316 Scientists (Eds.), Washington, DC (Integrated Ocean Drilling Program Management International, Inc.). doi:10.2204/iodp.proc.314315316.124.2009.
- Expedition 319 Scientists (2010), Site C0009, In: *Proc. IODP*, 319, D. Saffer, L. McNeill, T. Byrne, E. Araki, S. Toczko, N. Eguchi, K. Takahashi and Expedition 319 Scientists (Eds.), Integrated Ocean Drilling Program, Tokyo. doi:10.2204/iodp.proc.319.103.2010.
- Fuller, C. W., S. D. Willett, and M. T. Brandon (2006), Formation of forearc basins and their influence on subduction zone earthquakes, *Geology*, 34(2), 65-68. doi:10.1130/g21828.1.
- Gulick, S. P. S., N. L. B. Bangs, G. F. Moore, J. Ashi, K. M. Martin, D. S. Sawyer, H. J. Tobin, S. Kuramoto, and A. Taira (2010), Rapid forearc basin uplift and megasplay fault development from 3D seismic images of Nankai Margin off Kii Peninsula, Japan, *Earth Planet. Sci. Lett.*, 300(1-2), 55-62. doi:10.1016/J.Epsl.2010.09.034.
- Hasebe, N., and T. Tagami (2001), Exhumation of an accretionary prism — results from fission track thermochronology of the Shimanto Belt, southwest Japan, *Tectonophysics*, 331(3), 247-267. doi:10.1016/S0040-1951(00)00282-1.
- Hayman, N. W., T. B. Byrne, L. C. McNeill, K. Kanagawa, T. Kanamatsu, C. M. Browne, A. M. Schleicher, and G. J. Huftile (2012), Structural evolution of an inner accretionary wedge and forearc basin initiation, Nankai margin, Japan, *Earth Planet. Sci. Lett.*, 353-354, 163-172. doi:10.1016/j.epsl.2012.07.040.
- Hino, R., T. Tsuji, N. L. Bangs, Y. Sanada, J.-O. Park, R. von Huene, G. F. Moore, E. Araki, and M. Kinoshita (2015), Q P structure of the accretionary wedge in the Kumano Basin, Nankai Trough, Japan, revealed by long-offset walk-away VSP, *Earth Planets Space*, 67(1). doi:10.1186/s40623-014-0175-x.
- Ike, T., G. F. Moore, S. Kuramoto, J. O. Park, Y. Kaneda, and A. Taira (2008a), Tectonics and sedimentation around Kashinosaki Knoll: A subducting basement high in the eastern Nankai Trough, *Isl. Arc*, 17(3), 358-375. doi:10.1111/J.1440-1738.2008.00625.X.
- Ike, T., G. F. Moore, S. Kuramoto, J. O. Park, Y. Kaneda, and A. Taira (2008b), Variations in sediment thickness and type along the northern Philippine Sea Plate at the Nankai Trough, *Isl. Arc*, 17(3), 342-357. doi:10.1111/J.1440-1738.2008.00624.X.
- Itoh, Y. (1988), Differential Rotation of the Eastern Part of Southwest Japan Inferred from Paleomagnetism of Cretaceous and Neogene Rocks, *J. Geophys. Res.*, 93(B4), 3401-3411. doi:10.1029/Jb093ib04p03401.
- Kanamori, H. (1972), Tectonic implications of the 1944 Tonankai and the 1946 Nankaido earthquakes, *Phys. Earth Planet. Inter.*, 5, 129-139.

- Kimura, G., G. F. Moore, M. Strasser, E. Screaton, D. Curewitz, C. Streiff, and H. Tobin (2011), Spatial and temporal evolution of the megasplay fault in the Nankai Trough, *Geochem. Geophys. Geosyst.*, 12(3), Q0A008. doi:10.1029/2010gc003335.
- Kobayashi, K., and M. Nakada (1978), Magnetic anomalies and tectonic evolution of the Shikoku inter-arc basin, *J. Phys. Earth*, 26, 391-402.
- Kopp, H., and N. Kukowski (2003), Backstop geometry and accretionary mechanics of the Sunda margin, *Tectonics*, 22(6), 1072. doi:10.1029/2002tc001420.
- Kukowski, N., J. Greinert, and S. Henrys (2010), Morphometric and critical taper analysis of the Rock Garden region, Hikurangi Margin, New Zealand: Implications for slope stability and potential tsunami generation, *Mar. Geol.*, 272(1-4), 141-153. doi:10.1016/J.Margeo.2009.06.004.
- Lallemand, S., and X. Lepichon (1987), Coulomb Wedge Model Applied to the Subduction of Seamounts in the Japan Trench, *Geology*, 15(11), 1065-1069. doi:10.1130/0091-7613(1987)15<1065:Cwmatt>2.0.Co;2.
- Lin, W., M.-L. Doan, J. C. Moore, L. McNeill, T. B. Byrne, T. Ito, D. Saffer, M. Conin, M. Kinoshita, Y. Sanada, K. T. Moe, E. Araki, H. Tobin, D. Boutt, Y. Kano, N. W. Hayman, P. Flemings, G. J. Huftile, D. Cukur, C. Buret, A. M. Schleicher, N. Efimenko, K. Kawabata, D. M. Buchs, S. Jiang, K. Kameo, K. Horiguchi, T. Wiersberg, A. Kopf, K. Kitada, N. Eguchi, S. Toczko, K. Takahashi, and Y. Kido (2010), Present-day principal horizontal stress orientations in the Kumano forearc basin of the southwest Japan subduction zone determined from IODP NanTroSEIZE drilling Site C0009, *Geophys. Res. Lett.*, 37(13), L13303. doi:10.1029/2010gl043158.
- Lin, W., T. B. Byrne, M. Kinoshita, L. C. McNeill, C. Chang, J. C. Lewis, Y. Yamamoto, D. M. Saffer, J. Casey Moore, H.-Y. Wu, T. Tsuji, Y. Yamada, M. Conin, S. Saito, T. Ito, H. J. Tobin, G. Kimura, K. Kanagawa, J. Ashi, M. B. Underwood, and T. Kanamatsu (in Press), Distribution of stress state in the Nankai subduction zone, southwest Japan and a comparison with Japan Trench, *Tectonophysics*. doi:10.1016/j.tecto.2015.05.008.
- Loveless, J. P., and B. J. Meade (2010), Geodetic imaging of plate motions, slip rates, and partitioning of deformation in Japan, *J. Geophys. Res.*, 115(B2). doi:10.1029/2008jb006248.
- Martin, K. M., S. P. S. Gulick, N. L. B. Bangs, G. F. Moore, J. Ashi, J. O. Park, S. Kuramoto, and A. Taira (2010), Possible strain partitioning structure between the Kumano fore-arc basin and the slope of the Nankai Trough accretionary prism, *Geochem. Geophys. Geosyst.*, 11(5). doi:10.1029/2009gc002668.
- Moore, G. F., D. E. Karig, T. H. Shipley, A. Taira, P. L. Stoffa, and W. T. Wood (1991), Structural Framework of the ODP Leg 131 Area, Nankai Trough, In: *Proc. ODP, Init. Repts.*, 131, A. Taira, I. Hill and J. Firth, et al., (Eds.), College Station, TX (Ocean Drilling Program). doi:10.2973/odp.proc.ir.131.102.1991.

- Moore, G. F., A. Taira, A. Klaus, L. Becker, B. Boeckel, B. A. Cragg, A. Dean, C. L. Fergusson, P. Henry, S. Hirano, T. Hisamitsu, S. Hunze, M. Kastner, A. J. Maltman, J. K. Morgan, Y. Murakami, D. M. Saffer, M. Sanchez-Gomez, E. J. Sreaton, D. C. Smith, A. J. Spivack, J. Steurer, H. J. Tobin, K. Ujiie, M. B. Underwood, and M. Wilson (2001), New insights into deformation and fluid flow processes in the Nankai Trough accretionary prism: Results of Ocean Drilling Program Leg 190, *Geochem. Geophys. Geosyst.*, 2(10), 1058. doi:10.1029/2001GC000166.
- Moore, G. F., N. L. Bangs, A. Taira, S. Kuramoto, E. Pangborn, and H. J. Tobin (2007), Three-dimensional splay fault geometry and implications for tsunami generation, *Science*, 318(5853), 1128-1131. doi:10.1126/science.1147195.
- Moore, G. F., J. O. Park, N. L. Bangs, S. P. Gulick, H. J. Tobin, Y. Nakamura, S. Saito, T. Tsuji, T. Yoro, H. Tanaka, S. Uraki, Y. Kido, Y. Sanada, S. Kuramoto, and A. Taira (2009), Structural and seismic stratigraphic framework of the NanTroSEIZE Stage 1 transect, *Proc. IODP*, 314/315/316. doi:10.2204/iodp.proc.314315316.102.2009.
- Moore, G. F., B. B. Boston, A. F. Sacks, and D. M. Saffer (2013), Analysis of normal fault populations in the Kumano Forearc Basin, Nankai Trough, Japan: 1. Multiple orientations and generations of faults from 3-D coherency mapping, *Geochem. Geophys. Geosyst.*, 14(6), 1989-2002. doi:10.1002/ggge.20119.
- Moore, G. F., B. B. Boston, M. Strasser, M. B. Underwood, and R. A. Ratliff (2015), Evolution of Tectono-Sedimentary Systems in the Kumano Basin, Nankai Trough Forearc, *Mar. Pet. Geol.*, 67, 604-616. doi:10.1016/j.marpetgeo.2015.05.032.
- Moore, J. C., and B. Biju-Duval (1984), Tectonic Synthesis, Deep Sea Drilling Project Leg 78A: Structural Evolution of Offscraped and Underthrust Sediment, Northern Barbados Ridge Complex, In: *Init. Repts. Deep Sea Drill. Proj.*, 78A, B. Biju-Duval and J. C. Moore (Eds.), U.S. Government Printing Office, Washington, D.C., doi:10.2973/dsdp.proc.78a.133.1984.
- Moore, J. C., and P. Vrolijk (1992), Fluids in Accretionary Prisms, *Rev. Geophys.*, 30(2), 113-135.
- Morita, S., J. Ashi, K. Aoike, and S. i. Kuramoto (2004), Evolution of Kumano basin and sources of clastic ejecta and pore fluid in Kumano mud volcanoes, Eastern Nanaki Trough, paper presented at Proceedings of the International Symposium on Methane Hydrates and Fluid Flow in Upper Accretionary Prisms, Engineering Geology Laboratory, Department of Civil & Earth Resources Engineering, Kyoto University, Kyoto, 2004.
- Morley, C. K. (1988), Out-of-Sequence Thrusts, *Tectonics*, 7(3), 539-561. doi:10.1029/Tc007i003p00539.
- Moxon, I. W., and S. A. Graham (1987), History and controls of subsidence in the Late Cretaceous-Tertiary Great Valley forearc basin, California, *Geology*, 15(7), 626. doi:10.1130/0091-7613(1987)15<626:hacosi>2.0.co;2.

- Nishio, Y., A. Ijiri, T. Toki, Y. Morono, M. Tanimizu, K. Nagaishi, and F. Inagaki (2015), Origins of lithium in submarine mud volcano fluid in the Nankai accretionary wedge, *Earth Planet. Sci. Lett.*, 414, 144-155. doi:10.1016/j.epsl.2015.01.018.
- Okino, K., Y. Shimakawa, and S. Nagakoa (1994), Evolution of the Shikoku Basin, *J. Geomagn. Geoelectr.*, 46, 463-479.
- Okino, K., Y. Ohara, S. Kasuga, and Y. Kato (1999), The Philippine Sea: New survey results reveal the structure and the history of the marginal basins, *Geophys. Res. Lett.*, 26(15), 2287-2290. doi:10.1029/1999gl900537.
- Pape, T., P. Gegrags, S. Hammerschmidt, P. Wintersteller, J. G. Wei, T. Fleischmann, G. Bohrmann, and A. J. Kopf (2014), Hydrocarbon seepage and its sources at mud volcanoes of the Kumano forearc basin, Nankai Trough subduction zone, *Geochem. Geophys. Geosyst.*, 15(6), 2180-2194. doi:10.1002/2013gc005057.
- Park, J. O., T. Tsuru, S. Kodaira, P. R. Cummins, and Y. Kaneda (2002), Splay fault branching along the Nankai subduction zone, *Science*, 297(5584), 1157-1160. doi:10.1126/science.1074111.
- Platt, J. P. (1986), Dynamics of Orogenic Wedges and the Uplift of High-Pressure Metamorphic Rocks, *Geol. Soc. Am. Bull.*, 97(9), 1037-1053. doi:10.1130/0016-7606(1986)97<1037:Doowat>2.0.Co;2.
- Ramirez, S. G., S. P. S. Gulick, and N. W. Hayman (2015), Early sedimentation and deformation in the Kumano forearc basin linked with Nankai accretionary prism evolution, southwest Japan, *Geochem. Geophys. Geosyst.*, 16(5), 1616-1633. doi:10.1002/2014GC005643.
- Sacks, A., D. M. Saffer, and D. Fisher (2013), Analysis of normal fault populations in the Kumano forearc basin, Nankai Trough, Japan: 2. Principal axes of stress and strain from inversion of fault orientations, *Geochem. Geophys. Geosyst.*, 14(6), 1973-1988. doi:10.1002/ggge.20118.
- Seno, T., S. Stein, and A. E. Gripp (1993), A Model for the Motion of the Philippine Sea Plate Consistent with Nuvel-1 and Geological Data, *J. Geophys. Res.*, 98(B10), 17941-17948. doi:10.1029/93jb00782.
- Simpson, G. D. H. (2010), Formation of accretionary prisms influenced by sediment subduction and supplied by sediments from adjacent continents, *Geology*, 38(2), 131-134. doi:10.1130/g30461.1.
- Song, T. R., and M. Simons (2003), Large trench-parallel gravity variations predict seismogenic behavior in subduction zones, *Science*, 301(5633), 630-633. doi:10.1126/science.1085557.
- Stockmal, G. S. (1983), Modeling of Large-Scale Accretionary Wedge Deformation, *J. Geophys. Res.*, 88(Nb10), 8271-8287. doi:10.1029/Jb088ib10p08271.

- Strasser, M., G. F. Moore, G. Kimura, Y. Kitamura, A. J. Kopf, S. Lallemand, J. O. Park, E. J. Screaton, X. Su, M. B. Underwood, and X. X. Zhao (2009), Origin and evolution of a splay fault in the Nankai accretionary wedge, *Nat. Geosci.*, 2(9), 648-652. doi:10.1038/Ngeo609.
- Strasser, M., B. Dugan, K. Kanagawa, G. F. Moore, S. Toczko, L. Maeda, Y. Kido, K. T. Moe, Y. Sanada, L. Esteban, O. Fabbri, J. Geersen, S. Hammerschmidt, H. Hayashi, K. Heirman, A. Hüpers, M. J. Jurado Rodriguez, K. Kameo, T. Kanamatsu, H. Kitajima, H. Masuda, K. Milliken, R. Mishra, I. Motoyama, K. Olcott, K. Oohashi, K. T. Pickering, S. G. Ramirez, H. Rashid, D. Sawyer, A. Schleicher, Y. Shan, R. Skarbek, I. Song, T. Takeshita, T. Toki, J. Tudge, S. Webb, D. J. Wilson, H. Y. Wu, and A. Yamaguchi (2014), Site C0002, In: *Proc. IODP*, 338, M. Strasser, B. Dugan, K. Kanagawa, G. F. Moore, S. Toczko, L. Maeda and the Expedition 338 Scientists (Eds.), Integrated Ocean Drilling Program, Yokohama doi:10.2204/iodp.proc.338.103.2014.
- Suppe, J. (2007), Absolute fault and crustal strength from wedge tapers, *Geology*, 35(12), 1127-1130. doi:10.1130/G24053a.1.
- Taira, A., J. Katto, M. Tashiro, M. Okamura, and K. Kodama (1988), The Shimanto Belt in Shikoku Japan: Evolution of a Cretaceous to Miocene accretionary prism, *Mod. Geol.*, 12, 5-46.
- Tearpock, D. J., and R. E. Bischke (1991), *Applied Subsurface Geological Mapping*, Prentice Hall, NJ.
- Tobin, H., T. Hirose, D. Saffer, S. Toczko, L. Maeda, Y. Kubo, B. Boston, A. Broderick, K. Brown, A. Crespo-Blanc, E. Even, S. Fuchida, R. Fukuchi, S. Hammerschmidt, P. Henry, M. Josh, M. J. Jurado, and H. Kitajima, Kitamura, M., Maia, A., Otsubo, M., Sample, J., Schleicher, A., Sone, H., Song, C., Valdez, R., Yamamoto, Y., Yang, K., Sanada, Y., Kido, Y., and Hamada, Y., (2015a), Site C0002, In: *Proc. IODP*, 348, H. Tobin, Hirose, T., Saffer, D., Toczko, S., Maeda, L., Kubo, Y., and the Expedition 348 Scientists (Eds.), College Station, TX (Integrated Ocean Drilling Program). doi:10.2204/iodp.proc.348.103.2015.
- Tobin, H., T. Hirose, D. Saffer, S. Toczko, L. Maeda, Y. Kubo, B. Boston, A. Broderick, K. Brown, A. Crespo-Blanc, E. Even, S. Fuchida, R. Fukuchi, S. Hammerschmidt, P. Henry, M. Josh, M. J. Jurado, and H. Kitajima, Kitamura, M., Maia, A., Otsubo, M., Sample, J., Schleicher, A., Sone, H., Song, C., Valdez, R., Yamamoto, Y., Yang, K., Sanada, Y., Kido, Y., and Hamada, Y., (2015b), Methods, In: *Proc. IODP*, 348, H. Tobin, Hirose, T., Saffer, D., Toczko, S., Maeda, L., Kubo, Y., and the Expedition 348 Scientists (Eds.), College Station, TX (Integrated Ocean Drilling Program). doi:10.2204/iodp.proc.348.102.2015.
- Tsuji, T., J. Ashi, and Y. Ikeda (2014a), Strike-slip motion of a mega-splay fault system in the Nankai oblique subduction zone, *Earth Planets Space*, 66(1), 120. doi:10.1186/1880-5981-66-120.
- Tsuji, T., R. Kamei, and R. G. Pratt (2014b), Pore pressure distribution of a mega-splay fault system in the Nankai Trough subduction zone: Insight into up-dip extent of the seismogenic zone, *Earth Planet. Sci. Lett.*, 396, 165-178. doi:10.1016/j.epsl.2014.04.011.

- Underwood, M. B., R. Orr, K. Pickering, and A. Taira (1993), Provenance and Dispersal Patterns of Sediments in the Turbidite Wedge of Nankai Trough, In: *Proc. ODP, Sci. Results*, 131, I. A. Hill, A. Taira and J. V. Firth, et al., (Eds.), College Station, TX (Ocean Drilling Program). doi:10.2973/odp.proc.sr.131.105.1993.
- von Huene, R., and D. W. Scholl (1991), Observations at convergent margins concerning sediment subduction, subduction erosion, and the growth of continental crust, *Rev. Geophys.*, 29(3), 279-316.
- Wang, K. L., and Y. Hu (2006), Accretionary prisms in subduction earthquake cycles: The theory of dynamic Coulomb wedge, *J. Geophys. Res.*, 111(B6), B06410. doi:10.1029/2005jb004094.
- Wells, R. E., R. J. Blakely, Y. Sugiyama, D. W. Scholl, and P. A. Dinterman (2003), Basin-centered asperities in great subduction zone earthquakes: A link between slip, subsidence, and subduction erosion?, *J. Geophys. Res.*, 108(B10), 2507. doi:10.1029/2002jb002072.
- Wendt, J., D. D. Oglesby, and E. L. Geist (2009), Tsunamis and splay fault dynamics, *Geophys. Res. Lett.*, 36(15), L15303. doi:10.1029/2009gl038295.
- Wiersberg, T., A. M. Schleicher, K. Horiguchi, M.-L. Doan, N. Eguchi, and J. Erzinger (2015), Origin and in situ concentrations of hydrocarbons in the Kumano forearc basin from drilling mud gas monitoring during IODP NanTroSEIZE Exp. 319, *Appl. Geochem.*, 61, 206-216. doi:10.1016/j.apgeochem.2015.06.002.
- Xie, X., and P. Heller (2009), Plate tectonics and basin subsidence history, *Geol. Soc. Am. Bull.*, 121(1/2), 55-64. doi:10.1130/B26398.1.
- Zehnder, A. T., and R. W. Allmendinger (2000), Velocity field for the trishear model, *J. Struct. Geol.*, 22(8), 1009-1014. doi:10.1016/S0191-8141(00)00037-7.

## Chapter 4

### **Forearc Slope Deformation above the Japan Trench Megathrust: Implications for Subduction Erosion**

In preparation for publication as:

Boston, B., Moore, G. F., Nakamura, Y., Kodaira, S. Forearc Slope Deformation above the Japan Trench Megathrust: Implications for Subduction Erosion.

*Abstract*— Subduction erosion is a commonly invoked model that is used to explain the tectonic subsidence of the Japan Trench forearc slope, although other models have explained the morphology and history of the margin. New multichannel seismic reflection and bathymetric data collected after the 2011 Tohoku earthquake provide the opportunity to investigate the detailed structure of the overriding plate near the earthquake epicenter and obtain new constraints on formation models. We use regional-residual separation of the local bathymetry to constrain fault scarp extents and local landward dipping forearc basins. Seismic images of these basins clearly show landward dipping horizons in the shallow section. These basins indicate a different mechanism for formation than the surrounding forearc slope, and we propose that these basins formed from local uplift. A regional basal unconformity mapped ~150 km along-trench has a highly variable relief, indicating that forearc slope subsidence occurs at multiple wavelengths in response to multiple different sources. We characterize the upper to middle slope transition and propose that this region may be the landward limit of major subduction erosion and also the main region for large mass wasting. Normal faults found in this setting have maximum lengths of ~20 km, limiting their role in margin processes. Our results place

constraints on the extent of major subduction erosion at the Japan Trench margin, and indicate that subduction erosion should be revisited as the sole model of formation for similar margins.

#### **4.1. Introduction**

The great 2011 Mw 9.0 Tohoku earthquake produced large coseismic slip of 30-60 m (e.g., Simons et al., 2011; Ide et al., 2011; Fujii et al., 2011; Chu et al., 2011; Wei et al., 2012), creating a tsunami with local coastal heights as great as 40 m (Mori et al., 2011). The earthquake occurred where the Cretaceous Pacific Plate subducts beneath northern Honshu (Fig. 4.1). This margin is considered an end-member case erosional margin (von Huene and Culotta, 1989; von Huene et al., 1994) defined by subsidence and normal faulting throughout the forearc slope. This tectonic erosion is thought to remove material from the upper plate through hydrofracturing (von Huene et al., 2004). However, part of the subsidence may be caused by changes in plate convergence rates that alter the plate boundary geometry (Regalla et al., 2013). The morphology of the overriding plate plays a direct role in tsunamigenesis, where horizontal displacement of a steep slope can vertically displace the water column contributing to tsunami formation (Tanioka and Satake, 1996). This type of horizontal seafloor motion is argued to have increased the tsunami height from the Tohoku earthquake (Hooper et al., 2013), revealing the importance of morphology to the margin. The coseismic slip area of large earthquakes generally correlates with the area with overlying forearc basins (Song and Simons, 2003; Wells et al., 2003; Fuller et al., 2006). However, the Japan Trench margin is now known to have great earthquakes but lacks large forearc basins. Further characterization of forearc slope deformation in regions, such as the Japan Trench, will highlight upper plate contributions to large earthquakes and tsunami generation.

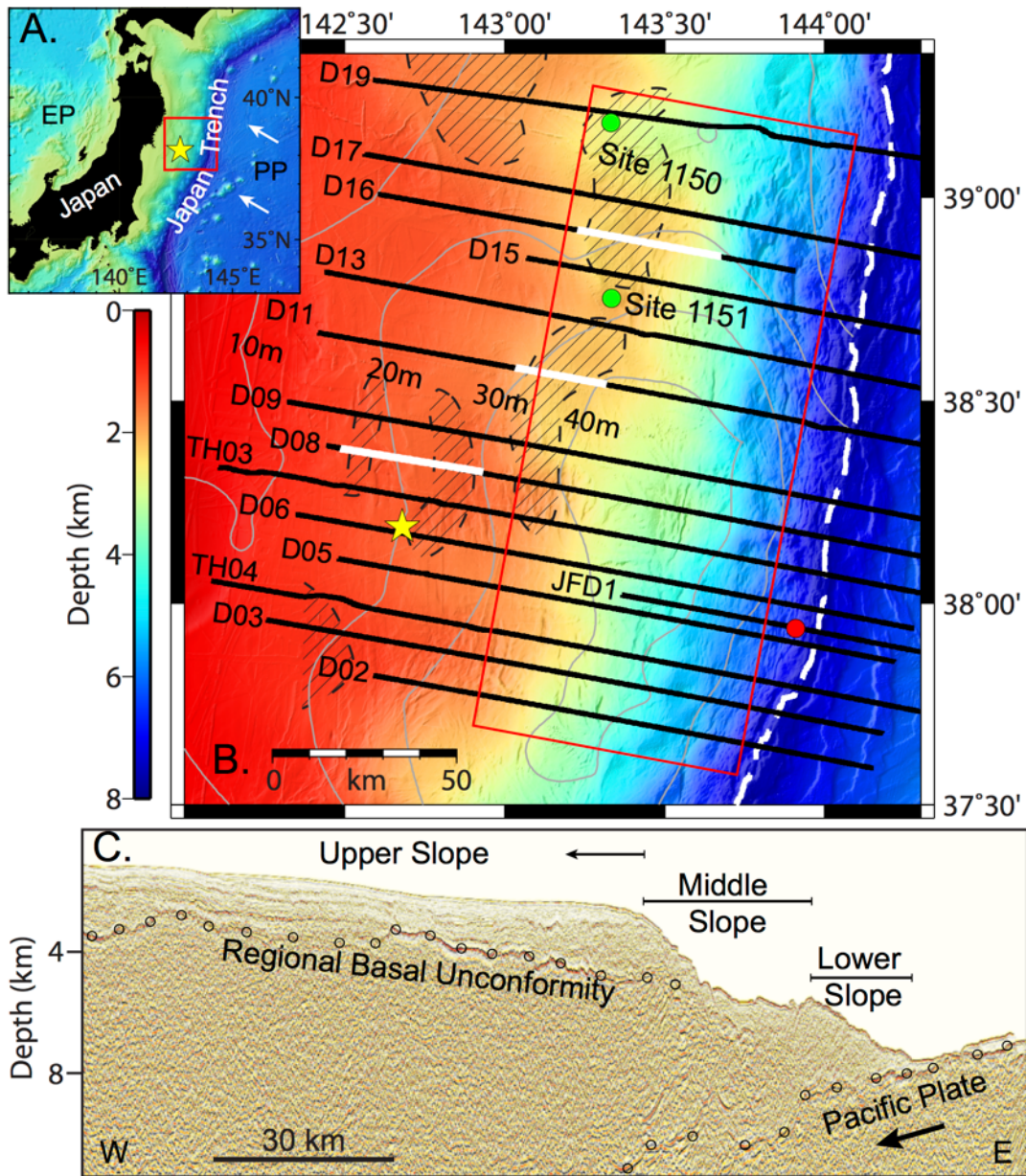


**Figure 4.1.** Japan Trench survey location and tectonic setting. **A.** Tectonic setting of the Japan Trench. The red box is the location of Fig. 4.1B, the yellow star shows the 2011 Tohoku earthquake epicenter (Chu et al., 2011), and white arrows show the convergence direction of the Pacific Plate – PP=Pacific Plate and EP= Eurasian Plate. **B.** Bathymetry map of the study region. Black lines are seismic profiles with white sections displayed in Fig. 4.3. White dashed curve is the deformation front (Boston et al., 2014). Grey contours show coseismic slip area for the 2011 earthquake (Wei et al., 2012). Diagonally shaded areas are identified as isolated basins (Arai et al., 2014). Green circles are ODP Sites and red circle is IODP Site C0019. The star is the earthquake epicenter. Red box is the location of Fig. 4.7. **C.** Seismic profile D17 with forearc slope morphology, the regional basal unconformity, and subducting Pacific Plate marked. The lower slope is the general location of the actively accreting prism.

The structure and lithology of the forearc region of northeastern Japan have been previously investigated by drilling and seismic surveys (e.g., Scientific Party, 1980; von Huene and Arthur, 1982; Tsuru et al., 2002; Suyehiro et al., 2003). In this region, the upper slope is underlain by ~2 km thick sequences of Neogene sediments (Fig. 4.1) dated by drilling during Deep Sea Drilling Project (DSDP) Legs 56 and 57 (Scientific Party, 1980). A regional unconformity separates silicified Cretaceous basement rocks from the overlying forearc slope strata (Scientific Party, 1980). This unconformity is interpreted to be a subaerial erosional surface marking sea level in the Miocene (von Huene et al., 1982), and we identify it as the regional basal unconformity (RBU). The Cretaceous basement is thought to have been an accretionary prism during the Paleogene (von Huene et al., 1982). The youngest overlying strata extend trenchward to a prominent boundary, against which a small frontal accretionary prism has formed along the lower slope (Fig. 4.1) (von Huene et al., 1994; Tsuru et al., 2000). Forearc basins have been found throughout the upper slope (Arai et al., 2014; von Huene and Arthur, 1982), and previous workers suggested that landward dipping forearc basins were formed through slip on a listric normal fault on the landward edge of the young basin (von Huene and Culotta, 1989). The shallow Neogene strata are largely characterized by normal faults that extend to the seafloor (Tsuru et al., 2000; Tsuru et al., 2002). Regional seismic reflection surveys show that the shallow structure in the northern Japan Trench forearc is similar throughout the margin (Tsuru et al., 2002; von Huene et al., 1994). However, north-south wide-angle seismic surveys find along-trench structural variations within the deep overlying plate that correlate with the segmentation of the interplate coupling (Fujie et al., 2013; Hayakawa et al., 2002). Observed seafloor fault scarps within the lower half of the middle prism are suggested to have been created during coseismic slip of the Tohoku earthquake (Tsuji et al., 2013). The frontal prism, penetrated

at Integrated Ocean Drilling Program (IODP) Site C0019 (Fig. 4.1), shows moderately to steeply dipping accreted mudstones above a plate boundary fault zone, ~5-15 m thick (Kirkpatrick et al., 2015).

Although many seismic reflection studies since the Tohoku earthquake have focused on imaging the trench axis and deformation front, which defines the seaward boundary of the frontal prism (e.g., Kodaira et al., 2012; Nakamura et al., 2013; Boston et al., 2014), the aim of this paper is to investigate the upper forearc slope using seismic reflection surveys collected in 2011 and 2013 in order to delineate the morphology of the margin. Many previous surveys have studied the full margin by using widely spaced reflection lines (e.g., Arai et al., 2014; Tsuru et al., 2002). We expand on these studies by focusing near the Tohoku epicenter with a denser survey grid that allows us to investigate in greater detail the margin's complex morphology and history. In this paper, we present data from 15 recently collected seismic reflection lines combined with regional bathymetry to characterize the Japan Trench regional basal unconformity, deformation styles within the forearc basins, and normal fault connectivity particularly in the middle to upper forearc slope to determine how the overriding plate has evolved over this megathrust region.

## **4.2. Methods**

This project focuses on an along-trench transect above the Tohoku megathrust earthquake in the central Japan Trench region and utilizes bathymetry and seismic reflection surveys. We used a compilation bathymetry grid of the Japan Trench region from *Boston et al., 2014* (Fig. 4.1). We applied a directional median filter (Kim and Wessel, 2008) for regional-residual separation of the bathymetry using a range of filter widths of  $20 \pm 10$  km that reduced the estimated median absolute deviation for the grid. This filtering technique prevents a biased

median due to a sloping regional trend, and we produced maps for, regional bathymetry, median absolute deviation, regional slope azimuth, and residual bathymetry (Fig. 4.2).

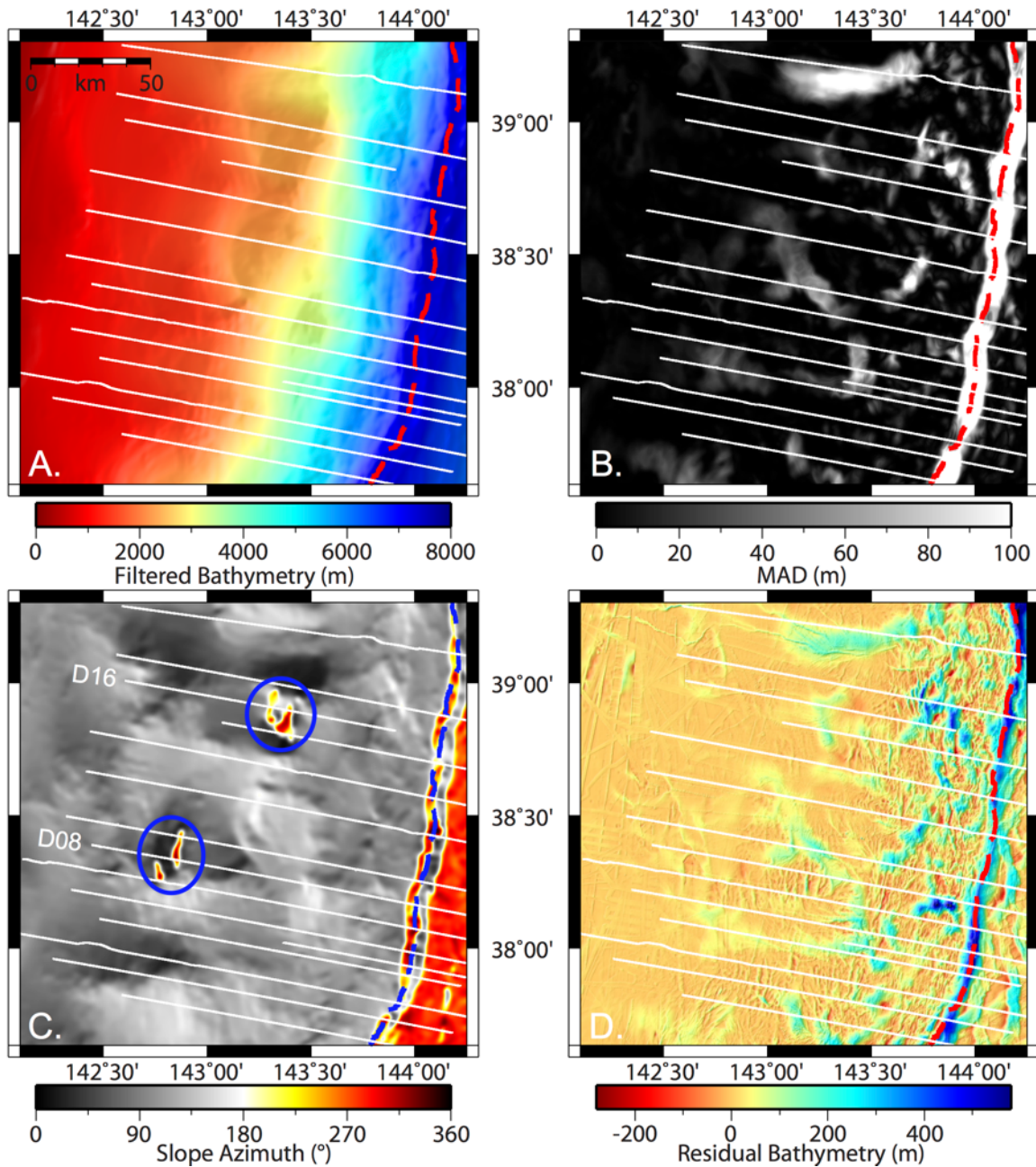


**Figure 4.2.** Regional-residual separation of bathymetry. White lines are the seismic profiles and the red or blue dashed line is the deformation front (Boston et al., 2014). **A.** Regional filtered bathymetry. **B.** Distribution of median absolute deviation (MAD) values from results in Fig. 4.2A. **C.** Slope azimuth of the regional bathymetry. Blue circles highlight two landward tilted forearc basins. **D.** Residual bathymetry.

We processed and analyzed 15 seismic reflection dip lines collected during four surveys in 2011 and 2013 on R/V *Kairei* (Fig. 4.1). The seismic system used a 6,000 m long, 12.5 m group interval, 444-channel hydrophone streamer cable to record seismic returns at a sampling interval of 2 ms. The source was a 7,800 in<sup>3</sup> air-gun array fired at 50 m intervals. This acquisition geometry generated a common mid-point (CMP) interval of 6.25 m. The seismic grid has an average along-strike line spacing of ~10 km. MCS processing included a conventional workflow of trace edit, CMP binning, predictive deconvolution, band-pass filter, velocity analysis, normal moveout correction, radon filter, and CMP stacking (Yilmaz, 2001). We performed Kirchhoff post-stack depth migration (PoSDM) on all the lines. To constrain our velocity model, we used velocities based on previous local refraction and reflection studies (e.g., Tsuru et al., 2000) for the initial velocity model. We iterated the velocity model through PoSDM to a final seismic depth section that produced the clearest image. Pre-stack depth migration (PSDM) was applied to lines D02, JFD1, TH03, D11, D17, and D19, iterating through horizon-based residual velocity analysis to produce a precise velocity model. We applied automatic gain control to all the final seismic images to enhance deeper reflections.

### **4.3. Results and Interpretations**

#### **4.3.1. Tilted Forearc Basins**

Our new bathymetry analysis provides new insights into the modern forearc basin processes of the Japan Trench forearc slope (Fig. 4.2). The median absolute deviation provides uncertainty bounds of the regional-residual bathymetry separation where different length-scale features are present. Because the forearc slope contains a continuum of length scales, we selected a final range of filter widths,  $20 \pm 10$  km, that included forearc basin features but reduced the median absolute deviation. The separation results are assessed by the spatial distribution of the

median absolute deviation between filter widths, and we find a generally low deviation except at a few locations such as the trench axis (Fig. 4.2B). Calculating the slope azimuth of the regional bathymetry shows a general seaward dip, except in two forearc basins (Fig. 4.2C). Instead, these two forearc basins have a seafloor that dips landward, suggesting a different process created these basins than the surrounding forearc slope. Whereas the landward dipping portion of the northern forearc basin covers the majority of the basin's area (~20 x 30 km), the southern basin landward dipping portion is small and more linear.

Seismic constraints validate our identification of these basins and provide clear images of tilted basins. Seismic lines D08 and D16 image the two landward dipping basins, whereas seismic line D11 reveals a buried landward dipping basin but with seaward dipping seafloor (Figs. 4.3 and 4.4). Line D08 images the southern basin and shows the bottom horizons onlapping onto the RBU, indicating the unconformity locally had high relief when buried by sediment. The overlying basin does not show major offset from normal faults; normal faults extending up from depth do not cut the overlying sediments, indicating that these faults are not currently active. We do not find any clear evidence for differential compaction altering the dip direction of the seafloor, as the small amount of sediment in this basin makes this unlikely. Line D16 shows a different style of landward dipping strata in the northern basin (Figs. 4.3 and 4.4). Here, both the oldest and youngest horizons have been tilted landward, with older, deeper horizons dipping more steeply. Along seismic line D11, the seafloor currently dips seaward but deeper horizons follow the anticlinal RBU. These seismic lines show both a current and a past history of landward tilted forearc basins.

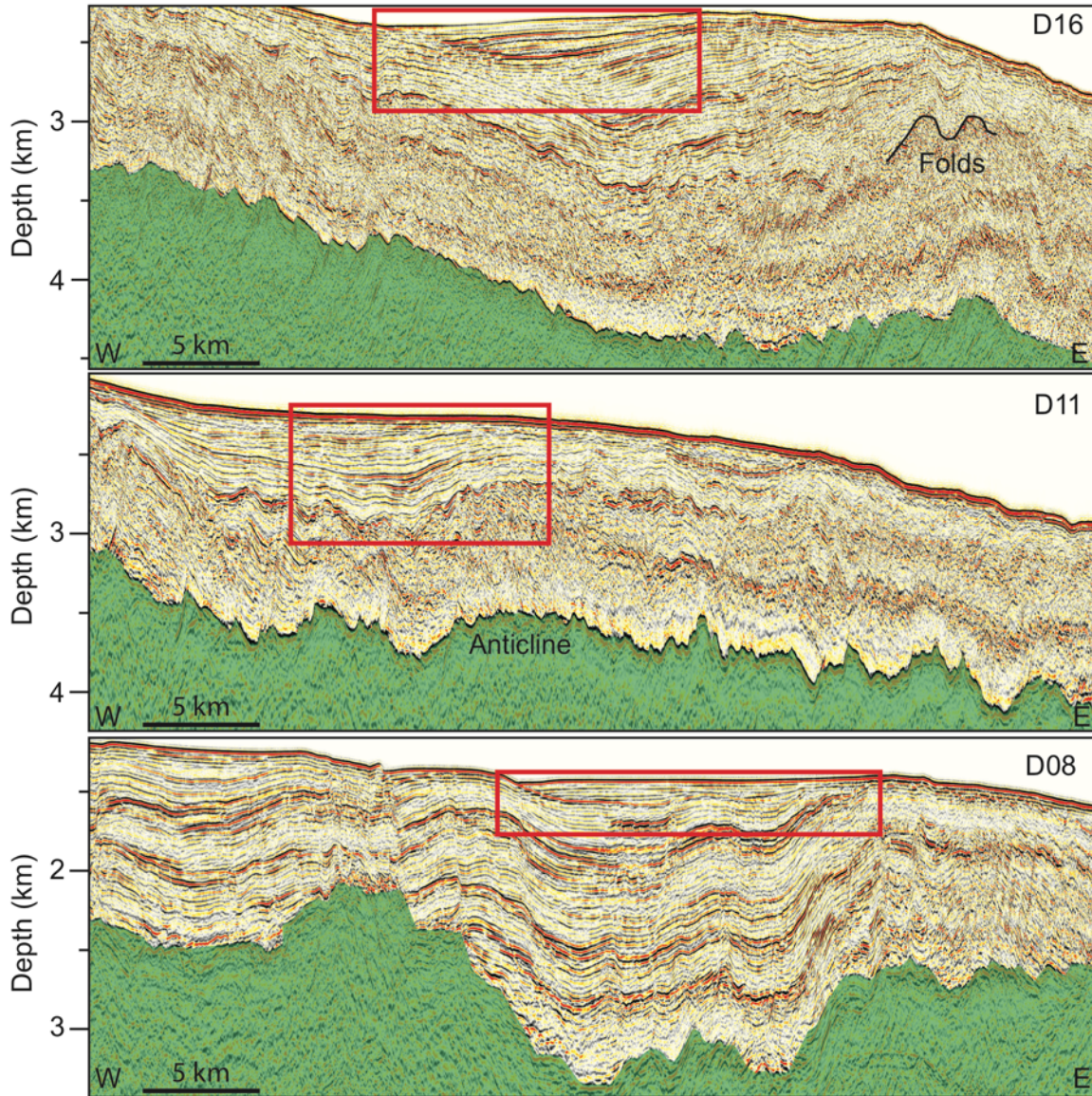


**Figure 4.3.** Seismic profiles of landward dipping basins. Locations in Fig. 4.1. Green is the regional basal unconformity. Red boxes are locations of the images shown in Fig. 4.4.

#### 4.3.2. The Regional Basal Unconformity and Slope Sediments

The RBU has recorded the Japan Trench forearc subsidence and deformational history since the period it marked sea level. We image the RBU within a region extending ~150 km along the trench. The unconformity appears as a positive high-amplitude reflection boundary (e.g., Fig. 4.1C) separating overlying continuous reflections from chaotic basement reflections,

consistent with previous seismic reflection interpretations throughout the margin (e.g., von Huene et al., 1982; Tsuru et al., 2002). The mapped RBU includes both confident and less confident interpretations, where poor signal return, multiple removal techniques, or the local geology reduces deeper image quality. The seaward extent of the unconformity is difficult to locate owing to poor image quality there. DSDP Legs 56 and 57 drilled through the basal unconformity outside our survey area (Scientific Party, 1980), but DSDP Site 584 was unable to penetrate to that depth (Shipboard Scientific Party, 1986). Ocean Drilling Program (ODP) Site 1150 is near seismic line D19, and ODP Site 1151 is near seismic line D15 (Fig. 4.1). Dating from these two sites indicate the upper sediments are Miocene and younger in age, however, the distance between lines and well sites is too significant for accurate correlation in this tectonic setting (Suyehiro et al., 2003). Neither of these ODP sites reached the deep basal unconformity. Our seismic data allow for a focus study of the RBU within a smaller area than previous studies.

The RBU morphology does not merely mimic the seafloor. The RBU exhibits >1 km relief within our survey area (Fig. 4.5), whereas the seafloor remains fairly consistent on the western portion of the survey. Both high and low relief features with variable wavelengths are found throughout many seismic lines. RBU depressions of ~1.5 km deep and ~30 km long, such as in line D11, are some of the largest. However, broader antiformal morphology seen in line D06 also is present. Many features of the RBU are not present line-to-line indicating their length is less than the seismic grid interval. The seaward ~50 km of the RBU consistently dips seaward in each seismic line (Fig. 4.5), however, the landward portion shows variable morphology.

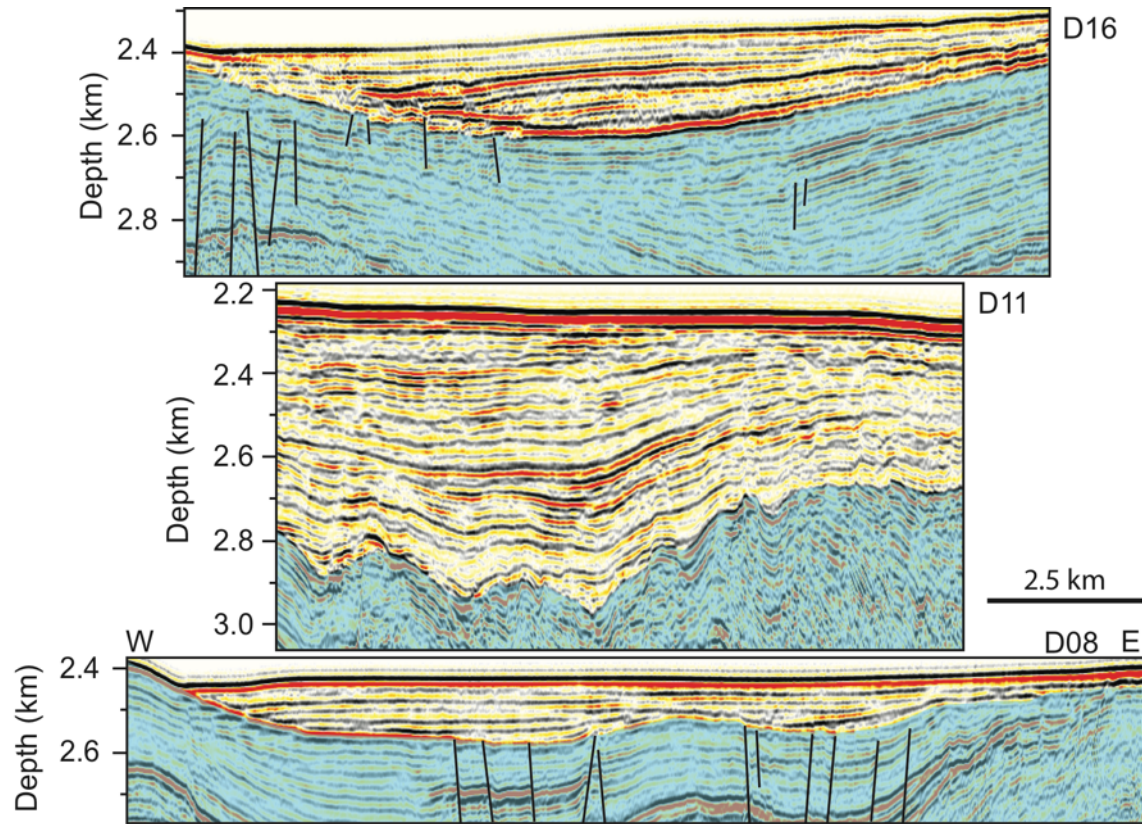


**Figure 4.4.** Shallow basins at the Japan Trench forearc. Locations are in Fig. 4.3. Blue region marks the onlapping surface.

We produced both a map view of the RBU (Fig. 4.6A), from gridding and smoothing with a 25 km Gaussian filter of seismic interpretations, and an isopach map of the sedimentary fill above the unconformity (Fig. 4.6B), created using the filtered bathymetry grid and the smoothed unconformity grid. The map view of the RBU shows a consistent increase in depth towards the east side of the map, which generally follows the deformation front's trace (Fig. 4.6). The isopach map reveals that the slope fill varies in thickness by ~3000 m and thins towards its seaward edge (Figs. 4.5 and 4.6). This thinning pattern is consistent throughout all the lines. This is also the location of a break in seafloor dip to the middle slope.

### 4.3.3 Characteristics of the Upper to Middle Slope Transition

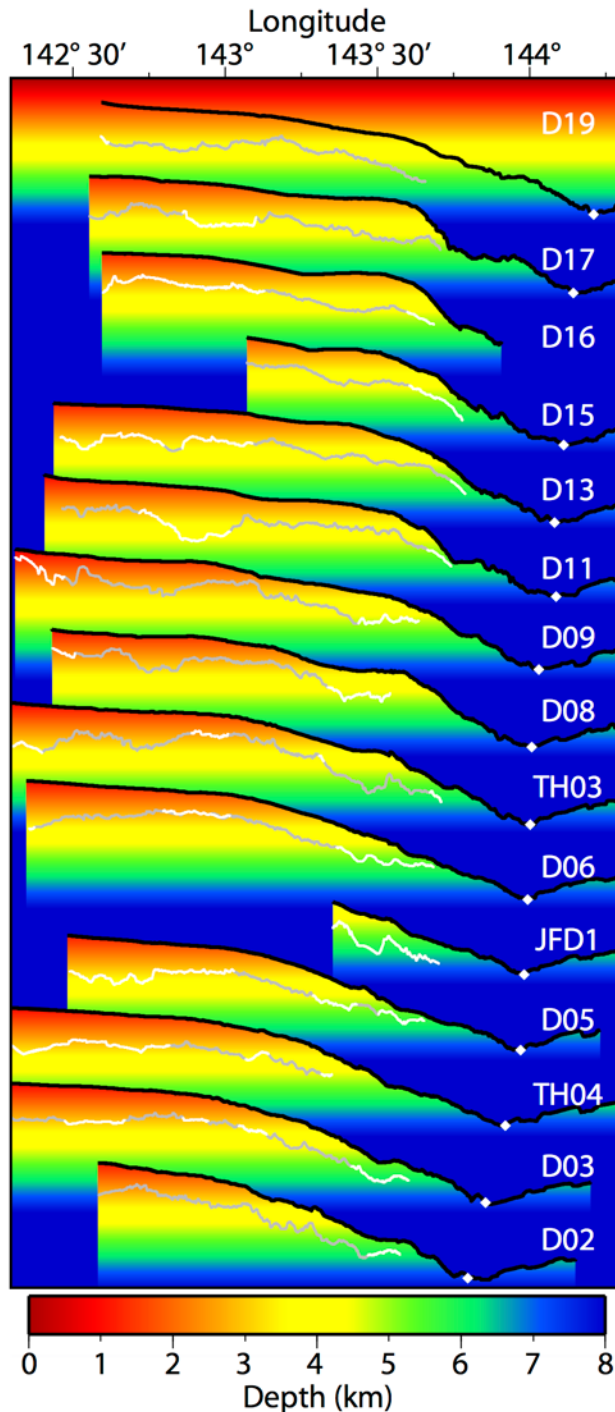


**Figure 4.5.** Seafloor and RBU profiles from seismic lines. The seafloor is in black and the RBU is in grey with high confidence and white in lower confidence. White diamonds are the location of the deformation front (Boston et al., 2014).

We define the upper and middle slope at the Japan Trench margin in the manner of Arai et al. (2014), where the upper slope has a relatively flat seafloor inclined at less than  $3^\circ$  and the middle slope has a relatively steep slope that starts at approximately 3 km depth. Our focus is on the transition between the two slopes (Fig. 4.1C).

Regional-residual separation of the bathymetry grid (Figs. 4.2 and 4.6) allows for better analysis of both short-length-scale bathymetric features and the regional bathymetry at the upper to middle slope transition. The residual bathymetry largely highlights fault scarps, channels, and small-scale basins. We find the lateral continuity of normal fault scarps is as great as  $\sim 20$  km, but commonly is only  $\sim 10$  km (Fig. 4.7).

Anticlines or ridges are most commonly found near the lower slope but are also located further landward and interspersed between normal faults. This fault pattern

indicates the upper to middle slope transition is not solely a normal fault boundary.

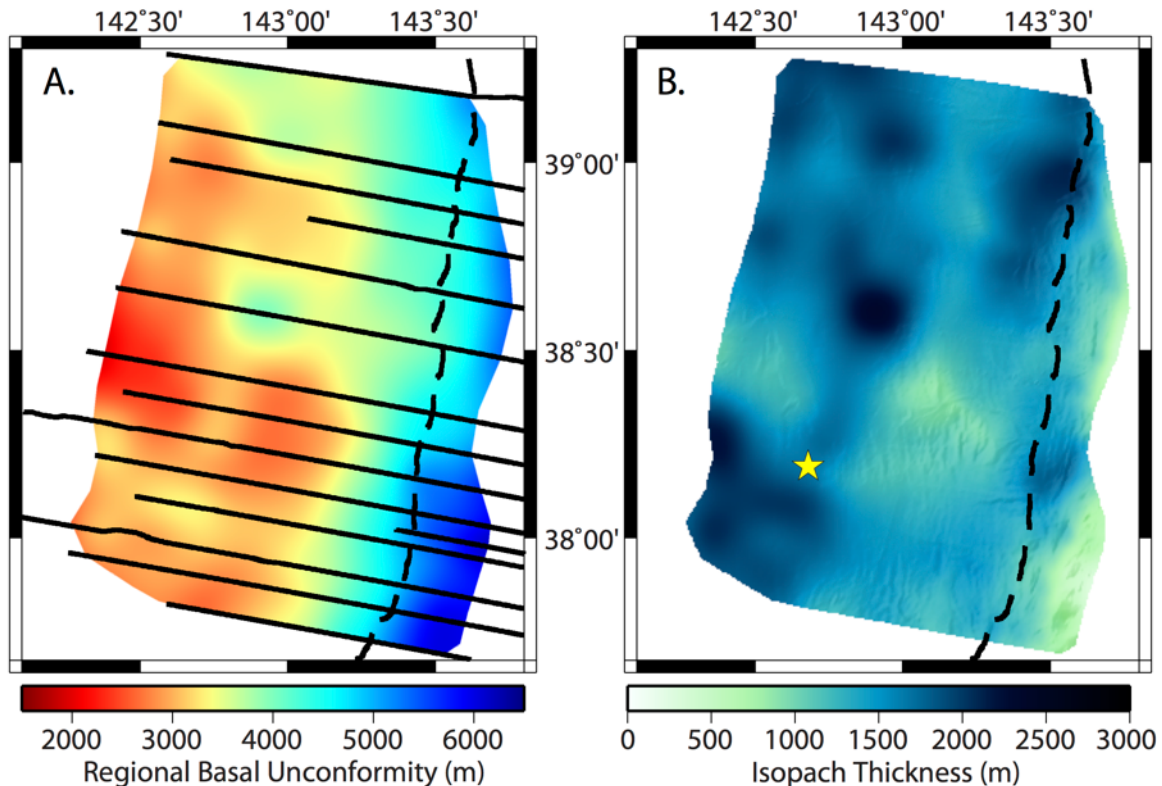


**Figure 4.6.** Map view of the RBU and slope fill sediment thickness map. **A.** Smoothed surface of the regional basal unconformity. Black lines are the seismic profiles to show interpretation constraints. Black dashed line in A. and B. is the deformation front shifted landward by 45 km. **B.** Isopach map of sediments above TK, with seafloor shaded relief. Black lines show seismic profiles and constraints on the smoothed grid and the star is the 2011 Tohoku earthquake epicenter. One general trend of thinning near the eastern edge is found throughout the region. However, the overall region shows multiple thicker basins.

Our seismic lines show that the transition between the upper and middle slope is complex (Fig. 4.8). Line D03 shows a large anticline on the seaward edge (Fig. 4.8), ~30 km west of the deformation front. This anticline is ~4-6 km long along strike and contains a local bathymetric high (Fig. 4.7). Line D05 shows a smooth seafloor with normal faults offsetting the sediment fill and a ~500 m high ridge. Line D09 reveals that normal faults offset the RBU and slope fill but do not extend up to the seafloor. Basin fill thickness of ~1 km is found near the center of the profile where the seismic amplitude of the RBU becomes weaker and thus forces a less confident

interpretation. Line D13 shows the seafloor slopes seaward, to the east, but bedding dips landward and fills a forearc basin similar to seismic line D11 (Figs. 4.3 and 4.4). The nearby location of these basins and similarities in tilting suggests that this previous tilting event was continuous for greater than 10 km along-trench. The basin in which lines D11 and D13 are located is bounded to the north by a small bathymetric high where ODP Site 1151 is located (Figs. 4.3 and 4.1). This separates the basin of D11 and D13 from the northern basin of line D16, which has a landward dipping seafloor. Furthermore at line D13, an anticline of ~2.5 km in width is found on the seaward edge of the overlying basin fill, and it does not deform the RBU (Fig. 4.8). However, the RBU dips landward where the overlying fill dips seaward with the RBU forming a much broader anticline of ~15 km wide. Line D17 shows thickening of the upper slope sediment fill near the upper to middle slope transition until a steep slope break. Here, the slope fill goes from ~2.5 km thick to <1 km thick over a distance of ~5 km. At the slope break, the seafloor and the RBU are offset by multiple normal faults. Line D19, ~12 km north of D17, shows a very different morphology. Line D19 shows slope fill that is heavily deformed by normal faults like in D17, but the RBU remains fairly continuous. An anticline on the RBU appears to have a deeper landward dipping reflection beneath it and deforms the seafloor. Slope fill thickens seaward on line D19 until this anticline and then thins seaward. The acquisition geometry of line D19 within this transition zone has a kink in it, caused by the need to avoid debris in the water, and this kink may cause seismic artifacts. Nonetheless, the disparate seismic profiles reveal a complex and nonuniform transition between the upper and middle slope. Both seismic and bathymetric data show normal faults are limited to lateral extents of ~20 km with anticlines interspersed between them.

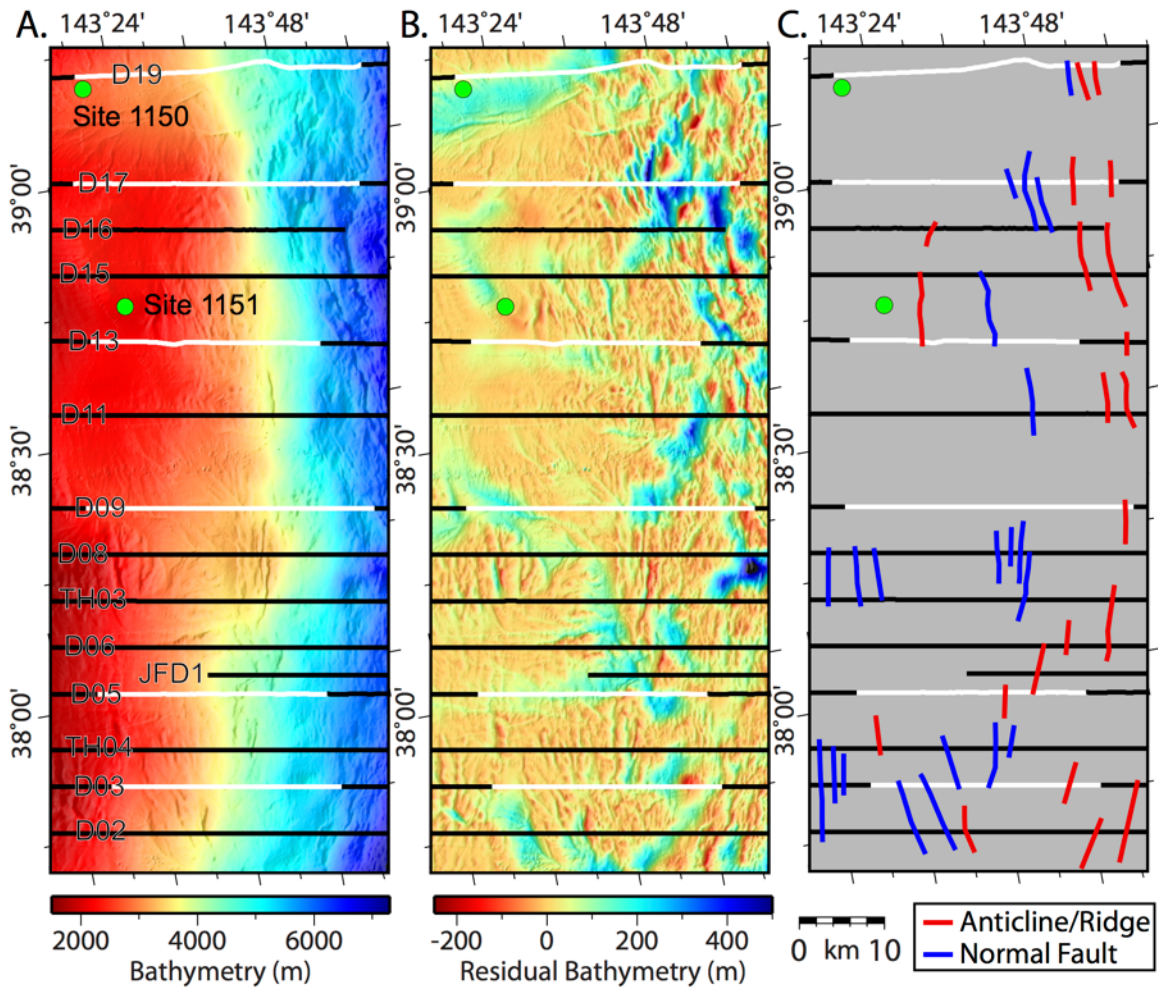


**Figure 4.7.** Bathymetry and residual bathymetry at the upper to midslope boundary and structural interpretations. The location of this region is shown in Figure 4.1B. Black lines are seismic lines with the white sections presented in Fig. 8. **A.** Bathymetry with seismic line names. **B.** Residual Bathymetry. **C.** Seafloor breaching large-scale features constrained from seismic profiles.

#### 4.4. Discussion

Our results provide new insights into subduction erosion at the Japan Trench margin. Listic normal faults on the landward edge of the forearc basin were previously thought to deform overlying strata (von Huene and Culotta, 1989). However, we do not find evidence for a basin-forming listric fault system. Compaction of sediments at D16 is unlikely to be responsible for the landward tilt because the sediments thicken seaward, and compaction of them would

cause a tilt away from land. We propose that the basins dip landward in response to local uplift at the east side of the basins. This is based on multiple seismic lines displaying anticlines on the seaward edge of the landward dipping forearc basin strata. Owing to the width (~20 km) of these basins, a buried normal fault beneath the RBU causing the tilt is less viable but would also suggest additional recent deep processes occurring. The location of RBU anticlines near the tilted basin (e.g., D11 and D16) also indicates that tilting was not from a normal fault. Uplift within this region suggests that subduction erosion is not the only factor responsible for the current morphology of the forearc slope. The Japan arc and backarc experienced a change from trench-perpendicular extension to shortening in the Miocene (Kato et al., 2006). This onshore shortening may have extended seaward to the upper slope basins. Furthermore, benthic foraminifera assemblages indicate shallowing of the forearc seafloor at Site 438/439 since 3.5 Ma, which indicates uplift of the region (Arthur et al., 1980). The subducting plate geometry may also have changed during this time period due to accelerations in plate convergence rate and decreased plate buoyancy, and may explain the regional subsidence patterns (Regalla et al., 2013). However, the middle slope has a larger and increasing amount of subsidence towards the trench that cannot be explained by plate convergence rates. The RBU consistently dips seaward and slope fill consistently thins at the middle slope (Figs. 4.5 and 4.6), whereas the RBU at the upper slope expresses no uniform pattern. This pattern suggests subduction erosion may occur under the middle slope, but other processes play a larger role in the upper slope deformation. Subducting siliceous sediments at the Japan Trench have a maximized dehydration rate zone of ~50-60 km from the deformation front (Kimura et al., 2012). This dehydration zone is at the seaward edge of the upper slope to the middle slope, and this water influx may cause hydrofracturing of the overriding plate and subduction erosion within this area (von Huene et al.,

2004). This pattern indicates that major subduction erosion has a landward limit. However, the location of the slope transition is also in the general location of a sharp bend in the subducting Pacific Plate, where the subduction angle changes from  $< 5^\circ$  to  $> 13^\circ$  in a short distance and a bending axis located at  $\sim 143^\circ\text{E}$  -  $143.5^\circ\text{E}$  in our study area (Fujie et al., 2006; Ito et al., 2005). Work by others has suggested that the plate interface could be rough or that some earthquakes occur on subfaults off from the main plate boundary fault and that there is no large bend in the subducting plate (Zhan et al., 2012). Thus, the role in the subducting plate bend on the middle slope deformation is still unclear. Our results indicate a landward limit on major subduction erosion and that other mechanisms influence the Japan Trench upper slope.

Seafloor steepening and slope fill thinning at the upper to middle slope transition suggests seafloor erosion is present at the middle slope (Figs. 4.6 and 4.8). Additionally, seismic reflectors become chaotic within the middle slope implying further deformation. Previous bathymetry analysis, deep-sea submersible observations, and tsunami modeling indicate potential submarine landslide locations at the middle slope region that may have impacted tsunami generation during the Tohoku event (Kawamura et al., 2012; Tappin et al., 2014). We find no direct evidence of major mass wasting events on the upper slope, within our seismic resolution, but middle slope erosion suggests the upper to middle slope transition is the landward boundary for major mass wasting events.

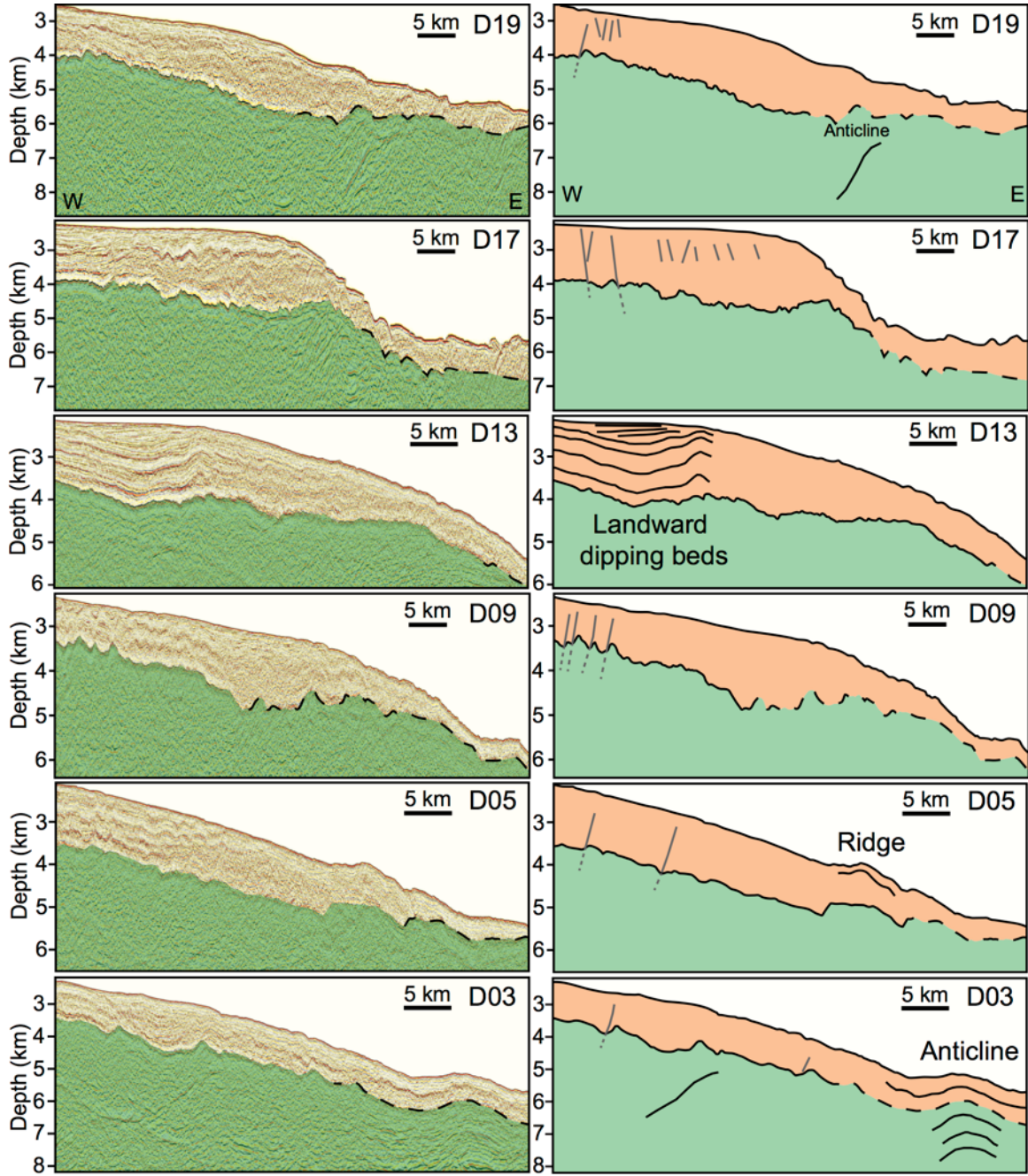


**Figure 4.8.** Seismic profiles of the western midslope boundary (left column) and general interpretations (right column). Locations are in Fig. 4.6. Green is the regional basal unconformity with dashed regions having lower certainty.

Based on previous work, a major normal fault at the upper to middle slope transition has been inferred to let the middle and lower slope act as a pop-up structure (Tsuji et al., 2011; Tsuji et al., 2013). Other erosional subduction zones, such as the central Chilean margin, are also suggested to have a master normal fault at the seaward upper slope boundary (Contreras-Reyes et al., 2015). Release of gravitational potential energy in such setting can induce a pop-up structure and influence tsunamigenesis (McKenzie and Jackson, 2012). However, this interpretation of a pop-up structure implies that the major normal fault is regional tectonic feature. Our results do not show a regional normal fault, with faults lengths only as great as ~20 km (Figs. 4.7 and 4.8). Due to wide grid spacings, we still lack an understanding of how these faults grow throughout the margin (e.g., Walsh et al., 2003). Aftershock data showed normal fault type mechanisms widely distributed in the overriding plate (Asano et al., 2011), however, a densely-spaced ocean bottom seismograph survey revealed a 45-km-wide aseismic wedge for the overriding prism's toe (Obana et al., 2013). Nakamura et al. (2014) showed a clear velocity contrast between low velocity accreted sediments and a higher velocity backstop for seismic line JFD1. However, this backstop interface is further seaward than the upper to middle slope transition. Due to the range of deformational styles at the upper to middle slope transition and lack of regional fault connectivity, normal faults at the upper to middle slope transition, and their presumed pop-up structure, are not an indicator of a large tsunami source area at the Japan Trench margin.

Forearc basins have been correlated with large earthquakes (Song and Simons, 2003; Wells et al., 2003). We find multiple forearc basins and slope sediment thickness as great as ~3 km (Fig. 4.6). The location of the 2011 Tohoku earthquake epicenter does not correlate with any thick basin location (Fig. 4.6). The spatial widths of these basins, as great as ~50 km, is much smaller than the slip area of the Tohoku earthquake (Fig. 4.1) and therefore may have a smaller

component in influencing deeper earthquake processes. However, the role of forearc basins at the Japan Trench margin is still elusive since our surveys focused in only a region of a great earthquake.

#### **4.5. Conclusions**

New seismic reflection profiles and interpretations of the Japan Trench forearc slope provide new insights for marginal processes. This dataset shows that relief on the regional basal unconformity must have existed before overlying sediments were deposited and uplift tilted some forearc basins, and that the unconformity was offset by normal faults. Forearc slope fill and forearc basins contain sediment thicknesses as great as ~3 km, but their locations show no correlation with the Tohoku earthquake epicenter. The upper to middle slope transition shows both extensional and shortening features, with normal faults (maximum lengths of ~ 20 km) located near anticlines, indicating that single normal faults are not capable of affecting margin-wide processes. We find thinning of sediments and seaward dip of the regional basal unconformity at this transition on all of the seismic lines in our survey area, which can be explained by a subduction erosion model. However, along the upper slope, we observe that the regional basal unconformity contains a more variable pattern of deformation and that uplift occurred in selected regions, indicating that a purely erosional model is not appropriate for this complex forearc region. This pattern suggests a landward limit to major subduction erosion at the Japan Trench upper to middle slope transition, which may have implications for similar behavior at other erosional margins.

#### **Acknowledgments**

Funding was provided through the National Science Foundation (grants OCE-1260718 and OCE-1138051). The authors are grateful to the scientists and crews of KR11-05 Leg 2, KR11-

E03, KR11-E05, and KR13-01. We thank Paradigm Geophysical and Landmark Graphics (Halliburton) for their academic software licenses that made this work possible.

## References

- Arai, K., Inoue, T., Ikehara, K., Sasaki, T., 2014. Episodic subsidence and active deformation of the forearc slope along the Japan Trench near the epicenter of the 2011 Tohoku Earthquake. *Earth Planet. Sci. Lett.* 408, 9-15. doi:10.1016/j.epsl.2014.09.048.
- Arthur, M.A., von Huene, R., Adelseck, C.G., 1980. Sedimentary evolution of the Japan fore-arc region off northern Honshu, Legs 56 and 57, Deep Sea Drilling Project, in: Lee, M., Stout, L.N. (Eds.), *Initial Reports of the Deep Sea Drilling Project, Legs 56 and 57 (Part 1)*, Washington, D.C., pp. 521-612.
- Asano, Y., Saito, T., Ito, Y., Shiomi, K., Hirose, H., Matsumoto, T., Aoi, S., Hori, S., Sekiguchi, S., 2011. Spatial distribution and focal mechanisms of aftershocks of the 2011 off the Pacific coast of Tohoku Earthquake. *Earth Planets Space* 63, 669-673. doi:10.5047/Eps.2011.06.016.
- Boston, B., Moore, G.F., Nakamura, Y., Kodaira, S., 2014. Outer-rise normal fault development and influence on near-trench décollement propagation along the Japan Trench, off Tohoku. *Earth Planets Space* 66, 135. doi:10.1186/1880-5981-66-135.
- Chu, R., Wei, S., Helmberger, D.V., Zhan, Z., Zhu, L., Kanamori, H., 2011. Initiation of the great Mw 9.0 Tohoku–Oki earthquake. *Earth Planet. Sci. Lett.* 308, 277-283. doi:10.1016/j.epsl.2011.06.031.
- Contreras-Reyes, E., Ruiz, J.A., Becerra, J., Kopp, H., Reichert, C., Maksymowicz, A., Arriagada, C., 2015. Structure and tectonics of the central Chilean margin (31°–33°S): implications for subduction erosion and shallow crustal seismicity. *Geophys. J. Int.* 203, 776-791. doi:10.1093/gji/ggv309.
- Fujie, G., Ito, A., Kodaira, S., Takahashi, N., Kaneda, Y., 2006. Confirming sharp bending of the Pacific plate in the northern Japan trench subduction zone by applying a travelttime mapping method. *Phys. Earth Planet. Inter.* 157, 72-85. doi:10.1016/j.pepi.2006.03.013.
- Fujie, G., Miura, S., Kodaira, S., Kaneda, Y., Shinohara, M., Mochizuki, K., Kanazawa, T., Murai, Y., Hino, R., Sato, T., Uehira, K., 2013. Along-trench structural variation and seismic coupling in the northern Japan subduction zone. *Earth Planets Space* 65, 75-83. doi:10.5047/eps.2012.06.003.
- Fujii, Y., Satake, K., Sakai, S., Shinohara, M., Kanazawa, T., 2011. Tsunami source of the 2011 off the Pacific coast of Tohoku Earthquake. *Earth Planets Space* 63, 815-820. doi:10.5047/Eps.2011.06.010.

- Fuller, C.W., Willett, S.D., Brandon, M.T., 2006. Formation of forearc basins and their influence on subduction zone earthquakes. *Geology* 34, 65-68. doi:10.1130/g21828.1.
- Hayakawa, T., Kasahara, J., Hino, R., Sato, T., Shinohara, M., Kamimura, A., Nishino, M., Sato, T., Kanazawa, T., 2002. Heterogeneous structure across the source regions of the 1968 Tokachi-Oki and the 1994 Sanriku-Haruka-Oki earthquakes at the Japan Trench revealed by an ocean bottom seismic survey. *Phys. Earth Planet. Inter.* 132, 89-104. doi:10.1016/S0031-9201(02)00046-8.
- Hooper, A., Pietrzak, J., Simons, W., Cui, H., Riva, R., Naeije, M., Terwisscha van Scheltinga, A., Schrama, E., Stelling, G., Socquet, A., 2013. Importance of horizontal seafloor motion on tsunami height for the 2011 Mw=9.0 Tohoku-Oki earthquake. *Earth Planet. Sci. Lett.* 361, 469-479. doi:10.1016/j.epsl.2012.11.013.
- Ide, S., Baltay, A., Beroza, G.C., 2011. Shallow dynamic overshoot and energetic deep rupture in the 2011 Mw 9.0 Tohoku-Oki earthquake. *Science* 332, 1426-1429. doi:10.1126/science.1207020.
- Ito, A., Fujie, G., Miura, S., Kodaira, S., Kaneda, Y., Hino, R., 2005. Bending of the subducting oceanic plate and its implication for rupture propagation of large interplate earthquakes off Miyagi, Japan, in the Japan Trench subduction zone. *Geophys. Res. Lett.* 32. doi:10.1029/2004gl022307.
- Kato, N., Sato, H., Umino, N., 2006. Fault reactivation and active tectonics on the fore-arc side of the back-arc rift system, NE Japan. *J. Struct. Geol.* 28, 2011-2022. doi:10.1016/j.jsg.2006.08.004.
- Kawamura, K., Sasaki, T., Kanamatsu, T., Sakaguchi, A., Ogawa, Y., 2012. Large submarine landslides in the Japan Trench: A new scenario for additional tsunami generation. *Geophys. Res. Lett.* 39, L05308. doi:10.1029/2011gl050661.
- Kim, S.-S., Wessel, P., 2008. Directional median filtering for regional-residual separation of bathymetry. *Geochem. Geophys. Geosyst.* 9, Q03005. doi:10.1029/2007gc001850.
- Kimura, G., Hina, S., Hamada, Y., Kameda, J., Tsuji, T., Kinoshita, M., Yamaguchi, A., 2012. Runaway slip to the trench due to rupture of highly pressurized megathrust beneath the middle trench slope: The tsunamigenesis of the 2011 Tohoku earthquake off the east coast of northern Japan. *Earth Planet. Sci. Lett.* 339-340, 32-45. doi:10.1016/j.epsl.2012.04.002.
- Kirkpatrick, J.D., Rowe, C.D., Ujiie, K., Moore, J.C., Regalla, C., Remitti, F., Toy, V., Wolfson-Schwehr, M., Kameda, J., Bose, S., Chester, F.M., 2015. Structure and lithology of the Japan Trench subduction plate boundary fault. *Tectonics* 34, 53-69. doi:10.1002/2014tc003695.
- Kodaira, S., No, T., Nakamura, Y., Fujiwara, T., Kaiho, Y., Miura, S., Takahashi, N., Kaneda, Y., Taira, A., 2012. Coseismic fault rupture at the trench axis during the 2011 Tohoku-oki earthquake. *Nat. Geosci.* 5, 646-650. doi:10.1038/Ngeo1547.

- McKenzie, D., Jackson, J., 2012. Tsunami earthquake generation by the release of gravitational potential energy. *Earth Planet. Sci. Lett.* 345-348, 1-8. doi:10.1016/j.epsl.2012.06.036.
- Mori, N., Takahashi, T., Yasuda, T., Yanagisawa, H., 2011. Survey of 2011 Tohoku earthquake tsunami inundation and run-up. *Geophys. Res. Lett.* 38, L00G14. doi:10.1029/2011gl049210.
- Nakamura, Y., Kodaira, S., Miura, S., Regalla, C., Takahashi, N., 2013. High-resolution seismic imaging in the Japan Trench axis area off Miyagi, northeastern Japan. *Geophys. Res. Lett.* 40, 1713-1718. doi:10.1002/grl.50364.
- Nakamura, Y., Kodaira, S., Cook, B.J., Jeppson, T., Kasaya, T., Yamamoto, Y., Hashimoto, Y., Yamaguchi, M., Obana, K., Fujie, G., 2014. Seismic imaging and velocity structure around the JFAST drill site in the Japan Trench: low Vp, high Vp/Vs in the transparent frontal prism. *Earth Planets Space* 66, 121. doi:10.1186/1880-5981-66-121.
- Obana, K., Kodaira, S., Shinohara, M., Hino, R., Uehira, K., Shiobara, H., Nakahigashi, K., Yamada, T., Sugioka, H., Ito, A., Nakamura, Y., Miura, S., No, T., Takahashi, N., 2013. Aftershocks near the updip end of the 2011 Tohoku-Oki earthquake. *Earth Planet. Sci. Lett.* 382, 111-116. doi:10.1016/j.epsl.2013.09.007.
- Regalla, C., Fisher, D.M., Kirby, E., Furlong, K.P., 2013. Relationship between outer forearc subsidence and plate boundary kinematics along the Northeast Japan convergent margin. *Geochem. Geophys. Geosyst.* 14, 5227-5243. doi:10.1002/2013gc005008.
- Scientific Party, 1980. Initial Reports of the Deep Sea Drilling Project, 56, 57, Washington (U.S. Govt. Printing Office). doi:10.2973/dsdp.proc.5657.1980.
- Shipboard Scientific Party, 1986. Site 584, in: Kagami, H., Karig, D.E., Coulbourn, W.T., et al. (Eds.), Initial Reports of Deep Sea Drilling Project, 87, Washington (U.S. Govt. Printing Office). doi:10.2973/dsdp.proc.87.105.1986.
- Simons, M., Minson, S.E., Sladen, A., Ortega, F., Jiang, J., Owen, S.E., Meng, L., Ampuero, J.P., Wei, S., Chu, R., Helmberger, D.V., Kanamori, H., Hetland, E., Moore, A.W., Webb, F.H., 2011. The 2011 magnitude 9.0 Tohoku-Oki earthquake: mosaicking the megathrust from seconds to centuries. *Science* 332, 1421-1425. doi:10.1126/science.1206731.
- Song, T.R., Simons, M., 2003. Large trench-parallel gravity variations predict seismogenic behavior in subduction zones. *Science* 301, 630-633. doi:10.1126/science.1085557.
- Suyehiro, K., Sacks, I.S., Acton, G.D., Oda, M., 2003. Proc. ODP, Sci. Results, 186, College Station, TX (Ocean Drilling Program). doi:10.2973/odp.proc.sr.186.2003.
- Tanioka, Y., Satake, K., 1996. Tsunami generation by horizontal displacement of ocean bottom. *Geophys. Res. Lett.* 23, 861-864. doi:10.1029/96gl00736.
- Tappin, D.R., Grilli, S.T., Harris, J.C., Geller, R.J., Masterlark, T., Kirby, J.T., Shi, F., Ma, G., Thingbaijam, K.K.S., Mai, P.M., 2014. Did a submarine landslide contribute to the 2011 Tohoku tsunami? *Mar. Geol.* 357, 344-361. doi:10.1016/j.margeo.2014.09.043.

- Tsuji, T., Ito, Y., Kido, M., Osada, Y., Fujimoto, H., Ashi, J., Kinoshita, M., Matsuoka, T., 2011. Potential tsunamigenic faults of the 2011 off the Pacific coast of Tohoku Earthquake. *Earth Planets Space* 63, 831-834. doi:10.5047/eps.2011.05.028.
- Tsuji, T., Kawamura, K., Kanamatsu, T., Kasaya, T., Fujikura, K., Ito, Y., Tsuru, T., Kinoshita, M., 2013. Extension of continental crust by anelastic deformation during the 2011 Tohoku-oki earthquake: The role of extensional faulting in the generation of a great tsunami. *Earth Planet. Sci. Lett.* 364, 44-58. doi:10.1016/j.epsl.2012.12.038.
- Tsuru, T., Park, J.O., Takahashi, N., Kodaira, S., Kido, Y., Kaneda, Y., Kono, Y., 2000. Tectonic features of the Japan Trench convergent margin off Sanriku, northeastern Japan, revealed by multichannel seismic reflection data. *J. Geophys. Res.* 105, 16403-16413. doi:10.1029/2000jb900132.
- Tsuru, T., Park, J.O., Miura, S., Kodaira, S., Kido, Y., Hayashi, T., 2002. Along-arc structural variation of the plate boundary at the Japan Trench margin: Implication of interplate coupling. *J. Geophys. Res.* 107, 2357. doi:10.1029/2001jb001664.
- von Huene, R., Arthur, M.A., 1982. Sedimentation across the Japan trench off northern Honshu Island. Geological Society, London, Special Publications 10, 27-48. doi:10.1144/GSL.SP.1982.010.01.02.
- von Huene, R., Langseth, M., Nasu, N., Okada, H., 1982. A summary of Cenozoic tectonic history along the IPOD Japan Trench transect. *Geol. Soc. Am. Bull.* 93, 829. doi:10.1130/0016-7606(1982)93<829:asoth>2.0.co;2.
- von Huene, R., Culotta, R., 1989. Tectonic erosion at the front of the Japan Trench convergent margin. *Tectonophysics* 160, 75-90.
- von Huene, R., Klaeschen, D., Cropp, B., Miller, J., 1994. Tectonic structure across the accretionary and erosional parts of the Japan Trench margin. *J. Geophys. Res.* 99, 22349-22361. doi:10.1029/94JB01198.
- von Huene, R., Ranero, C.R., Vannucchi, P., 2004. Generic model of subduction erosion. *Geology* 32, 913-916. doi:10.1130/g20563.1.
- Walsh, J.J., Bailey, W.R., Childs, C., Nicol, A., Bonson, C.G., 2003. Formation of segmented normal faults: a 3-D perspective. *J. Struct. Geol.* 25, 1251-1262. doi:10.1016/S0191-8141(02)00161-X.
- Wei, S.J., Graves, R., Helmberger, D., Avouac, J.P., Jiang, J.L., 2012. Sources of shaking and flooding during the Tohoku-Oki earthquake: A mixture of rupture styles. *Earth Planet. Sci. Lett.* 333, 91-100. doi:10.1016/J.epsl.2012.04.006.
- Wells, R.E., Blakely, R.J., Sugiyama, Y., Scholl, D.W., Dinterman, P.A., 2003. Basin-centered asperities in great subduction zone earthquakes: A link between slip, subsidence, and subduction erosion? *J. Geophys. Res.* 108, 2507. doi:10.1029/2002jb002072.

Yilmaz, Ö., 2001. *Seismic Data Analysis: Processing, Inversion, and Interpretation of Seismic Data*. SEG, Tulsa, OK. doi:10.1190/1.9781560801580.

Zhan, Z., Helmberger, D., Simons, M., Kanamori, H., Wu, W., Cubas, N., Duputel, Z., Chu, R., Tsai, V.C., Avouac, J.-P., Hudnut, K.W., Ni, S., Hetland, E., Culaciati, F.H.O., 2012. Anomalously steep dips of earthquakes in the 2011 Tohoku-Oki source region and possible explanations. *Earth Planet. Sci. Lett.* 353-354, 121-133. doi:10.1016/j.epsl.2012.07.038.

## Chapter 5

### Concluding Remarks

#### 5.1. Dissertation Summary

Results presented in this dissertation provide new insights into subduction zones focusing on three different geological settings, from the incoming plate and deformation front (Chapter 2), to the inner accretionary prism (Chapter 3) and the landward forearc slope (Chapter 4).

Chapter 2 focused on the deformation front at the Japan Trench and the incoming Pacific Plate. Our depth-migrated regional and high-resolution seismic lines that image the incoming plate along the Japan Trench off Tohoku show trench-parallel faults that offset the igneous crust on the outer-rise seaward of the trench. Throw analysis of the outer-rise normal faults indicates more offset in the north than south of our survey area with continuing formation of faults towards the trench. This chapter also investigated the material being subducted by measuring the sediment thickness of the Pacific Plate and found that it is not uniform but fluctuates between 0 and 600 m with a general increase in thickness towards the trench, which will directly influence how the prism forms and develops. Chapter 2 also showed new evidence for recent sediment deposition on normal fault footwalls and near-trench topographic lows along the Japan Trench. This late stage deposition adds to the regional sediment fluctuations to create more sediment variation in this region than previously thought. Furthermore, densely spaced faults within the sediments of the incoming plate sediment reveal only a few meters of slip. This chapter expanded on previous studies to show up-dip décollement propagation over both horst and graben systems along the Japan Trench revealing a clear correlation between subducted structure and deformation front location. This led to a new proposal that the décollement geometry and

normal faults reflect stresses and displacements at the tips of actively subducting active normal faults.

The inner accretionary prism system has been insufficiently studied due to its deep location and poor geophysical images, but was the topic of study for Chapter 3 of this dissertation. Whereas the seismic data does not directly image thrust faults beneath the Kumano Basin, the seismic data does image folded horizons within the Miocene prism and allows for the interpretation of the top of the prism. An interpreted buried outer prism thrust fault is found under the Kumano Basin and appears to have been reactivated after forearc basin formation. Trishear modeling confirms this interpretation with ~580 m of slip occurring on a steeply dipping thrust fault as the basin developed, but the fault is currently not active. The interior of the inner prism was found to contain steeply dipping beds with bedding strike perpendicular to the plate convergence direction, indicating continued tilting and deformation before forearc basin deposition. These new results provide insights into the regional and small-scale structural geology of an inner accretionary prism, how the inner prism develops, and how the inner prism becomes a stable region for forearc basin deposition.

Chapter 4 uses depth-migrated regional seismic lines to image the forearc slope over the 2011 Tohoku epicenter. Forearc basins are tilted landward in both the bathymetry and the seismic lines and interpreted to be from local uplift. Uplift is not expected at an erosional margin and indicates other factors are involved in how the margin subsided. Additionally, the regional basement unconformity was mapped within the survey region finding a highly variable depth and dip in the upper slope. This pattern indicates that prism subsidence and morphology of the regional basement unconformity may be from multiple sources instead of just from subduction erosion. Middle slope deformation is found throughout the margin and is more uniform

compared to upper slope deformational styles. These results will have an impact on the community's understanding of the Japan Trench tectonics and erosional margins by providing new evidence of forearc slope deformation.

## **5.2. Broader Impacts**

The 2011 Mw 9.0 Tohoku earthquake surprised many because of previous notions that the Japan Trench could not produce larger than Mw 8 earthquakes. Damage from both the earthquake and tsunami affected the lives of hundreds of thousands of Japanese along the coast but also affected people, land, and property throughout the Pacific. Work on near-trench properties along the Japan Trench helps one to understand the dangers poised beneath the sea. As evidence for coseismic slip propagating to the trench axis continues to be unearthed, as exemplified by the Tohoku event, the role of the near-trench décollement will be vital to unraveling tsunamigenic events. Our results will impact other disciplines through international collaborations and may be expanded to additional subduction zones. The Integrated Ocean Drilling Program (IODP) drilled Site C0019 within our survey area. Our results will impact conclusions from sedimentology, structure, and physical properties by helping expand results away from the well site to better understand the regional setting. This work provides a regional overview to the local drill site that will help in our understanding of the 2011 Tohoku earthquake. Presently, an IODP proposal to drill along this margin is under consideration, with this work and additional seismic expeditions greatly enhancing the community's understanding of both this margin and the slip to the trench for the 2011 Tohoku earthquake. The effects of normal faults on the deformation front should be studied at other margins where large horst blocks are subducting, such as the Middle America Trench off Costa. Furthermore, our results

have additional implications for the hydration of the plate and upper mantle from both large- and small-scale faulting with future projects planned to investigate this at the Japan Trench outer rise.

The Nankai Trough project provided new perspectives on wedge dynamics. This project provides new insight on how inner prisms form and evolve at an accretionary margin. It has implications for how the dynamic backstop, of the inner prism, is stable during the earthquake cycle. Our results indicate that the deep inner prism is heavily deformed. However, the timing of this deformation is not well constrained. It is also not clear if this type of deformation occurred coseismically, which would have further implications on tsunami risk during the initial inner prism formation. Whereas these results should be considered for most wedge evolution, the Kumano portion of the Nankai Trough does display different morphology than many accretionary prisms: the sharp slope break landward of the out-of-sequence-thrust fault zone, which is not present at many other margins, may limit its general applicability.

The Japan Trench forearc slope project highlights new images and interpretations on the margin. The deep processes of subduction erosion are poorly constrained, and this work has new implications on how and where subduction erosion may occur along the Japan Trench. With nearly half of the world's convergent margins being classified as erosive, this suggests additional processes play a larger role in shaping convergent margins than just subduction erosion. This work also proposed locations for mass wasting events due to thinning of slope sediments and a steep seafloor. This type of hazard is becoming more apparent worldwide.

Further research on subduction zones is vital for scientific understanding of these regions and for the social impact these regions create. Earthquakes and tsunamis generated at subduction zones still devastate local communities, with a potentially increasing threat to coastal communities due to sea level rise. In addition to sea level rise, increasing coastal development

increases the risk to both people and property. Subduction zones have long been challenging to study due to their great water column depth, sediment cover, and complex geology, but further exploration and research will help define the fundamental properties of this dynamic tectonic setting.